Modeling and Real-Time Optimal Energy Management for Hybrid and Plug-in Hybrid Electric Vehicles

by

Jian Dong

B.A., Tongji University, 2009

A Dissertation Submitted in Partial Fulfillment

of the Requirements for the Degree of

DOCTOR OF PHILOSOPHY

in the Department of Mechanical Engineering

Supervisory Committee

Modeling and Real-Time Optimal Energy Management for Hybrid and Plug-in Hybrid Electric Vehicle

by

Jian Dong

B.A., Tongji University, 2009

Supervisory Committee

Dr. Zuomin Dong, Department of Mechanical Engineering
Supervisor

Dr. Curran Crawford, Department of Mechanical Engineering
Co-Supervisor

Dr. Wusheng Lu, Department of Electrical Engineering
Outside Member

Abstract

Today, hybrid electric propulsion technology provides a promising and practical solution for improving vehicle performance, increasing energy efficiency, and reducing harmful emissions, due to the additional flexibility that the technology has provided in the optimal power control and energy management, which are the keys to its success.

In this work, a systematic approach for real-time optimal energy management of hybrid electric vehicles (HEVs) and plug-in hybrid electric vehicles (PHEVs) has been introduced and validated through two HEV/PHEV case studies. Firstly, a new analytical model of the optimal control problem for the Toyota Prius HEV with both offline and real-time solutions was presented and validated through Hardware-in-Loop (HIL) real-time simulation. Secondly, the new online or real-time optimal control algorithm was extended to a multi-regime PHEV by modifying the optimal control objective function and introducing a real-time implementable control algorithm with an adaptive coefficient tuning strategy. A number of practical issues in vehicle control, including drivability, controller integration, etc. are also investigated. The new algorithm was also validated on various driving cycles using both Model-in-Loop (MIL) and HIL environment.

This research better utilizes the energy efficiency and emissions reduction potentials of hybrid electric powertrain systems, and forms the foundation for development of the next generation HEVs and PHEVs.

Table of Contents

List of Figures

List of Tables

List of Abbreviations

ADVISOR:	ADvanced VehIcle SimulatOR
AER:	all-electric-range
AMFDS:	American Federal Urban Driving Schedule
ANN:	artificial neural network
ANL:	Argonne National Laboratory
ARSM:	Adaptive Response Surface Method
ASM:	Automotive Simulation Models
BEV:	battery electric vehicle
CAD/CAM/CAE:	Computer aided design/manufacturing/engineering
cc:	cubic centimeter
DC:	direct current
DOE:	Department of Energy
DOH:	degree of hybridization
DP:	dynamic programming
ECMS:	Equivalent Consumption Minimization Strategy
EREV:	extended range electric vehicle
ESS:	energy storage system
GA:	Genetic Algorithms
GHG:	greenhouse gas
GIS:	geographical information systems
GO:	global optimization
GPS:	Global Positioning System
HEV:	hybrid electric vehicle
HIL:	hardware-in-the-loop
ICE:	internal combustion engine
IESVic:	Integrated Energy Systems at the University of Victoria
ITS:	intelligent transportation systems
L-A:	lead-acid
Li-I:	lithium-ion
MIL:	Model-in-the-Loop
MPC:	Model Predictive Control
NEDC:	New European Drive Cycle
NiMH:	nickel metal hydride
NREL:	National Renewable Energy Laboratory
NYCC:	New York City Cycle
PSAT:	Powertrain Systems Analysis Tool
PHEV:	plug-in hybrid electric vehicle
PI:	Proportional-Integral
PMP:	Pontryagin’s Minimum Principal

PTW:	pump-to-wheels
QP:	quadratic programming
SA:	Simulated Annealing
SI:	spark ignition
SIL:	Software-in-the-Loop
SOC:	state of charge
SQP:	Sequential Quadratic Programming
THS:	Toyota Hybrid System
V2I:	vehicle-to-infrastructure
V2V:	vehicle-to-vehicle
VP:	virtual prototyping
WTP:	well-to-pump
ZEV:	zero-emission vehicle

Acknowledgments

Financial supports from the Natural Science and Engineering Research Council of Canada (NSERC), Natural Resources of Canada, and China Scholarship Council are gratefully acknowledged.

Dedication

I would like to thank Dr. Zuomin Dong, Dr. Curran Crawford, Dr. Wusheng Lu and the members of the UVic Green Vehicle Research team for the precious guidance and feedback over the course of this work.

I am also grateful to the many bright students and researchers I met here at UVic, for the interesting discussions on hybrids, smart cars, intelligent technologies, for those working nights before the project deadline and the beer nights after the deadline, for the support provided to build and implement the Hardware-in-the-loop test environment, for the generous knowledge sharing, technical help as well as moral encourage by my dear colleagues. Thank you very much guys.

I would like to say thanks to all my friends for their presence in my life, especially important when one lives far away from home. The years in Victoria have been my most precious memory from the first time I was picked up at the airport and then during all the great times that followed until now. I have always enjoyed my stay in Victoria. Thank you all for the wonderful company.

Finally, I would like to thank my dear parents who have supported me over the past years. I could not have made it without their encouraging support. I love you and thank you!

Chapter 1. Introduction

1.1 Research Problem

1.1.1 Background

Increasing concerns on various environmental issues, such as global warming and greenhouse gas (GHG) emissions, as well as uncertain oil supplies have made hybrid electric vehicles (HEVs) a promising alternative to conventional Internal Combustion Engine (ICE) vehicles, due to their ability to considerably improved energy efficiency and reduced emissions.

The energy efficiency improvement of HEVs is partially due to their capability of recovering braking energy, and partially due to their ability to allow the ICE to operate at the high efficiency operation conditions with the additional degree of freedom from two energy sources on board of the vehicle, the electrical energy storage system (ESS) and the fuel tank. The presence of this additional degree of freedom, however, also demands an appropriate energy management strategy to exploit the optimal operation effectively.

Recently, plug-in hybrid electric vehicles (PHEVs), HEVs with oversized batteries that can be recharged using grid power at station, present an even more promising solution to greener vehicles due to their ability to further reduce the petroleum consumption and greenhouse gas (GHG) emissions by using grid power generated from renewable energy sources and excess electric generation capacity at off-peak hours. The added part-time pure electric vehicle (PEV) mode supports better emissions control in highly populated urban areas and contributes to further improvement of powertrain efficiency. In some region, the lower cost of electricity comparing to petroleum fuels present additional incentive to the new PHEVs. According to the cost-benefit analysis for PHEV shown in [1], the running cost of gasoline and electricity consumption is

about 0.153 $/mile for a conventional vehicle and 0.078 $/mile for a PHEV with the same vehicle platform, using the U.S. average retail gasoline rate for February 2014 (3.5 dollar/gallon)[2] and average residential electricity rate for December 2013 (0.12 dollar/kWh)[3]. PHEVs also eliminate the problem of "range anxiety" associated to PEVs, because the ICE functions as a backup when the batteries are depleted, giving PHEVs driving range comparable to other vehicles with gasoline tanks. Other benefits include improved national energy security, fewer fill-ups at the filling station, the convenience of home recharging, opportunities to provide emergency backup power in the home, and "vehicle-to-grid"(V2G) applications[4].

1.1.2 Research Motivation

A major challenge for the development of hybrid vehicles (both HEVs and PHEVs) is the control of multiple energy sources and converters and, in the case of a hybrid vehicle, power flow control for both the mechanical and the electrical paths. This necessitates the utilization of an appropriate control or energy management strategy. A supervisory control strategy, which is usually implemented in the vehicle central controller, is defined as an algorithm, essentially a law regulating the operation of the drive train of the vehicle. Generally, it inputs the measurements of the vehicle operating conditions such as speed or acceleration, requested torque by the driver, current roadway type or traffic information, in-advance solutions, and even the information provided by the Global Positioning System (GPS). The outputs of a control strategy are decisions to turn ON or OFF certain components or to modify their operating points by commanding local component controllers. As an example, the IC engine can be commanded to run near its optimal efficiency curve, using an EM as a buffer for load balancing.

The primary objectives of hybrid drivetrain energy management system are meeting the driver's demand for the traction power, sustaining the battery charge and

optimization of drivetrain efficiency, fuel consumption, and emissions. Recently, achieving smooth gear shifting and minimizing excessive driveline vibrations, known as drivability, are included in the drivetrain control strategy. For PHEV, there're some additional challenges for control and optimization, due to the necessity of accounting for the cost, energy depletion and pollution due to the use of electrical energy in place of fuel.

The current focus of hybrid vehicle controller design is on the development of real-time implementable optimal energy management strategies that can approximate the global optimal solution closely. In reality the true global optimal solution can only be obtained through computation intensive offline optimization techniques such as Dynamic Programming, consider all energy use possibilities of the entire trip. Due to the intensity of the computation and the need to have "future" driving conditions, the approach can only serve as benchmark study for optimal energy management, and cannot be applied directly in real-time optimal control. The benchmark results present the best possible results that a control system can achieve in principle, and serve as a reference to guide the development of "real-time optimizer". The ultimate goal of this dissertation is to develop a systematic methodology for formalization of online control algorithm for hybrid vehicles (both HEV and PHEV), which approximates the offline global optimal solution as closely as possible; and is easy to implement in practical applications and fast enough for real-time use without dependence on specific driving cycles at the same time.

1.2 Literature Review

A review on related literatures to better understand the state-of-the-art of the research, better define the research problem, and introduce innovative new optimal energy management technique has been conducted with the following outcomes.

1.2.1 Advanced HEV/PHEV Powertrain Architecture

Hybrid electric vehicle can be distinguished by their powertrain configuration. They have broken out into the following distinct categories:

- series hybrid electric vehicles in which there is no mechanical connection between the internal combustion engine and the wheel. The vehicle is primly propelled only by electric motors with an engine/generator set providing the electric power coming from an electric battery or when required the engine/generator can also be used to charge the battery.
- parallel hybrid electric vehicles, where engine and electric motor(s) are connected mechanically (via gear set, chain, belt and etc.) and can transmit power simultaneously to propel the vehicle, usually through a conventional transmission.
- power-split or series-parallel hybrid electric vehicles, where the powertrain combines a parallel and series hybrid feature usually by using a power-split device such like planetary gear set in Prius HEV[5]. Usually more than 2 electric motors are used and the power path from the engine to the wheel can be either mechanical or electrical depending on the current operating conditions.

With the addition of a large ESS, HEVs can have the ability to acquire electric charge from the power grid, forming PHEV, and if the electric drive of the PHEV is powerful enough to complete all driving cycles independently, the PHEV becomes an extended-range electric vehicles (EREV). PHEV and EREV can have all of these different powertrain architectures. The merits and drawbacks of each configuration are summarized in the following table:

Table 1. Advantages and Disadvantages of Different Types of HEV

	Advantages	**Disadvantage**	**Industrial Application**
Series	● Ideal for urban and suburban driving conditions. Engine tends to be smaller and more efficient since it is not	● Less efficient than parallel hybrids for highway driving due to energy conversion	BMW i3 range extender.

	directly connected to the wheels and are not subject to the highly variable power demands of stop-and-go driving. ● Easy for packaging and design, since only electrical connections between each component and no need for a complicated multi-speed transmission and clutch. ● Relatively simple control system.	losses between mechanical and electrical power. ● More cost and weight than parallel hybrid due to the need of larger, more complicated battery and motor and the addition of a generator to meet its power needs.	
Parallel	● More efficient than series hybrid since mechanical energy from engine is delivered direct to the wheel with no energy conversion. ● Cheaper. Only a cheap clutch or belt driven torque converter is needed instead of a gen set and high power battery for series hybrid. ● More powerful since both the traction motor and engine are directly coupled to the drive train.	● Engine operating conditions (speed) is dependent on the vehicle speed, since it is coupled to (via the transmission) the ground. ● More complex control than series hybrid is needed.	Honda's Insight, Civic, and Accord hybrids. General Motors Parallel Hybrid Truck (PHT) and BAS Hybrids such as Saturn VUE, Aura Greenline, Chevrolet Malibu
Power-Split and Series-Parallel	● Combines the advantages of series and parallel hybrid vehicles. ● Has a direct mechanical path for the ICE, which is very efficient in steady operating conditions like cruising. ● Has an electromechanical	● Further complexity and cost	Toyota Prius, Ford, General Motors Volt, Lexus, Nissan

	path which allows for efficient operation of the ICE in unsteady driving, such as speed variations seen in city driving		

An alternative way to classify hybrid vehicles is by the degree of electrification:

- Micro hybrids feature stop/start functionality with no electric propulsion support. Other features include efficient generator, regenerative braking, comfort stop/start.
- Mild hybrids can have all of the above plus limited electrification of propulsion with typically about 15% of the total power from the electric drive, 5-12 kW power and less than 1kWh ESS capacity.
- Full hybrids feature a high electrification of propulsion, typically more than 20 kW and more than 1kWh storage capacity. They have a power assist feature, usually in association with a smaller internal combustion engine than is needed for the base vehicle and limited zero emission (EV only) operation using its own on-board electric motor.
- Plug-in hybrid electric vehicles (PHEV) have a larger rechargeable battery, which can be restored to full charge by connecting a plug to an external electric power source (usually a normal electric wall socket). A PHEV shares the characteristics of both a conventional hybrid electric vehicle and an all-electric vehicle.
- Extended range electric vehicles (EREV) are PHEVs with a bigger battery for driving ranges of 40-80 miles using only the battery (EV-only), after which the gas engine starts to provide power. The “range anxiety” is one of the main barriers for the commercial success of electric vehicles, and EREV’s ability to extend the vehicle's range when the battery is depleted helps alleviate this concerns.
- Battery electric vehicles (BEV) are full electric vehicles. They only have an electric drive train which derives all its power from its rechargeable battery pack and thus has no internal combustion engine and fuel tank.

1.2.2 Powertrain Modeling for Energy Management

The modeling approach for vehicle powertrain can be classified as static and dynamic:

1) The static or quasi-static approach assumes that the prescribed driving cycle is followed exactly by the vehicle. A relatively larger simulation time step compared to dynamic modeling is usually used (typically a time step of 1s) based on averaged speed, torque, and acceleration during that time interval. Efficiency map or power loss map obtained from steady-state testing of real components are used to model the powertrain.

2) The dynamic approach is based on first-principles description of each powertrain component, with differential equations that describes the evolution of its state. It takes into account transient phenomena and hence is often more accurate than the static modeling.

Based on the information flow, the modeling approaches for vehicle powertrain can also be categorized as backward and forward approach:

a) In the backward approach (as shown in Fig 1), the demanded speed profile is the direct input to the vehicle model. Based on the speed profile, payload and grade profiles, along with the vehicle characteristics, the net tractive force at the wheel and the resultant torque and speed request is calculated and propagated from the wheel to the engine via the drivetrain components. This approach does not require a driver model and is considered as non-causal. The engine operating point is determined backwards through the drivetrain components based on the steady-state efficiency maps and so the backward approach is also considered as “quasi-static”. Since the demanded drive cycle must be met at each time step, this approach cannot capture the limit of the physical system. Due to its faster simulation time compared to the forward approach, the back approach is usually used at the initial design phase

(e.g. for component sizing, energy oriented analysis and etc.), while it is not suitable to be applied to control-oriented development or Hardware-in-the-loop simulation. Advisor developed at National Renewable Energy Laboratory(NREL) is based on this approach[6].

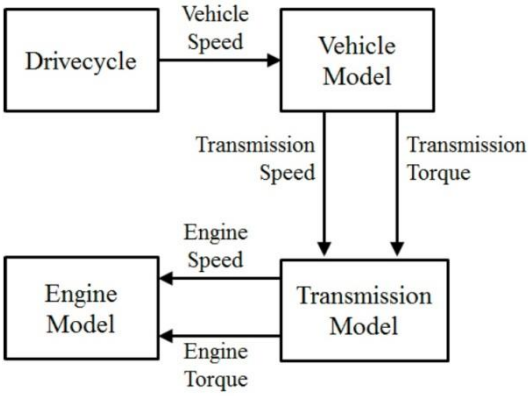

Fig 1. Backward modeling approach for vehicle powertrain[7].

b) Forward approach features a driver model (as shown in Fig 2), which typically uses a PI controller to emulate the real world driver behavior to follow the demanded speed profile. The torque request is generated out from the driver model and is then propagated forwardly through engine to the wheel via the drivetrain components such as transmission, torque converter, differential, final drive and etc. Ultimately based on this propagated torque, the tractive force at the tire is produced. The vehicle speed that results from the applied force based on the vehicle dynamics function is fed back to the driver model and compared with the demanded speed to generate the torque request. The demanded speed profile doesn't necessarily be followed and so the forward approach can capture the limits of the physical system and provide insight into the vehicle drivability. Forward approach is causal and it naturally includes longitudinal vehicle dynamics into the modeling. It is more accurate and is well-suited for control-oriented development, vehicle dynamic performances evaluation (e.g. full-throttle acceleration test) and Hardware-in-the-loop implementation[8]. The powertrain simulation software Autonomie[9] and its predecessor PSAT[10] developed by Argonne National Lab(ANL) are based on this

approach.

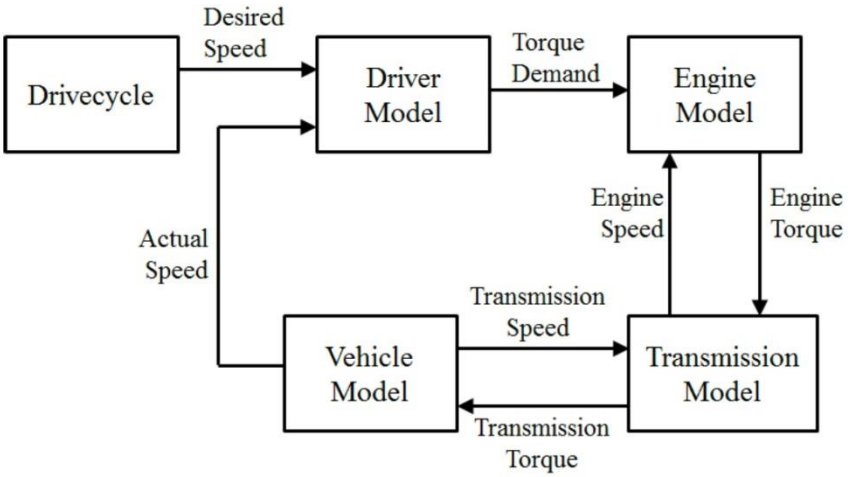

Fig 2. Forward modeling approach for vehicle powertrain[7].

1.2.3 Energy Management (Supervisory Control Strategies) for HEV

Energy management or supervisory control strategy, essentially a set of laws or an algorithm regulating the operation of main components in the drivetrain at every time step, plays a critical role in determining the hybrid electric vehicle's performance，which is usually implemented in the vehicle central controller. Generally, it is responsible for determining the operating mode of the HEV, the On/Off commands as well as power/torque split among those major powertrain components such as engine and electric motors based on the current vehicle operating conditions such as vehicle speed, acceleration, driver torque request, traffic and GPS information and etc. The energy management strategy, i.e. power/torque split strategy, can be determined either by a set of predefined rules or by optimization based algorithm. The primary goal is to satisfy the driver's torque request with minimum fuel consumption and emissions (usually engine is kept running in its most efficient region) and with other optimum vehicle performance such as drivability. Moreover, fuel economy, emissions and drivability are conflicting objectives and therefore a trade-off between them needs to be taken into consideration.

Table 2. Classification of HEV energy management strategies

Rule-Based		Optimization-Based	
Fuzzy Logic	Deterministic	Offline Global Optimization	Online (Real-Time) Optimization
• Predictive • Adaptive • Conventional	• State Machine • Power Follower • Thermostat Control	• Dynamic Programming • Linear Programming • Quadratic Programming • Stochastic DP • Game Theory • Genetic Algorithm • Particle Swarm Optimization	• Equivalent Consumption Minimization Strategy • Pontryagin's Minimum Principle • Model Predictive Control • Neural Network • Approximate Dynamic Programming

As shown in Table 2, energy management strategies can be mainly classified into two categories: rule-based and optimization-based algorithms.

Rule-based algorithms rely on heuristics, expert knowledge and engineering intuition, which comprised of a large number of pre-defined control logic statements. Rule-based control algorithms include deterministic rule-based and fuzzy rule-based methods [11-13]. Rule-based control is very commonly used in industrial applications, since compared to the optimization-based control, it is relatively simpler to implement, more intuitive for calibration, more flexible to introduce additional rules (since it does not need to change the overall algorithm structure), more computational efficient in real-time and does not require any knowledge of future drive cycle. However, rule-based control methods suffer from several inherent drawbacks: they guarantee no optimality of the results, provide poor adaptability since the overall performances rely on particular vehicle structure and driving conditions, and can be fairly time consuming when developing a new rule-based supervisory control strategy.

The optimization-based methods for HEV supervisory control has been extensively studied in [14-18]. The main purpose is to find the global optimal solution that minimizes the cost function representing fuel consumption and emission over the whole driving cycle, not just instantaneously, for example, to determine at a given time step whether to charge the battery assuming that charge will be used up at some point in the future, although the future driving cycle might not be known in advance.

There have been two general categories for optimization-based methods: offline and online approaches. Various offline optimal control approaches have been proposed including dynamic programming, linear programming, genetic algorithms, game theory and etc. [19]. Among these techniques, dynamic programming (DP) [11,17,18, 20] is the only one that can achieve global optimality. It is, however, not practically implementable due to its non-causal nature and computational burden. Nevertheless, these serve as good theoretical benchmarks and rule extraction reference for online control strategies.

The current focus of HEV controller design is on the development of online real-time implementable energy management strategies that can approximate the offline global optimal solution closely without or with minimum *a priori* knowledge of the driving cycle. In addition, this kind of control algorithm usually requires much fewer calibration parameters than those based on rule-based heuristic methods due to its model-based nature.

An online analytical solution based on optimal control theory for a parallel HEV problem was found in [15]. However, the Lagrangian parameters of this solution is determined based on the future trip preview and the approach is not applicable to other general powertrain architecture. [21, 22] applied Stochastic Dynamic Programming (SDP) to the HEV energy management problem, where an optimal energy management policy is computed by iteratively solving a stochastic dynamic program over an infinite

horizon. In this control scheme, the driver's power request is modeled as a random Markov process to accurately represent the nondeterministic nature of this variable. Despite the improvements in fuel and emission, the main drawback of SDP is the significant amount of driving data and the huge computational time needed for validating and evaluating the algorithm. Model predictive control (MPC) obtained by system identification has also been investigated for the energy management problem for HEV[23, 24]. MPC features optimization over a moving finite prediction time-horizon, where a future control sequence is calculated for fuel minimization and then only the first element of the computed control sequence is applied to the HEV model. The process is repeated at the next time step by moving the prediction horizon one step forward. Improved fuel economy is noticed with respect to that of an conventional controller in PSAT software[23]. However, due to the burdensome time-horizon optimization at each time step, MPC is hard to implement on-line (in real time) directly. Also since the future driver torque demand is assumed to be exponentially decreasing over the prediction horizon [23, 25], while in reality it is usually unknown, the optimality of the MPC approach remains susceptible. Other techniques such as artificial neural network applied to HEV [26-28] with better fuel saving results claimed. The NN controller can adapt to different driving cycle and driver’s style, assuming comprehensive the training table are implemented. Its main drawback lies in algorithm complexity, non-intuitive training and needs of propagation to retrain the NN, slow processing time and possible needs of an additional large processor[29].

The Equivalent Consumption Minimization Strategy (ECMS)[14, 30] utilizes a weighted cost function of electrical and fuel energies. The performance is dependent on the tuning of the equivalent factor between the two energy sources, where much less calibration effort is required than rule-based controllers. This equivalent factor can be tuned based on the current driving conditions and battery SOC deviation. ECMS can also be easily adapted to different vehicle architectures without changing the algorithm

structure.

Another optimal control solution similar to ECMS is based on Pontryagin's Minimum Principle (PMP)[18, 20, 31] which converts a global optimal control problem into an instantaneous optimization problem. The results of PMP have been shown to be superior to ECMS[31] and almost same as the global optimal results obtained from DP[20, 31] given that the costate in PMP is well tuned based on the whole trip information. With innovation thriving of the on-board vehicle telematics devices, the development of intelligent energy management systems has allowed optimal parameter tuning based on past driving profiles or predicted future driving conditions by using machine learning techniques[32-34]. However, the drawback lies in both the computation burden for real-time implementation and the accuracy of the predicted future condition which might subject to sudden and unpredictable pattern change.

The merits and drawbacks of rule-based methods and various optimization-based methods for HEV supervisory control are summarized in Table 3.

Table 3. Advantages and disadvantages of heuristic methods and optimization-based methods.

	Heuristic Methods	**Optimization Methods**
Advantages	• Simple to develop. • Intuitive calibration. • Computationally efficient. • No requirement for future drive cycle knowledge.	• (Quasi-) optimal control policies. • Small number of calibration parameters. • Good adaptability to different architectures.
Disadvantages	• No guarantee for optimality. • Time-consuming calibration. • Poor adaptability to different vehicle architectures.	• Requires accurate component models. • Non-intuitive calibration. • Computational burden in real time. • Requirement for future drive

		cycle knowledge might be needed.

Practically, heuristic methods and optimization methods are combined together in the control scheme to deal with the energy management for a hybrid vehicle. The vehicle operating modes (as shown in Fig 3) and transition between the modes are usually determined by predefined event-triggered rules based on current operating conditions, while the power/torque split inside an operating mode is determined by either rules or by the aforementioned optimization techniques. However, since the optimality of the optimal control depends on the whole driving profile, instead of one single time step, the above combined strategies cannot guarantee optimality.

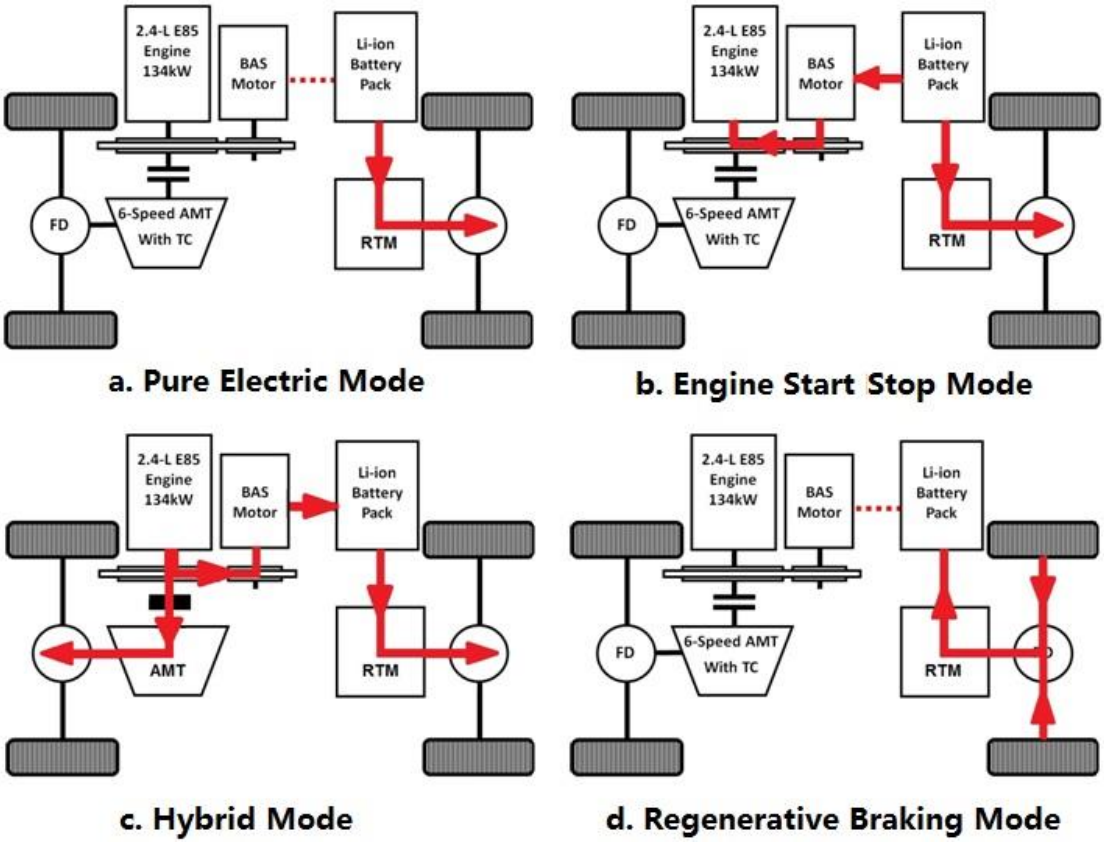

Fig 3. Typical operating modes for HEV

1.2.4 Energy Management (Supervisory Control Strategies) for PHEV

Compared to conventional HEV supervisory control, where the battery SOC is

maintained around a nominally constant value during the whole driving cycle, the energy storage system with much higher capacity in PHEV and its capability of depleting the battery to a pre-defined low threshold SOC and recharging it directly from the power grid adds more complexity as well as flexibility into the energy management problem for PHEV. In fact, most of the available electrical energy is supplied from the grid, hence introducing the full-cycle well-to-wheel (WTW) assessment of energy use and GHG emissions into the energy optimization problem. This implies that the performance of PHEVs are significantly influenced by additional variables, such as the upstream marginal electricity generation mix, fuel choices and their well-to-wheel assessment, battery capacity and the resulting all-electric-range (AER), the consumer's interaction related information such as trip distance. To evaluate a PHEV, full-cycle energy analysis can be conducted by using tools like GREET[24] developed by Argonne National Laboratory (ANL), which tracks the energy use and emission from the primary energy source to the vehicle's operation, which is known as a "well-to-wheels" (WTW) analysis[30, 35, 36].

Like for HEV, there're mainly two categories of PHEV supervisory control approaches: rule-based (heuristics-based) and optimization-based methods. The simplest way to control PHEV is to use the Charge Depleting-Charge Sustaining (CDCS) rule-based strategy. Regardless of its architecture, a PHEV is capable of operating in two modes: Charge-Depleting (CD) mode and Charge-Sustaining (CS) mode. CDCS strategy operates the vehicle first in CD mode, where battery is used exclusively (except during hard acceleration) to power the vehicle until its battery SOC is depleted to a predetermined low threshold level, and then the vehicle will operate in CS mode where engine will start to provide power along with battery and the battery SOC will be kept at a nominally constant value as in a conventional HEV. CD mode is sometimes also referred to as Electric Vehicle (EV) mode or All Electric Range (AER) mode. Instead of using pure EV mode, another way to control PHEV is to use the

blended strategy during CD mode, where the vehicle is operated under a combination mode of both CD and CS mode, which is also termed blended mode. Under blended mode, engine is turned on and off fairly frequently during the whole cycle as shown in Fig 4, and typically the CD range (distance) is increased when using blended mode compared to the case when using pure EV mode. Based on CDCS heuristic methods, several control approaches have been proposed in the literature on this topic[29, 37-39]. CDCS method is simple and easy to implement and doesn't rely on future cycle's knowledge. However, this kind of heuristic control approach can by no means provide optimal results.

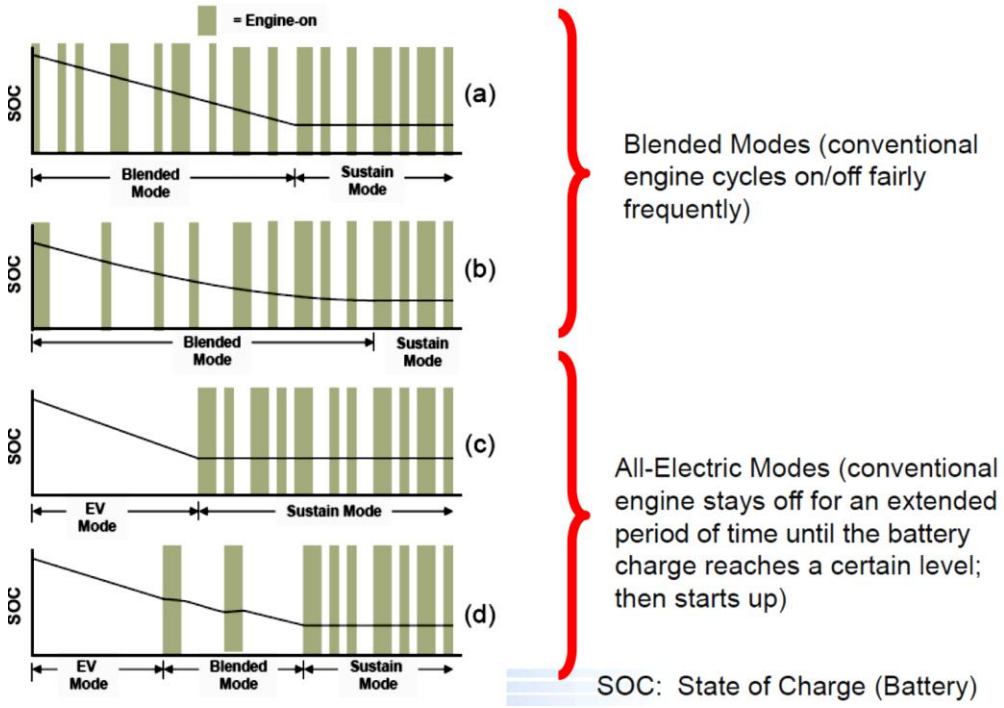

Fig 4. CDCS control strategy for PHEV

It was found that blended mode strategies have a significant benefit over CDCS control strategies since the blended strategy can ration a vehicle's battery energy throughout an entire trip by saving the battery energy for later portions of the cycle to increase the average engine efficiency, assuming that trip distance has been known in advance ([17, 32, 34, 40]). In [34], the blended mode strategy was shown to improve a

power-split PHEV's fuel economy by up to 9% comparing to CDCS strategy, due to more efficient operation of the engine.

Unlike CDCS, which does not need any knowledge of the future trip, the optimality of the optimization based supervisory control strategies, such as DP, ECMS and PMP that provide blended mode solutions, are based on the vehicle speed and grade profiles known in advance. However, a real-time implementable controller can be designed using information extracted from an optimal control policy[41].

Moreover, as shown in [17, 29, 32, 40], the performance of PHEV is highly trip-dependent. Near-to-optimal fuel economy can be achieved if the control strategy depletes the battery proportionally to the driving distance and the battery SOC reaches its depleted minimum value by the end of the trip. This gives the chance to apply optimal control strategies, such as PMP, in real-time with only the trip distance known in advance. With the rapid development of intelligent transportation systems (ITS), geographical information systems (GIS), global positioning systems (GPS), vehicle-to-vehicle (V2V) and vehicle-to-infrastructure (V2I) interactions, drive cycle modeling and prediction becomes possible based on historical and current traffic patterns and trip data accessed in real-time, which will further facilitate developing the optimal energy management for PHEV.

1.2.5 Development and Validation of Supervisory Control System as part of MBD

Model-Based Design (MBD) is a mathematical and visual method of addressing problems associated with designing complex control system[42]. It's commonly used in aerospace and automotive applications. MBD provides an efficient approach for establishing a common framework for communication throughout the design process while supporting the Vehicle Development Process (VDP) cycle ("V" diagram)[43].

In MBD of control systems, there are four major development steps: 1) modeling a plant, 2) analyzing and synthesizing a controller for the plant, 3) simulating the plant and controller both offline and in real-time, and 4) integrating all these phases by deploying the controller.

As part of the MBD process, development and validation of the control system is conducted by connecting controller to the plant to examine the performance of the whole system. This can be realized at different steps of the process, first with MIL (Model-in-the-Loop) or SIL (Software-in-the-Loop), then in HIL (Hardware-in-the-Loop) and finally in VIL (Vehicle-in-the-loop).

MIL – In this case, both the controller and plant model are set up in desktop Simulink environment. Extremely fast development occurs at this stage as you can make small changes to the control model and immediately test the system.

SIL -- This is a case where the control model is slightly more "real" in the sense that you are no longer executing the model but rather you have probably coded the model into C or C++ and then inserted this coded model back into your overall plan simulation. This is essentially a test of your coding system (whether autocoded or human coded). Design iteration slows down slightly from MIL but coding failures start to become evident.

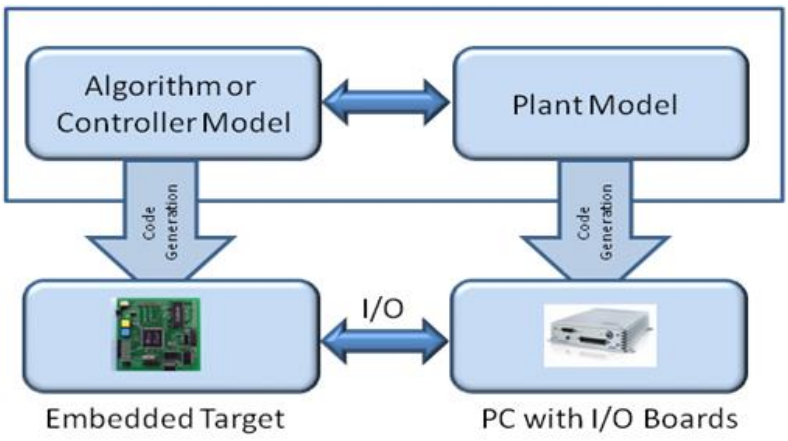

Fig 5. Hardware-in-the-loop(HIL)

HIL -- This is a case where the control system is fully installed into the final control hardware and can only interact with the plant through the proper IO of the controller, as shown in Fig 5. For testing and development of embedded electronic controllers, the hardware controller and associated software are connected to a mathematical simulation of the system plant, which is executed on a computer in real time with IO simulations to fool the controller into believing that it is installed on the real plant. In this case, the only difference between the final application and the HIL environment is the fidelity of the plant model and the test vectors that you are using. HIL is often used only for software validation rather than development as the design iteration is very slow at this point. However, this test is closest to the final application and therefore exposes most of the problems that will be seen.

VIL -- Finally, the controller is integrated into the real vehicle and is communicated with the real components in the vehicle through CAN bus. The vehicle does not move in real traffic or roads, but with a real test driver on dynamometer, where a predefined driving cycle simulating the real road conditions is used for the driver to follow.

1.3 Organization of the Dissertation

This chapter provides a literature review of the advanced hybrid powertrain architectures, methodologies for modeling energy flow and fuel consumption in hybrid vehicles, energy management strategies for both HEV and PHEV as well as their hardware-in-the-loop (HIL) validation methods. Chapter 2 uses Toyota Prius HEV as a case study of practical relevance to present an analytical formalization of the optimal control problem for HEV associated with both offline and online (real-time) solution for the energy management problem, as well as the HIL real-time validation of the proposed control algorithm[44]. Chapter 3 extends the online (real-time) control algorithm to a multi-regime PHEV[43], where the optimal control objective function is modified and a fast real-time implementable control algorithm with an adaptive

coefficient tuning strategy is developed accordingly. A few practical issues (drivability issues, controller integration, and etc.) are also investigated. The algorithm is validated on various driving cycles in both MIL and HIL environment.

1.4 Original Research Contribution

The research carried out within the framework of this thesis leads to the following contributions:

- Developed a systematic methodology for solving HEV and PHEV optimal energy management problem. (Chapter 2.2 and 3.4)
- Conducted a comparative study of various optimal control algorithms (DP, QP and PMP) for HEV and PHEV energy management. (Chapter 2.3, 2.4 and 3.4)
- Developed a dynamic simulator using forward approach for both the Prius HEV powertrain system and the proposed new multi-regime series-parallel PHEV powertrain system. (Chapter 2.1 and 3.2)
- Developed fast offline global optimization techniques based on PMP and QP for HEV (Prius). (Chapter 2.3.2)
- Developed an online adaptive optimal control strategy based on PMP that is close to offline optimal solution and computes fast enough in real-time for HEV (Prius). (Chapter 2.4)
- Formulated an optimal control problem for PHEV powertrain taking full cycle well-to-wheel impacts (GHG and PEU respectively) into consideration, based on a combined fuel and electric source cost evaluation. (Chapter 3.4)
- Proposed a fast online adaptive optimal control algorithm based on PMP for a PHEV with a complex series-parallel architecture that can compute fast enough in real-time and need only the trip distance known in advance. (Chapter

3.5)

- Investigated practical issues when implementing the control algorithm including drivability and controller integration. (Chapter 3.6)
- Investigated the impact of the co-state over various driving cycles for fuel and emission metrics for HEV and for WTW metrics (GHG and PEU) for PHEV respectively. (Chapter 2.7 and 3.7)
- Developed a HIL test setup and validated the proposed fast online optimal control algorithm in real-time environment for both HEV and PHEV. (Chapter 2.6 and 3.8)

Chapter 2. Modeling, Optimal Control and Its Real-Time Validation for HEV: Case Study on Toyota Prius Power-Split HEV

The current focus of HEV controller design is on the development of real-time implementable energy management strategies that can approximate the global optimal solution closely. In this chapter, the Toyota Prius power-split hybrid powertrain is used as a case study for developing online energy management strategy for hybrid electric vehicle.

Toyota Prius is the representative of the power-split (input-split) hybrid powertrain systems, which combines the advantages of both the series and parallel hybrid powertrain and has been appealing to the auto-makers in the past years. The addition of two additional electric machines and a Planetary Gear Sets (PGS) allows more flexibility in terms of control at some cost of complexity.

The production Toyota Prius uses a 'power follower' controller, which is a popular deterministic rule-based controller based on a set of predefined rules (other application example include Honda Insight). It operates on the criteria of sustaining the battery SOC and focuses on parallel topologies, where the electric motor serves as primarily a torque-assist device, whereas the engine is responsible for providing the base torque required for propulsion. The power follower, while being a practical and successful solution, is not ideal since it does not provide any optimality in terms of control. More details about the rule-based control for Prius HEV can be found in Chapter 2.1.6.

The ultimate goal of this work is to develop a close-to-optimal supervisory control strategy that is online implementable with fast computation speed and is applicable to general hybrid electric powertrains. To validate the control strategy, we choose the well-known Toyota Prius power-split powertrain as the baseline vehicle, since high-fidelity components and performance data source for this powertrain is available from literature as well as from commercial software (AUTONOMIE, PSAT and Advisor).

Our ultimate goal is to develop online control strategies for hybrid vehicle which requires no or little future driving cycle information, which will be discussed in Section 2.5.

2.1 Modeling of a Power-Split HEV Powertrain System

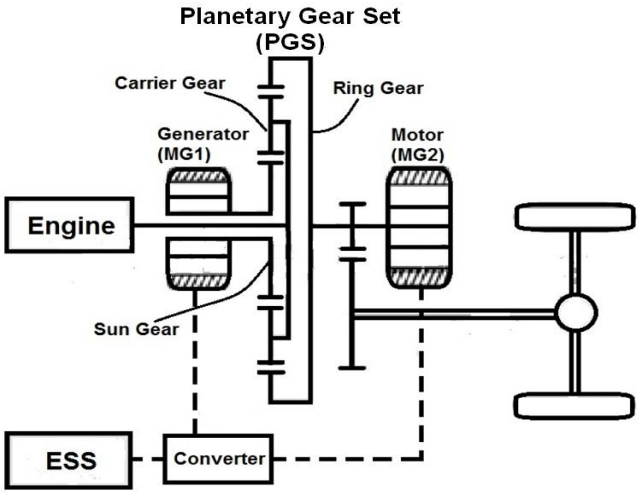

Fig 6. Toyota Hybrid System(THS) power-split powertrain system

The vehicle model considered in the work is the THS input-split hybrid electric powertrain system, which consists of a power-split transmission coupled with two electric machines, as shown in Fig 6.

The Planetary Gear Set (PGS) functions as a power split device, which is placed at the input of the transmission system. The engine shaft as the input shaft is connected to the carrier of the PGS. The output shaft from the ring gear is connected to the drive shaft of the vehicle. MG1 is connected to the sun gear, which is used to function as a generator most of the time to absorb mechanical power from the engine and supply power to the battery. MG2 is connected to the output shaft and functions as a motor most of the time to draw power from either MG1 or the Energy Storage System (ESS) to provide power to the vehicle. During vehicle deceleration, MG2 can also act as a generator for regenerative braking.

A forward approach is used to model the vehicle in the MATLAB/Simulink

environment. All the component data in this study comes from the high fidelity Prius04 model provided in AUTONOMIE[45], which is a state-of-the-art commercial software for vehicle modeling released newly by US Argonne National Laboratory with the support of automotive manufacturers and sponsored by US Department of Energy (DOE). The Prius04 model in AUTONOMIE has been validated within 5% fuel economy and battery SOC for several driving cycles[46], which is used in this work as a reliable data source and for performance validation of the developed model.

The following fundamental assumptions are made regarding the vehicle model:

- Only longitudinal dynamics are included. Indirect coupling effects due to vertical and lateral motions are neglected.
- The drivetrain losses are represented by lumped efficiency and friction models. Frictional losses of driveline components due to effects such as gear meshing and bearing friction are not modeled individually.
- The impacts of environmental factors such as temperature or ageing are not taken into consideration in the component models, since no information was available.

The powertrain dynamics and component models are described as follows.

2.1.1 Power-Split Transmission Dynamics

By analyzing the free-body diagrams of the four parts of the planetary gear set, a separate dynamic equation can be written for each body. The dynamic equations of the PGS can be summarized as below.

$$\begin{bmatrix} T_s \\ T_c \\ T_r \\ 0 \\ 0 \\ 0 \end{bmatrix} = \begin{bmatrix} J_s & 0 & 0 & 0 & R_s N & 0 \\ 0 & J_c & 0 & 0 & -R_s N & R_r N \\ 0 & 0 & J_r & 0 & 0 & -R_r N \\ 0 & 0 & 0 & J_p & R_p & R_p \\ 1/K & -(1+K)/K & 1 & 0 & 0 & 0 \\ 1/K & 0 & -1 & (K-1)/K & 0 & 0 \end{bmatrix} \cdot \begin{bmatrix} \dot{\omega}_s \\ \dot{\omega}_c \\ \dot{\omega}_r \\ \dot{\omega}_p \\ F_s \\ F_r \end{bmatrix} \quad (1)$$

where T_s is the torque output of the planetary system from the sun shaft. T_c is the torque input to the planetary system from the carrier shaft. T_r is the torque added to the planetary system ring shaft. J_s is the inertia of the sun gear. J_c is the Inertia of the carrier gear. J_r is the inertia of the ring gear. J_p is the inertia of a single planet with its own center as the frame of reference. R_s is the number of teeth around the circumference of the sun gear. R_r is the number of teeth on the interior of the circumference of the ring gear. R_p is the number of teeth of the planet gear. N is the number of planet gears in the planetary system. F_s is the reaction force on a planet due to the sun gear. F_r is the reaction force on a planet due to the ring gear.

On the basis of the kinematics of the planetary gear, the speed relationships are determined as follows[16]:

$$\begin{bmatrix} \omega_{gen}(t) \\ \omega_{mot}(t) \end{bmatrix} = \begin{bmatrix} -K & 1+K \\ 1 & 0 \end{bmatrix} \cdot \begin{bmatrix} R_{fd} \cdot \omega_{req}(t) \\ \omega_{eng}(t) \end{bmatrix} \quad (2)$$

where ω_{eng}, ω_{mot}, ω_{gen}, and ω_{req} are the speeds of the engine, motor, and generator, and the requested output speed for transmission, respectively. Further, K and R_{fd} are the gear ratio of the planetary gear set and the final gear ratio, respectively, where K is determined as follows:

$$K = \frac{R_r}{R_s} \quad (3)$$

Neglecting the inertia of the gears, which are trivial comparing to the inertia of the

power source components, the overall dynamics of the input-split powertrain are shown in equation (4).

Note that although there are three speed states, but only two of them are independent due to equation (2). Here we use engine speed and motor speed as the two independent states.

$$\begin{bmatrix} J_{eng}\dfrac{K}{1+K} & J_{gen} \\ \dfrac{J_{eng}+J_{gen}(1+K)^2}{1+K} & -J_{gen}K \end{bmatrix} \cdot \begin{bmatrix} \dfrac{d\omega_{eng}}{dt} \\ \dfrac{d\omega_{mot}}{dt} \end{bmatrix} = \begin{bmatrix} \dfrac{K}{1+K} & 1 & 0 & \dfrac{1}{R_{fd}} & \dfrac{-1}{R_{fd}} \\ \dfrac{1}{1+K} & 0 & 1 & 0 & 0 \end{bmatrix} \cdot \begin{bmatrix} T_{eng} \\ T_{mot} \\ T_{gen} \\ T_{req} \\ T_{brake} \end{bmatrix} \tag{4}$$

where R_{fd} is the final gear ratio. T_{eng} , T_{mot} and T_{gen} are the torque output of the engine, motor and generator, respectively. T_{brake} is the additional brake torque produced by the normal friction brake at the wheel. T_{req} is the requested torque demand at the wheel.

From equation (4), we have the following dynamic equation for the ring output shaft of the PGS gearbox.

$$\begin{aligned} J_{eq}\frac{d\omega_{mot}}{dt} &= T_{gb} - T_{resist} \\ &= [(T_{mot} + A_1 T_{eng} + A_2 T_{gen}) - T_{gb\_loss}] - \frac{T_{req} - T_{brake}}{R_{fd}} \end{aligned} \tag{5}$$

where J_{eq} is the equivalent inertia for the ring gear. T_{gb} is the total torque output from the PGS gearbox acting on the ring shaft, which is obtained by subtracting torque loss from the sum of the torque output from engine, motor and generator. T_{gb_loss} is the torque loss of the PGS gearbox, which is a function of the gearbox output speed ω_{mot}. T_{resist} is the resist torque acting on the ring shaft from the wheel, which is a combination of the road torque demand and the friction brake torque. A1 and A2 are lumped constants. The calculation of J_{eq}, A1 and A2 can be found as follows.

$$
\begin{aligned}
J_{eq} &= \frac{J_{eng} J_{gen} K^2}{J_{eng} + J_{gen}(1+K)^2} + J_{mot} \\
A_1 &= \frac{K}{1+K} - \frac{J_{eng} K}{J_{eng}(1+K) + J_{gen}(1+K)^3} \\
A_2 &= \frac{-J_{eng} K}{J_{eng} + J_{gen}(1+K)^2}
\end{aligned}
\tag{6}
$$

2.1.2 Vehicle Dynamics

Only the longitudinal dynamics is considered in this work. The torque demand at the wheel T_{req} can be determined by either the empirical equation (7) or by the second-degree polynomial curve fitting functions (8). Here we use equation (8) to model the vehicle dynamics[47].

$$
T_{req} = (mg\sin(\alpha) + mgC_{rr} + \tfrac{1}{2}\rho C_d A_f v^2 + m\frac{dv}{dt}) \cdot r \tag{7}
$$

$$
T_{req} = (F_{loss} + m\dot{v}) \cdot r = (F_0 + F_1 v + F_2 v^2 + m\frac{dv}{dt}) \cdot r \tag{8}
$$

where v is the vehicle speed, m is the vehicle mass, r is the wheel radius, α is the grade, C_{rr} is the rolling resistance, ρ is the density of air, C_d is the drag coefficient and A_f is the front area. F_{loss} is the force loss due to aerodynamic drag and rolling resistance. F_0, F_1 and F_2 are road load coefficients for the second-degree polynomial, which are obtained from AUTONOMIE.

Since the vehicle speed and the motor speed has the following relationship:

$$
\omega_{mot} = \omega_{req} = \frac{R_{fd}}{r} v \tag{9}
$$

Substituting equation (8) and (9) into (4), we then have the following dynamic equation for the chassis:

$$
\begin{aligned}
m_{eq}\frac{dv}{dt} &= R_{fd}\frac{T_{gb}}{r}+\frac{T_{brake}}{r}-F_{loss} \\
&= R_{fd}\frac{[(T_{mot}+A_1T_{eng}+A_2T_{gen})-T_{gb\_loss}]}{r}+\frac{T_{brake}}{r}-(F_0+F_1v+F_2v^2) \\
m_{eq} &= J_{eq}\frac{R_{fd}^{\ 2}}{r^2}+m
\end{aligned}
\tag{10}
$$

where m_{eq} is the equivalent mass including both the rotational inertia and the vehicle mass.

2.1.3 Battery Dynamics

The required power of the battery can be calculated as:

$$
P_{bat} = \eta_c^{\ m}(\eta_{gen}T_{gen}\omega_{gen}+\eta_{mot}T_{mot}\omega_{mot}) \tag{11}
$$

where the efficiencies of generator and motor, η_{mot} and η_{gen}, are obtained based on motor efficiency maps of each motor, which include the motor and inverter losses, and η_c is the converter efficiency, where:

$$
m = \begin{cases} 1, & when \quad charging: P_{bat} < 0 \\ -1, & when \quad discharging: P_{bat} \geq 0 \end{cases} \tag{12}
$$

The time derivative of *SOC* (battery state of charge), $\dot{SOC}$, can be calculated from the battery power, which gives the following dynamic equation of the battery:

$$
\dot{SOC} = \frac{d(SOC)}{dt} = f(P_{bat}(t)) = -\frac{1}{C_{bat}}\cdot\frac{V_{oc}-\sqrt{V_{oc}^2-4R_{in}P_{bat}}}{2R_{in}} \tag{13}
$$

where C_{bat} is the battery capacity. V_{oc} is the open-circuit voltage and R_{in} is the internal resistance of the battery. For a charge-sustaining HEV with a limited range of SOC, these parameters can be regarded as constants already known. Fig 7 shows the battery characteristics of the HEV battery used in this work.

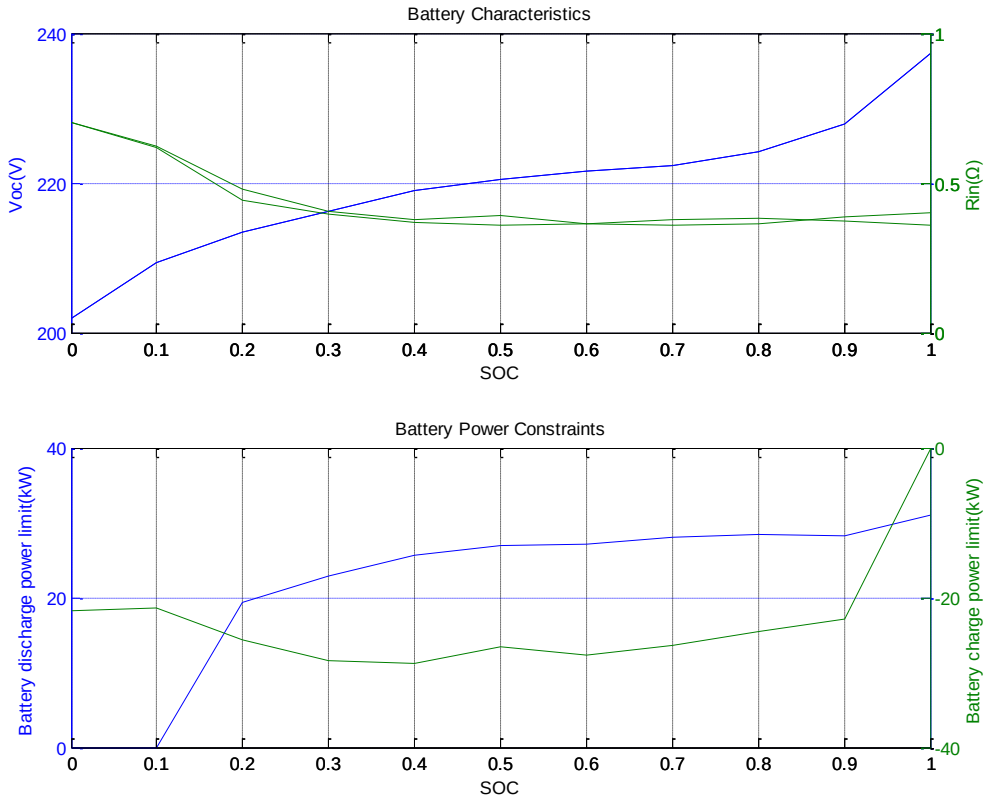

Fig 7. Battery characteristics of the HEV.

2.1.4 Engine, Motor and Generator Models

For discrete time optimization with a sample interval of 1s, the dynamic behavior of the engine and the two electric machines are fast with respect to the dynamics of powertrain and vehicle, and so can be neglected.

The fuel consumption is static function of two independent variables: engine speed and engine torque. The fuel rate $\dot{m}_{fc}$ of the engine can be obtained from the map of engine torque T_{eng} and speed ω_{eng}, which is shown in Fig 8.

$$\dot{m}_{fc} = L(T_{eng}, \omega_{eng}) \tag{14}$$

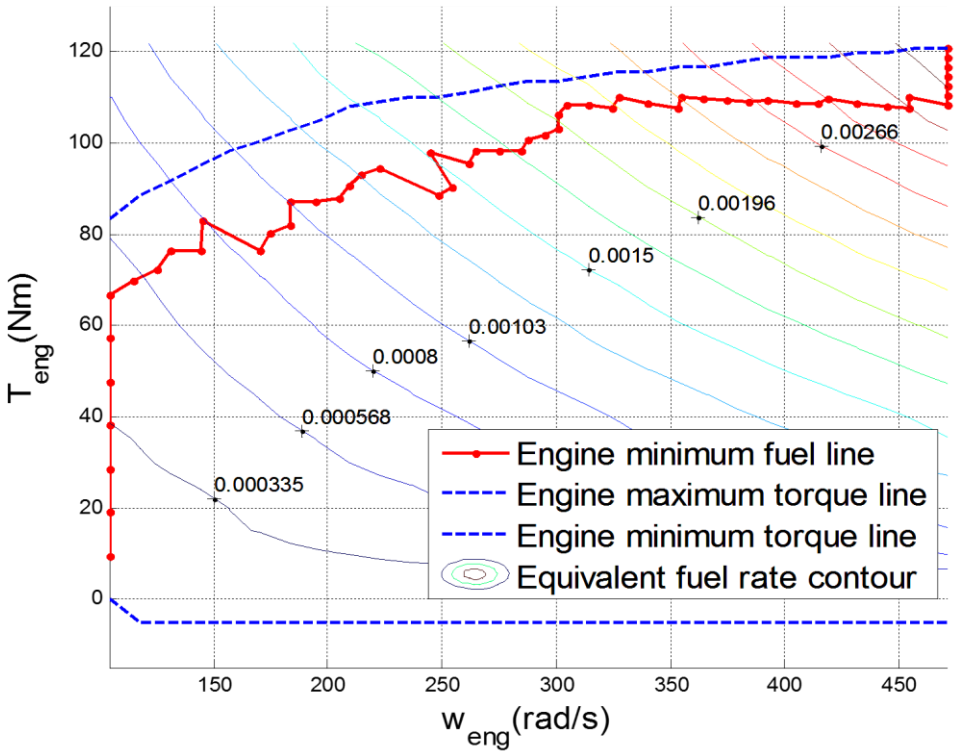

Fig 8. Engine hot fuel rate map of THS

Fig 9 and Fig 10 show the motor and generator efficiency map (combined with inverter efficiency), respectively. The torque limits of each component are also shown in the figure.

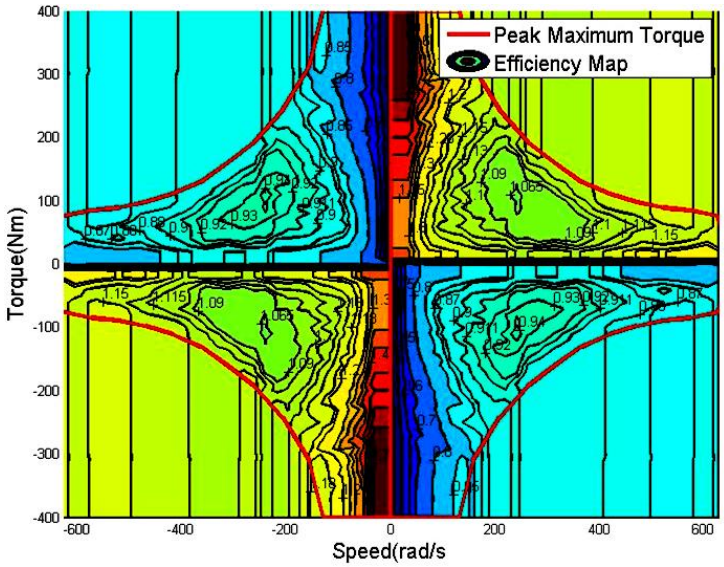

Fig 9. Motor and inverter combined efficiency map of THS.

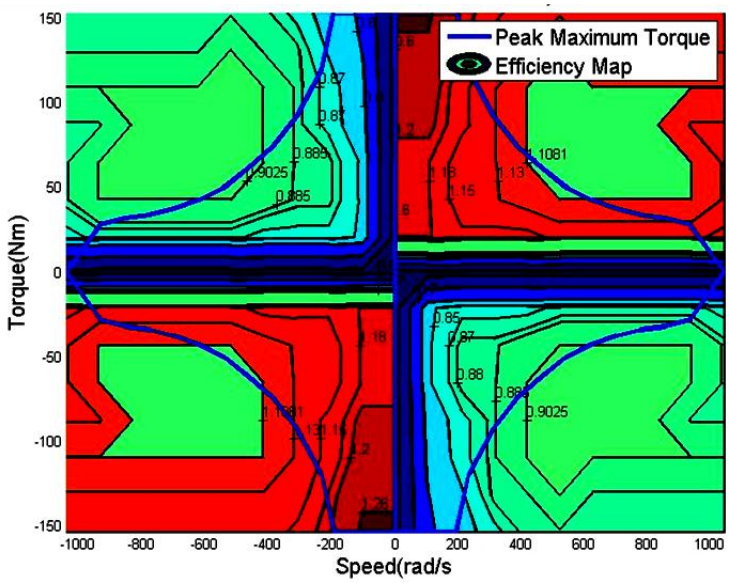

Fig 10. Generator and inverter combined efficiency map of THS.

2.1.5 Forward Discrete Simulation Model

Based on the above powertrain dynamics and component models, a forward-looking vehicle simulation model is built in a discrete-time format within the MATLAB/Simulink environment. A driver model from AUTONOMIE, essentially a PI controller with a torque estimation term, is used here to convert the error between the desired vehicle speed from a pre-defined driving cycle and the current vehicle speed feedback from the plant model into a torque demand T_{req}, which also match the equation used inside the developed plant model. The speed and torque demand along with the state feedback are then fed to the supervisory controller. The controller calculates the torque request as input to the plant model, which again gives back the states feedback. The sampling time for the main-loop simulation is set to 1 second. Fig 11 shows the topology of the simulation model.

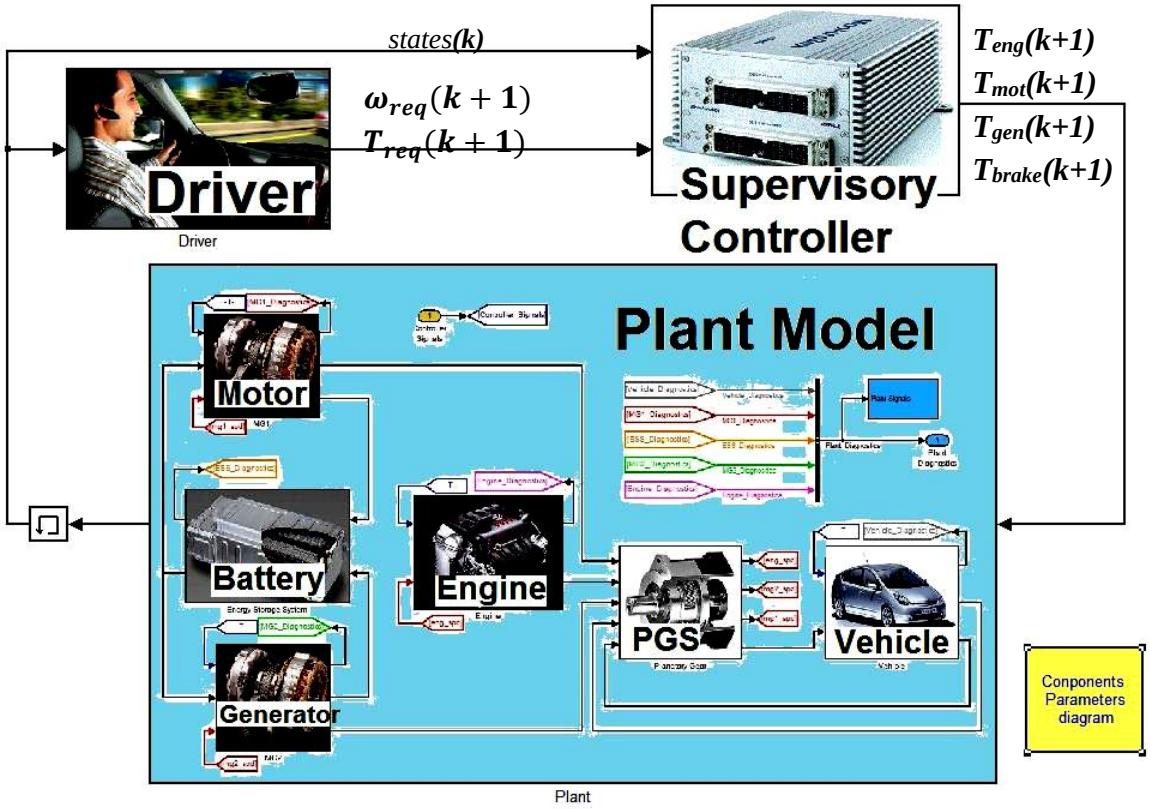

Fig 11. Topology of the simulation model in Simulink.

2.1.6 Rule-Based Control for HEV

The most common way of implementing supervisory control in a hybrid electric vehicle is to introduce a set of rules that, given the observed values of some meaningful parameters, decide the power split between the engine and the energy storage device. Unlike techniques based on optimal control or equivalent consumption minimization, rule-based control does not rely on formal (ODE) models and formal description of the problem. Instead, the rules are based on engineering intuition: the objective is to make each element of the powertrain work in high-efficiency conditions, and to recuperate as much energy as possible from regenerative braking. A simple rule structure looks like the one shown in Fig 12. The rules are usually in the form if-then-else, and efficiency maps or fuzzy-logic methods may be used in the implementation.

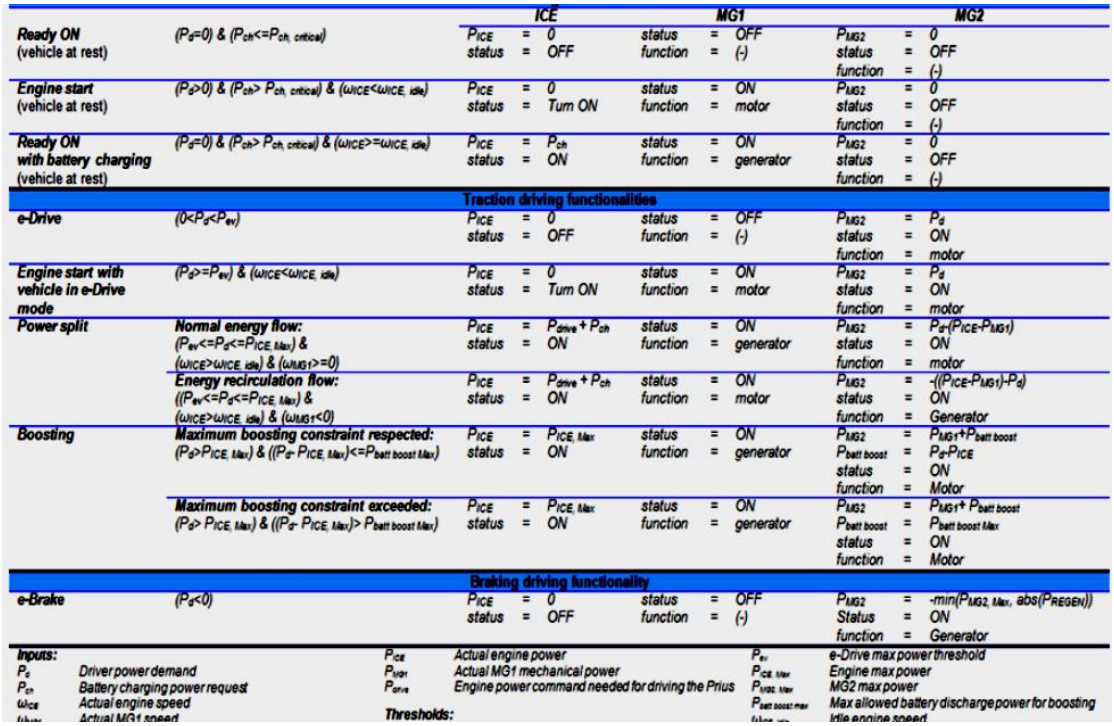

Fig 12. A sample of a rule-based control strategy for Prius HEV.

Since rule-based controllers are based only on instantaneous conditions, it is very easy to take into account the local constraints (i.e., limitations on power, torque, speed etc). On the other hand, it is impossible to formally guarantee the optimality of the solution and the respect of the integral constraints, for example the charge-sustainability: in this case, the rules can only force a given integral measure (typically the state of charge) to remain between two limits. The parameters of the rule-based controller (e.g. the threshold values that decide when to switch from a mode to another) are usually obtained through calibration based on modeling and simulation of the powertrain, possibly using optimization techniques. Optimal control results such as those described later (especially dynamic programming) can be used to benchmark or validate the effectiveness of the strategy or as a guideline to determine the control rules.

The main advantage of rule-based control is its conceptual simplicity and the ease of implementation on running vehicles. The rules can be made as complex and detailed as needed and (in principle) can take care of any special event that may affect the

vehicle, thus incorporating "limp-mode" capabilities in the supervisory control itself.

The main disadvantages are the lack of proof of optimality, and the fact that there is no standard methodology for synthesizing the rules (i.e., the rules are decided on a case-by-case basis but there is no way to determine a priori that a given set of rules is appropriate for a given application). Also, the presence of many thresholds and parameters makes it quite difficult to obtain an appropriate calibration that works for a wide variety of driving conditions.

Nonetheless, rule based strategies are widely used in production environment, possibly in conjunction with other algorithms based on optimal control. For example, it may be possible to implement effectively ECMS only in a part of the vehicle operating range, using the rule-based controller for the remaining conditions.

2.2 Optimal Control Problem Formulation for HEV

The goal of this project is to find an optimal control that minimizes the fuel consumption for a power-split HEV. In order to be able to use typical optimization tools, such as Dynamic Programming or Pontryagin's Minimum Principle, the problem must be first formulated mathematically in a suitable form.

A general mathematical formulation of such an optimal control problem with fixed final time t_f is described as follows. Consider a system described by the generic state equation

$$\dot{\mathbf{x}} = f(\mathbf{x}, \mathbf{u}, t) \tag{15}$$

where $\mathbf{x}$ is the state vector, $\mathbf{u}$ the control vector, t the time. Consider the optimal control problem of finding the sequence of controls $\mathbf{u}^*(t)$ that minimizes the cost function in the Bolza form:

$$J = E(\mathbf{x}(t_f), t_f) + \int_{t_0}^{t_f} L(\mathbf{x}(t), \mathbf{u}(t), t)dt$$

$$s.t. \begin{cases} \dot{\mathbf{x}}(t) = f(\mathbf{x}(t), \mathbf{u}(t), t) \\ 0 = g(\mathbf{x}(t), \mathbf{u}(t), t) \\ \mathbf{x}(t_0) = \mathbf{x}_0 \\ \mathbf{u}_{\min} \le \mathbf{u} \le \mathbf{u}_{\max} \\ \mathbf{x}_{\min} \le \mathbf{x} \le \mathbf{x}_{\max} \end{cases} \quad (16)$$

where *L(x(t),u(t),t)* is the Lagrangian or running cost subject to control and state constraints, as well as prescribed initial conditions on the system state. For HEV, it's also required that $x(t_f) = x_f$, which makes the problem become a fixed terminal-time and fixed terminal-state optimal control problem.

In the following sections, the generic optimal control problem introduced above is explicitly written for a charge-sustaining HEV.

2.2.1 Original Optimal Control Problem

For a charge-sustaining HEV, the objective in this work is to minimize the overall fuel consumption over a time horizon, which is the time integral of the fuel rate at each time step, while satisfying the following general rules:

- The driver's demand/power request for acceleration and deceleration needs to be satisfied (i.e. ω_{req} and T_{req} need to be met) whenever possible and optimality is sacrificed if the power request is not met.
- All component constraints such as rotational speed and torque limit (as shown in Fig 8, Fig 9 and Fig 10) need to be met.
- The trajectory of battery state of charge (SOC) must be maintained within a pre-defined range with SOC at the end of the trajectory equal to the start point.
- Normal friction brake is used only if the engine and motor/generator cannot provide all the commanded negative torque.

The objective function is defined as follows:

$$\min\left\{J=\int_{t_0}^{t_f}\dot{m}_{fc}(t)dt=\int_{t_0}^{t_f}L(\omega_{eng}(t),T_{eng}(t))dt\right\} \tag{17}$$

$$subject\quad to:$$

$$\begin{cases}
\dfrac{dSOC(t)}{dt}=f(P_{bat}(\mathrm{t}))=-\dfrac{1}{C_{bat}}\cdot\dfrac{V_{oc}-\sqrt{V_{oc}^2-4R_{in}P_{bat}(t)}}{2R_{in}}; & (17.a)\\
\dfrac{d\omega_{eng}(t)}{dt}=f(T_{eng}(\mathrm{t}),T_{mot}(\mathrm{t}),T_{gen}(\mathrm{t})); & (17.b)\\
SOC(t_0)=SOC(t_f) & (17.c)\\
SOC_{\min}\le SOC(t)\le SOC_{\max} & (17.d)\\
P_{bat_\min}\le P_{bat}(t)\le P_{bat_\min} & (17.e)\\
T_{eng_\min}(\omega_{eng}(t))\le T_{eng}(t)\le T_{eng_\max}(\omega_e(t)) & (17.f)\\
\omega_{eng_\min}\le\omega_{eng}(t)\le\omega_{eng_\max} & (17.g)\\
T_{gen_\min}(\omega_{gen}(t))\le T_{gen}(t)\le T_{gen_\max}(\omega_{gen}(t)) & (17.h)\\
\omega_{gen_\min}\le\omega_{gen}(t)\le\omega_{gen_\max} & (17.i)\\
T_{mot_\min}(\omega_{mot}(t))\le T_{mot}(t)\le T_{mot_\max}(\omega_{mot}(t)) & (17.j)\\
\omega_{mot_\min}\le\omega_{mot}(t)\le\omega_{mot_\max} & (17.k)
\end{cases}$$

where $\dot{m}_{fc}(t)$ is the rate of fuel consumption of the engine, which is a function of engine speed and torque. The battery power P_{bat} is bound-constrained, due to the battery charge/discharge power limit. The torques and speeds of engine, generator and motor are restricted by each component's capability such as the maximum speed or the maximum torque, which are time varying.

For charge-sustaining HEV, the initial battery state of charge $SOC(t_0)$ needs to be equal to the end point $SOC(t_f)$, where $SOC(t_0)$ is set to 0.7 in this study and $SOC(t)$ is determined according to the dynamic battery model equation described in (13).

Moreover, to ensure the torque and speed demand can be met at each time step, powertrain dynamics (17.b) needs to be satisfied according to (4), where the motor speed is restricted by (9) and T_{req} is calculated by (8).

Instead of minimizing the fuel use only, the cost function can also be a weighted sum of the fuel use and the exhaust emissions as follows:

$$J = \int_{t_0}^{t_f} [w_1 \dot{m}_{fc}(t) + w_2 CO_2(t) + w_3 HC(t) + w_4 CO(t) + w_5 NO_x(t)]dt \qquad (18)$$

where w_i are the weighting factors.

2.2.2 Simplification of the Original Optimization Problem

Since the fuel rate map is nonlinear and the original problem involves too many control variables and states, which is hard to deal with when considering solving the objective function over the whole driving cycle, the original problem is reduced to a single-variable minimization problem in terms of battery power P_{bat}, subject to *SOC* dynamic equition (13) and the P_{bat} boundary constraint at each time step.

The general idea is to limit engine operating region to those points along its fuel minimum line. To deal with constraints, those points violating boundary conditions are eliminated.

The detailed variable reduction procedures are described as follows.

Step 1. Determine the engine operating point

Since there're only two power source for this powertrain, the engine power can be approximated as the difference of the current power demand P_d and the battery power P_{bat}. Thus, an engine power vector is generated first as follows:

$$P_{eng}(i,t) = \begin{cases} P_d(t) - P_{bat}(i,t) & if\ P_d(t) \geq 0 \text{ (propelling mode)} \\ 0 & if\ P_d(t) < 0 \text{ (braking mode)} \end{cases} \qquad (19)$$

where P_d is calculated by:

$$P_d = \omega_{req} \cdot T_{req} \qquad (20)$$

For each engine power, the engine operating points are determined by using the power-specific engine fuel minimum line as shown in Fig 8, which can be calculated off-line and stored as a static map for online implementation. Specifically, engine speed and torque are determined at each time step as follows:

$$\omega_{eng}(t)=\begin{cases} f_{\min\_fuel\_line}(P_{eng}(t)), & if\ P_{eng}(t)\geq P_{eng\_on\_min}\ (\text{engine ON}) \\ \omega_{eng\_lb}(t), & if\ P_{eng}(t)<P_{eng\_on\_min}\ (\text{engine OFF}) \end{cases} \quad (21)$$

$$T_{eng}(t)=\begin{cases} P_{eng}(t)/\omega_{eng}(t), & if\ P_{eng}(t)\geq P_{eng\_on\_min}\ (\text{engine ON}) \\ 0, & if\ P_{eng}(t)<P_{eng\_on\_min}\ (\text{engine OFF}) \end{cases} \quad (22)$$

where $P_{eng\_on\_min}$, the minimum engine power for engine to be turned on, is set to 1kW in this study. Engine is set to OFF if its power is lower than this threshold value. And the engine speed lower bound $\omega_{eng\_lb}(t)$ is calculated based on generator speed limit at each time step:

$$\omega_{eng\_lb}(t)=\max\{\ 0,\ (\omega_{gen\_lb}(t)+K\omega_{mot}(t))/(1+K)\ \} \quad (23)$$

By using (21) and (22), all the other points in the fuel map are considered inferior and thereby eliminated from the feasible region leaving only those points along the fuel minimum line need to be examined. Consequently, the fuel consumption can be calculated as a function of P_{bat} at each time step:

$$\dot{m}_{fc}(i,t)=f(P_{bat}(i,t)) \quad (24)$$

Since all the calculations in Step 1 do not vary with time, Step 1 can be prepared offline, where equation (21), (22), (24) are pre-computed into a lookup table for online use.

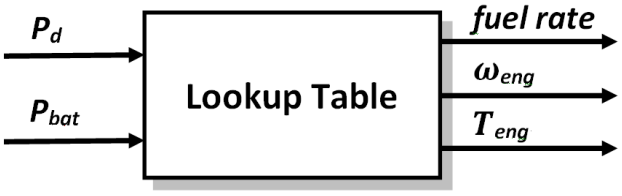

Fig 13. Pre-computed engine minimum fuel line lookup table

Step 2. Calculate the operating points for all other components

Note that the degree of freedom for control variables is two in the original problem, once the engine operating point (i.e. $\omega_{eng}(t)$ and $T_{eng}(t)$) is given, the operating

points of all other components can be obtained by following speed relationship (2) and powertrain dynamics (4). More specifically, the speed and torque of motor and generator can be calculated in a discrete-time format as shown in (25)-(27):

$$\begin{aligned} \omega_{mot}(k) &= \omega_{req}(k) = \frac{R_{fd}}{r} v_{req}(k) \\ \omega_{gen}(k) &= (1+K)\omega_{eng}(k) - K\omega_{mot}(k) \end{aligned} \tag{25}$$

$$\begin{aligned} T_{mot}(k) = & \frac{-K}{K+1} T_{eng}(k) + \frac{1}{R_{fd}} T_{req}(k) - T_{brake}(k) \\ & + J_{eng} \frac{K}{K+1} \frac{\omega_{eng}(k) - \omega_{eng}(k-1)}{T} + J_{mot} \frac{\omega_{mot}(k) - \omega_{mot}(k-1)}{T} \end{aligned} \tag{26}$$

$$\begin{aligned} T_{gen}(k) = & \frac{-1}{K+1} T_{eng}(k) + [\frac{J_{eng}}{K+1} + J_{gen}(K+1)] \frac{\omega_{eng}(k) - \omega_{eng}(k-1)}{T} \\ & - J_{gen} K \frac{\omega_{mot}(k) - \omega_{mot}(k-1)}{T} \end{aligned} \tag{27}$$

where $v_{req}(k)$ and $T_{req}(k)$ are the requested vehicle speed and torque given by the driver model. At time step k, $\omega_{eng}(k-1)$ and $\omega_{mot}(k-1)$ are assumed to be known variables, since they are the feedback states of the last time step obtainable from the plant model. Moreover, the brake torque produced by the normal friction brake $T_{brake}(k)$ is zero unless the motor cannot provide sufficient braking torque during braking, and can be calculated as follows.

$$T_{brake}(k) = T_{req}(k) - R_{fd} \cdot [T_{mot\_\max}(\omega_{mot}(k)) - J_{eq} \frac{\omega_{mot}(k) - \omega_{mot}(k-1)}{T}] \tag{28}$$

where the motor is assigned with its maximum torque $T_{mot\_\max}$ considering both maximum motor torque capacity and available battery power at speed $\omega_{mot}(k+1)$ during the case when motor alone cannot satisfy the braking request.

Step 3. Find the admissible set of the control variable $P_{bat}(k)$

Note that the $P_{bat}(k)$ in step 1 is used as the control variable, whose value is not necessarily coincident with the actual battery power value $P_{bat\_act}(k)$. To make sure that the corresponding actual battery power is within the boundary constraint, additional

examination needs to be conducted for each $P_{bat}(k)$.

Substitute (25) - (27) to (11), the actual battery power P_{bat_act} can be calculated. Accordingly, a P_{bat_act} vector corresponding to the P_{eng} vector in step 1 can be generated. Those points violating the component's boundary limits defined in (17.e) - (17.f) were eliminated. In this way, an admissible set of control variable: battery power $\{P_{bat\_feasible}(i,k)\}$ can be obtained at each time step k.

2.2.3 Simplified Optimal Control Problem

Combining Step 1 to Step 3, the original time-horizon optimization problem with multiple control variables and states can now be converted to a standard fixed final-time and fixed final-state optimal control problem with a single control variable (battery power P_{bat}) in discrete time format. The only system state is the battery state of charge *SOC*:

$$\min\left\{J=\sum_{k=1}^{N}\dot{m}_{fc}(k)=\sum_{k=1}^{N}g(P_{bat}(k))\right\} \tag{29}$$

$$\begin{cases} subject\quad to: & \\ \Delta SOC(k)=SOC(k+1)-SOC(k) & \\ \qquad\qquad =f(P_{bat}(k)) & (29.a)\\ \qquad\qquad =-\dfrac{1}{C_{bat}}\cdot\dfrac{V_{oc}-\sqrt{V_{oc}^2-4R_{in}P_{bat}(k)}}{2R_{in}} & (29.b)\\ SOC(k=N)=SOC(k=1)=0.7 & (29.c)\\ SOC_{\min}\le SOC(k)\le SOC_{\max} & (29.d)\\ P_{bat}(k)\in\{P_{bat\_feasible}(k)\} & \end{cases}$$

Comparing to the original problem in (17), only P_{bat} needs to be decided to solve the optimal control problem. At the same time, the optimal P_{bat} gives the optimal engine operating points. State variable SOC is subject to dynamic constraint (29.a), initial and global constraint (29.b) and instantaneous boundary constraint (29.c). Control variable P_{bat} also needs to stay in its feasible range by (29.d). Note: this P_{bat} feasible range is a result from all components boundary limits defined in (17.e) - (17.f), and can be

obtained by following step 3 in Section 2.3.2.

2.3 Accurate Off-line Solution of the HEV Optimal Control Problem

To solve the optimal control problem defined in (29), essentially to find the optimal trajectory of battery power P_{bat} that leads to minimum fuel consumption, offline approaches, which need to have the full knowledge of the given driving cycle in advance, are used first. These offline approaches can give the global optima (the optimal vehicle operating trajectory) over the whole driving cycle time span, instead of finding local optima at an instantaneous time step. Although offline approaches are not practically implementable due to their non-causal nature and computational burden, they serve as good theoretical benchmarks and rule extraction reference for online control strategies.

In this section, two offline approaches for solving the formulated optimization problem using Dynamic Programming (DP) and Quadratic Programming (QP) algorithms are derived respectively.

DP is the only optimal control technique capable of providing the accurate solution to the HEV optimal control problems using the complex model, considering all possible variations over the entire trip. It essentially searches all the possible solutions (in this case it refers to all possible vehicle operating trajectories from the start to the end of the trip) of an optimization problem and identifies the global optimum (the optimal trajectory). However, it requires extensive computation time. In contrast, QP provides fast computation time at the cost of optimality of the resulting trajectory, since it essentially derives a closed-formed optimal solution based on quadratic approximation of the problem which calculates much faster while also introduces inaccuracy.

2.3.1 DP Solution

The optimal control problem formulated in (29) can be seen as a multi-step decision problem: at each time instant, one has to decide the value of the control variable *u(k)*, such that for the next time interval the smallest objective value will be achieved over a certain trajectory, while satisfying the constraints.

In this section, deterministic dynamic programming algorithm, which throughout this thesis is referred to as dynamic programming (DP), is used to solve this multistage decision-making problems. The DP algorithm determines the optimal node (control variable P_{bat}) combination between the initial and final state. DP is commonly used for global optimization of the energy management problem of hybrid electric vehicles[14, 16, 31, 48]. This algorithm is based on Bellman's principle of optimality. More details can be found in [19]. In addition to serving as benchmark, DP has also been used to help developing rule-based controller by analyzing and extracting implementable rules from the DP resulting strategy[14, 18].

DP argues that the problem can be solved by recursively solving Bellman's equations to find time consistent policy functions, *i.e.*, to find the optimal sequence of control variables $u^*(k)$ along the time horizon that minimizes the cumulative cost function: $J = \sum_{k=1}^{N} L(x(k), u(k), k)$, and at the same time brings a dynamic system whose state evolves according to given equation: $x(k+1) = f(x(k), u(k), k)$. For problem (29), we take battery power $P_{bat}(k)$ as the control variable $u(k)$ and battery state of charge $SOC(k)$ as state variable $x(k)$. Note that $x(k)$ and $u(k)$ are also subjects to constraints (29.b) to (29.d).

To solve the problem, the operating space of state variable SOC is discretized, making a grid as shown in Fig 14, and DP essentially searches and evaluates all

possible trajectories within this SOC grid and finds the optimal one.

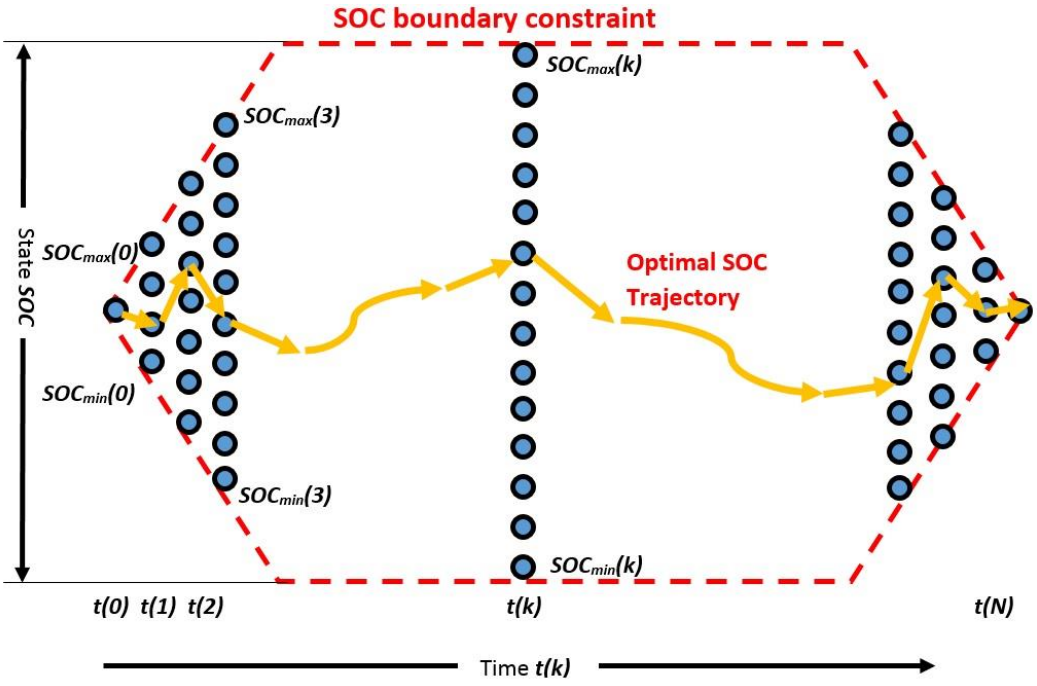

Fig 14. DP grid of the state variable SOC

In this work, DP is implemented by using MATLAB M-script. A backward-looking vehicle model is coded according to the dynamic model described in Section 2.1 and the same variable reduction procedures as presented in Section 2.2.2 are used so that the comparison between DP and other online or offline algorithms is fair. Simulation results can be found in Section 2.7.

The detailed procedures to implement the DP algorithm for Prius HEV are summarized as follows:

1) Initialize the grid matrices for state *SOC*, cost-to-go and other variables (P_{bat}, ω_{eng}, T_{eng}, ω_{mot}, T_{mot}, ω_{gen}, T_{gen} and etc.). Each matrix is of the size *M-by-N*, where *M* corresponds to the number of SOC grid [SOC_{min},…,SOC_{max}], and *N* corresponds to the length of the driving cycle.

2) Define the boundary of the SOC grid as shown in Fig 14, which can be calculated based on maximum and minimum charging and discharging limit of

the battery, as well as the SOC constraint (29.b) and (29.c).

3) The whole DP calculation process starts from the initial node *t(k=1)*, and goes towards the final node *t(k=N)*. At each time step *t=k*, calculation is conducted for each node *i=1* to *i=M*. For each node i at each time instant *t(k)*, find the route that gives minimum cost-to-go from all possible nodes in the previous time instant *t(k-1)*. The cost-to-go is calculated as $J = \sum_{t=0}^{t=k} \dot{m}_{fc}(t) = \sum_{t=0}^{t=k} g(P_{bat}(t))$, where the current optimal fuel consumption is summed to the optimal cumulative consumption over the preceding time step, so that the least total consumption can be obtained from all subsequent time steps. Calculate all the other variables (ω_{eng}, T_{eng}, ω_{mot}, T_{mot}, ω_{gen}, T_{gen} and etc.).

4) Record all the variables in their corresponding grid matrix. Note that if there are any variables violating the constraints, the corresponding node point in the grid matrix will be set to *NaN*.

5) Repeat the same calculation procedure until the end of the route is reached at *t(k=N)*.

6) After establishing the forward calculation of the nodes in the cost-to-go matrix, the DP algorithm proceeds backward from t(k=N) to t(k=0), by tracking the route that gives SOC(t(N))=0.7. The consequent recorded route from the previous forward calculation will be the optimal node combination between t(k=0) and t(k=N). The associated powertrain decision commands can also be obtained from previously recorded grid matrix.

Since DP is very time-consuming, several techniques have been taken in this work to speed up the simulation:

- Parallel computing: MATLAB lets you solve computationally and data-

intensive problems using multicore processors, GPUs, and computer clusters. By using constructs such as parallel for-loops (*parfor*) and special array types for distributed processing and for GPU computing, the computation time has been decreased for about 2-3 times on a 4-core computer.

- Vectorization: Since MATLAB is optimized for operations involving matrices and vectors, vectorizing the variables instead of using loop-based, scalar-oriented code improves the computation speed dramatically.

Although DP guarantees overall optimal solution, it is not practically implementable in real-time due to several disadvantages:

- The driving cycle needs to be known in advance.
- The generated rules cannot adapt to another route.
- DP is prone to 'curse of dimension': The computation burden grows exponentially with the increase of control input variables and the size of the grid.
- The DP generated rules cannot avoid frequent engine ON/OFF behavior.

Nevertheless, DP serves as a benchmark for other control strategies to compare with since it provides the 'best' performance that a control system can achieve and as a good rule extraction reference for online control strategies.

2.3.2 QP Solution

Let's recall the discrete-time optimal control problem formulated in (29), which is nonlinear and can be solved by nonlinear problem solvers, such as DP described in the last section. Due to the low computation efficiency of DP, the nonlinear optimization problem is approximated to a convex QP problem here, which improves the computation speed significantly and gives the global optimal solution with all

constraints satisfied at the cost of less optimality since quadratic approximation introduces inaccuracy into the model.

If we define the state variable as $x(k) = SOC(k)$ and the control input as $u(k) = f(P_{bat}(k))$ which satisfies:

$$u(k) = -\frac{1}{C_{bat}} \cdot \frac{V_{oc} - \sqrt{V_{oc}^2 - 4R_{in}P_{bat}(k)}}{2R_{in}} \tag{30}$$

From constraint (29.a), we have:

$$u(k) = x(k+1) - x(k) \tag{31}$$

Since:

$$\begin{aligned} u(1) &= x(2) - x(1) \\ u(2) &= x(3) - x(2) \\ &\vdots \\ u(N) &= x(N+1) - x(N) \end{aligned} \tag{32}$$

and from constraint (29.b) we have:

$$x(1) = x(N+1) \tag{33}$$

The sum of all equations in (32) along with equation (33) implies the following linear equality constraint enforcing on the control input $\mathbf{u} = [u(1), u(2), ..., u(N)]$:

$$\mathbf{c}^T\mathbf{u} = u(1) + u(2) + \cdots + u(N) = 0 \tag{34}$$

where $\mathbf{c} = \begin{bmatrix} 1 & 1 & \cdots & 1 \end{bmatrix}^T$.

From (30) and constraint (29.d), we have:

$$P_{bat\_\min}(k) \le P_{bat}(k) = \frac{V_{oc}^2 - (2C_{bat} \cdot u(k) + V_{oc})^2}{4R_{in}} \le P_{bat\_\max}(k) \quad for \quad k = 1, 2 \cdots N \tag{35}$$

Note the battery power boundary $P_{bat\_\min}(k)$ and $P_{bat\_\max}(k)$ are varied with time, which are depending on the feasible set $\{P_{bat\_feasible}(k)\}$ determined by Step 2 described in Section 2.2.2. The inequality constraint (35) can be converted to:

$$\begin{aligned} u(k) &\ge \frac{\sqrt{V_{oc}^2 - 4R_{in}P_{bat\_\max}(k)} - V_{oc}}{2C_{bat}R_{in}} \\ -u(k) &\ge -\frac{\sqrt{V_{oc}^2 - 4R_{in}P_{bat\_\min}(k)} - V_{oc}}{2C_{bat}R_{in}} \\ & for \quad k = 1, 2 \cdots N \end{aligned} \tag{36}$$

From constraint (29.c) and since the initial SOC $x(1) = 0.7$, we have:

$$\begin{aligned} SOC_{\min} &\le x(2) = u(1) + x(1) \le SOC_{\max} \\ SOC_{\min} &\le x(3) = u(2) + x(2) = u(2) + u(1) + x(1) \le SOC_{\max} \\ &\vdots \\ SOC_{\min} &\le x(N+1) = u(N) + x(N) \\ &= u(N) + u(N+1) + \cdots + u(1) + x(1) \le SOC_{\max} \end{aligned}$$

which implies that:

$$\begin{aligned} u(1) &\ge SOC_{\min} - x(1) \\ -u(1) &\ge -(SOC_{\max} - x(1)) \\ u(1) + u(2) &\ge SOC_{\min} - x(1) \\ -u(1) - u(2) &\ge -(SOC_{\max} - x(1)) \\ &\vdots \\ u(1) + u(2) + \cdots + u(N) &\ge SOC_{\min} - x(1) \\ -u(1) - u(2) - \cdots - u(N) &\ge -(SOC_{\max} - x(1)) \end{aligned} \tag{37}$$

Constraints (36) and (37) can be expressed as the following linear inequality constraints:

$$\mathbf{Au} \ge \mathbf{b} \tag{38}$$

where **A** is a *4N-by-N* constant matrix, and **b** is a 4N-by-1 vector. The elements of **A**

and **b** are given in Appendix 0.

Note that for vector **b**, at time step *k*, part of its components are not known at the current time step *k*, since battery power boundary $P_{bat\_\min}(k+1), P_{bat\_\min}(k+2), ..., P_{bat\_\min}(N)$ and $P_{bat\_\max}(k+1), P_{bat\_\max}(k+2), ..., P_{bat\_\max}(N)$ are related to the future driving cycle information. Nevertheless, in the case of off-line control, where the whole driving cycle is known in advance, battery power boundary at each time step can be calculated and vector **b** in (38) is treated as a known constant vector.

Furthermore, for steady state, equation (24) is found to be an almost linear function of battery power $P_{bat}(k)$. Fig 15 shows the simulation result of minimum fuel rate versus $P_{bat}(k)$. In this case, we can express the objective function (29) as:

$$\dot{m}_{fc}(k) = -a \cdot P_{bat}(k) + b(k) \tag{39}$$

where $a > 0$ is a constant slope which is found almost unchanged both during the same trip and under different driving cycles as shown in Fig 16, meaning that it's only related to the intrinsic property of a vehicle system.

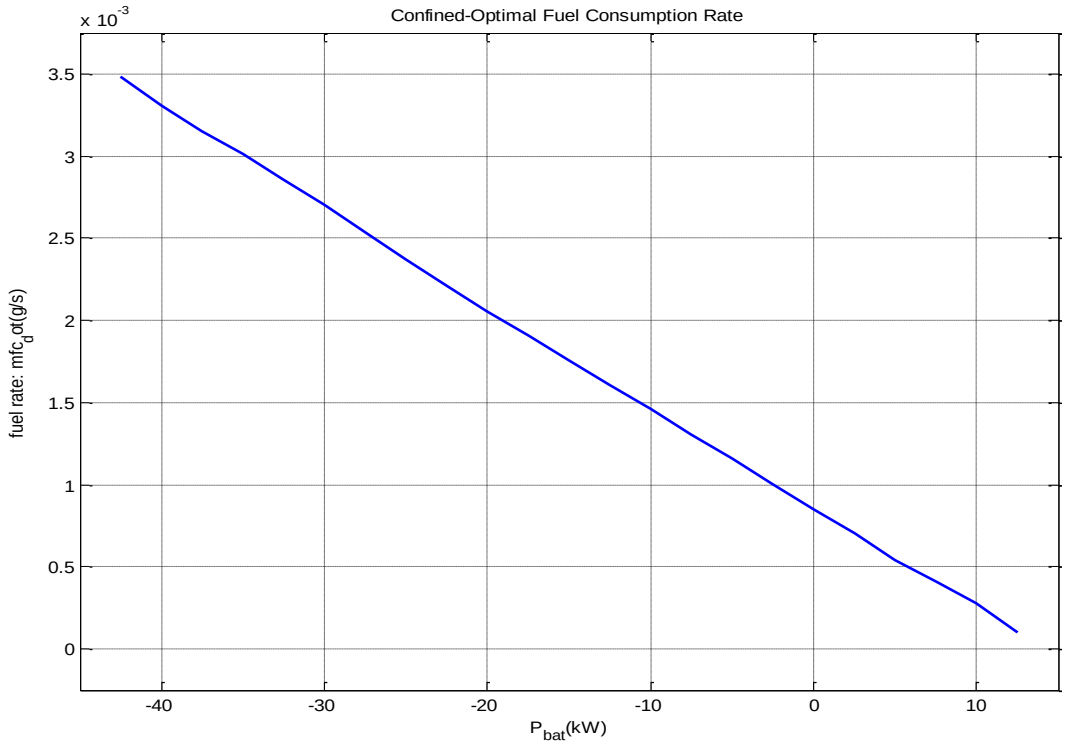

Fig 15. Minimum fuel rate vs P_{bat} at time instant t=330s of US06.

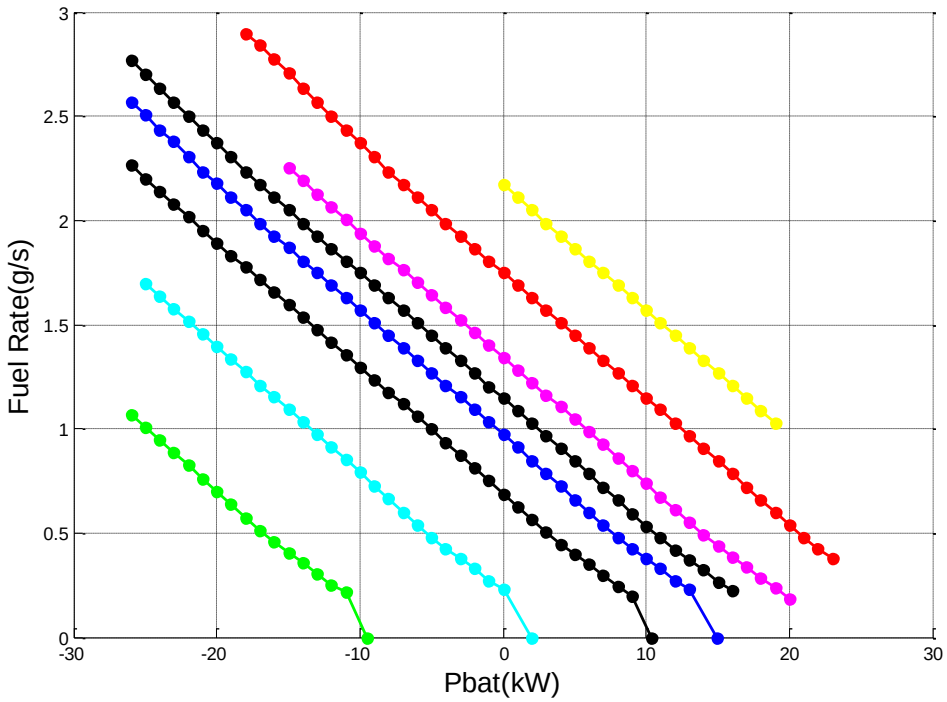

Fig 16. Minimum fuel rate vs Pbat at different time instant for different driving cycles.

Substituting (39) into the objective function (29), we have:

$$\begin{aligned} J = \sum_{k=1}^{N} \dot{m}_{fc}(k) &= \sum_{k=1}^{N} (a \cdot \frac{V_{oc}^2 - (2C_{bat} \cdot u(k) + V_{oc})^2}{4R_{in}} + b(k)) \\ &= \sum_{k=1}^{N} (4aC_{bat}^2 R_{in}^2 \cdot u^2(k) + 4C_{bat} R_{in} V_{oc} \cdot u(k)) + const. \\ &= \frac{1}{2}\mathbf{u}^T \mathbf{H}\mathbf{u} + \mathbf{u}^T \mathbf{h} \end{aligned} \tag{40}$$

where:

$$\mathbf{u} = \begin{bmatrix} u(1) \\ u(2) \\ \vdots \\ u(N) \end{bmatrix}, \quad \mathbf{H} = \begin{bmatrix} 8aC_{bat}^2 R_{in}^2 & 0 & \cdots & 0 \\ 0 & 8aC_{bat}^2 R_{in}^2 & \ddots & \vdots \\ \vdots & \ddots & \ddots & 0 \\ 0 & \cdots & 0 & 8aC_{bat}^2 R_{in}^2 \end{bmatrix} \text{ and}$$

$$\mathbf{h} = \begin{bmatrix} 4aC_{bat} R_{in} V_{oc} \\ 4aC_{bat} R_{in} V_{oc} \\ \vdots \\ 4aC_{bat} R_{in} V_{oc} \end{bmatrix}.$$

The original time horizon optimal control problem is now converted into the following convex Quadratic Programming (QP) problem with both linear equality and linear inequality constraints:

$$\min_{\mathbf{u}} J = \sum_{k=1}^{N} \dot{m}_{fc}(k) = \frac{1}{2}\mathbf{u}^T \mathbf{H}\mathbf{u} + \mathbf{u}^T \mathbf{h} \tag{41}$$

$$\begin{aligned} \textit{subject} \quad \textit{to}: \quad & \mathbf{A}\mathbf{u} \geq \mathbf{b} \\ & \mathbf{c}^T \mathbf{u} = 0 \end{aligned}$$

where $\mathbf{H} \succ 0$.

The problem in (41) can be solved by any standard QP solver. The optimal P_{bat} vector can then be obtained by (30).

In this work, we use the open-source MATLAB based toolbox SeDuMi[49] to solve the standard convex QP problem. The algorithm is carried out in MATLAB script

environment. For fair comparison, the resulted solution points from QP solver are reimplemented in the same vehicle model used for DP and PMP. The simulation results will be shown in Section 2.7.

The limitation of using QP algorithm for offline optimal control is that QP can only be applied to driving cycles with short length, due to the fact that QP solver solves the minimization problem in (41) once for the whole cycle and the dimension of the variable, which is directly related to the cycle length, cannot be too high. Nevertheless, QP can be used for a limited prediction horizon within a Model Predictive Control (MPC) structure using a receding horizon[50]. This means that the optimization is carried out over a moving finite prediction time-horizon, where a future control sequence is calculated for fuel minimization and then only the first element of the computed control sequence is applied. The process is repeated at the next time step by moving the prediction horizon one step forward.

2.4 Online Solution of the HEV Optimal Control Problem

Although DP and QP can give global optimal results of the optimal control problem, they are not able to be implemented for online application. To develop the supervisory optimal control strategy for a HEV, essentially to solve the reduced optimal control problem formulated in (29), on-line solution based on Pontryagin's Minimum Principal (PMP) and its real-time practically implementable approach is proposed in this section.

2.4.1 PMP Solution

Let's recall the fixed terminal-time and fixed terminal-state optimal control problem defined by (15) and (16), and define the Hamiltonian function as

$$H(\mathbf{x},\mathbf{u},t) = L(\mathbf{x},\mathbf{u},t) + \boldsymbol{\lambda}^T(t) \cdot f(\mathbf{x},\mathbf{u},t) \tag{42}$$

where $\boldsymbol{\lambda}^T(t)$ is the co-state vector (essentially a Lagrange multiplier). Pontryagin's

minimum principle states that the optimal solution $\mathbf{u}^*(t)$ which minimizes the objective function (16) such that the following conditions are satisfied:

- At each time, the optimal solution of the global problem is also the solution to the instantaneous problem of minimizing the Hamiltonian function, i.e.

$$\mathbf{u}^*(t) = \arg\min_{\mathbf{u}}(H(\mathbf{x},\mathbf{u},t)) \tag{43}$$

- The co-state variable appearing in the Hamiltonian function evolves according to the Euler-Lagrange equation:

$$\dot{\boldsymbol{\lambda}}(t) = -\frac{\partial H}{\partial \mathbf{x}} = -\frac{\partial L(\mathbf{x},\mathbf{u},t)}{\partial \mathbf{x}} - \boldsymbol{\lambda}^T(t)\cdot\frac{\partial f(\mathbf{x},\mathbf{u},t)}{\partial \mathbf{x}} \tag{44}$$

Equation (43) and (44) provide the solution to the problem, under the hypothesis that the optimal control $\mathbf{u}^*(t)$ exists and is unique. The existence and uniqueness of the solution have not been proved in the general case, but are generally accepted conditions in the typical HEV case, for which [14] provided a formal proof under some mildly simplifying hypotheses (constant co-state).

While the DP approach guarantees the global optimal solution by obtaining all possible optimal trajectories from the field of optimal control, PMP, as one method of trajectory optimization, yields us necessary—but not sufficient—conditions that the absolute (i.e., global optimal) trajectory must satisfy[14].

For a charge-sustaining HEV, the battery open circuit voltage V_{oc} and internal resistance R_{in} remains almost as constants throughout the driving cycle (typically in the SOC range of 0.5 to 0.8), as can be seen in Fig 17. Under these two assumptions, the optimal control obtained by PMP can be a global optimal or at least near-global optimal control for a charge-sustaining HEV according to [14].

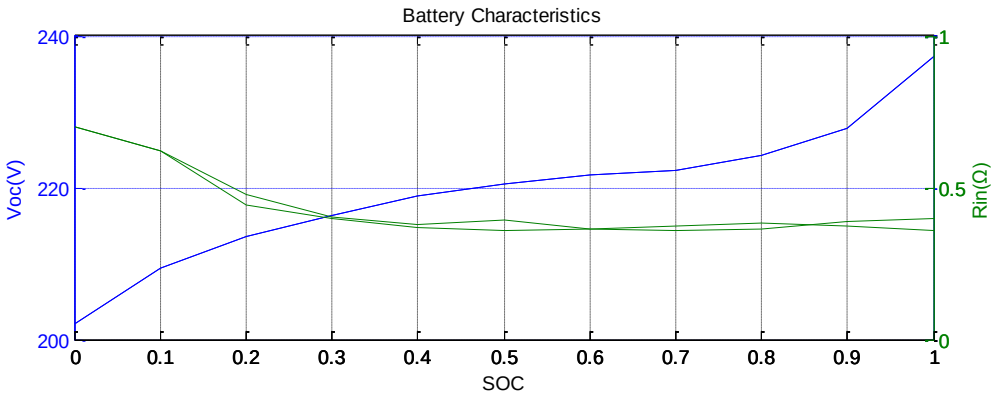

Fig 17. Battery characteristics for a Charge-Sustaining HEV

According to PMP theory, the time-horizon optimal control problem defined by (29) can be converted to a problem of instantaneous minimization of the Hamiltonian *H* defined as follows with a costate *p(k)* augmenting an P_{bat} related item with the fuel consumption:

$$\begin{aligned} H(P_{bat}(k),k) &= g(P_{bat}(k),k) + p(k)\cdot f(P_{bat}(k)) \\ &= g(P_{bat}(k),k) - p(k)\cdot\frac{V_{oc}-\sqrt{V_{oc}^2-4R_{in}P_{bat}(k)}}{2C_{bat}R_{in}} \end{aligned} \tag{45}$$

Based on (44) and the fact that V_{oc} and R_{in} are irrelevant to battery *SOC* for HEV, we also have the following:

$$\dot{p}(t) = -\frac{\partial H}{\partial SOC} = 0 \tag{46}$$

which means that the optimal costate *p(k)* can be represented as a constant throughout the driving cycle.

According to (44), the optimal $P_{bat}(k)$ is found such that the Hamiltonian $H(P_{bat}(k),k)$ is minimized at each time step, with constraint (29.d) satisfied :

$$
\begin{aligned}
&P_{bat}^{*}(k) = \arg\min(H(k)) \\
&subject \quad to: \\
&\qquad P_{bat}(k) \in \{P_{bat\_feasible}(k)\}
\end{aligned}
\tag{47}
$$

Fig 18 shows the Hamiltonian (red dot line) at time instant 200s of UDDS cycle. The Hamiltonian is convex in most of the cases as will be proved later.

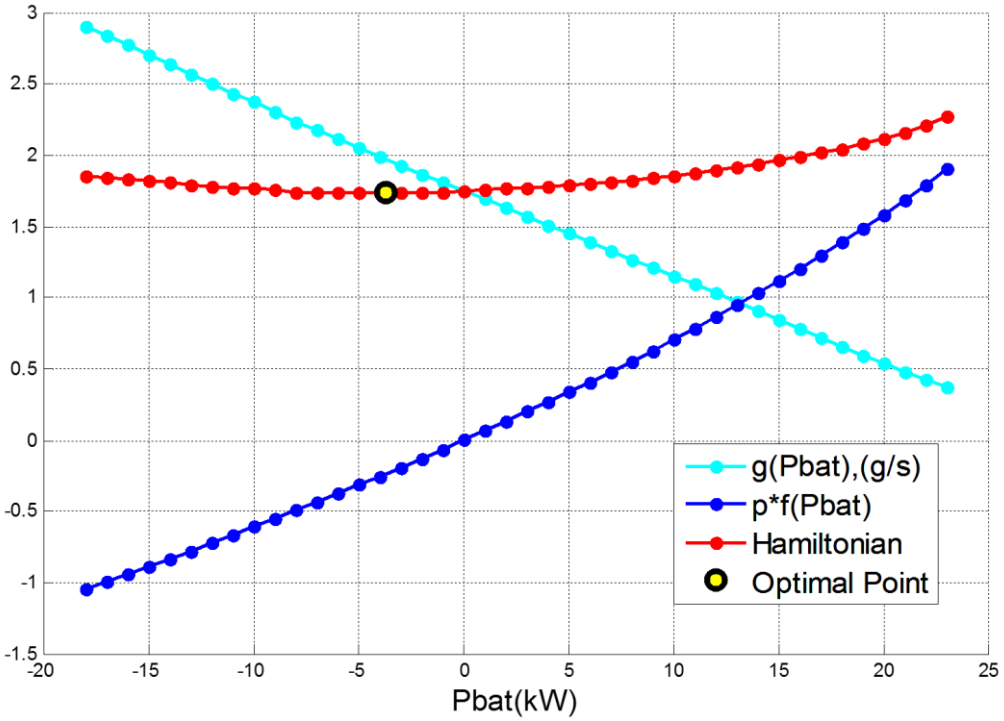

Fig 18. Hamiltonian at time instant t=200s of UDDS

If the fuel consumption curve (light blue) in Fig 18 can be approximated as a linear line as shown in (39), we can further derive the Hamiltonian as following by substitute $SOC(k+1)-SOC(k)=f(P_{bat}(k))=-\frac{1}{C_{bat}}\cdot\frac{V_{oc}-\sqrt{V_{oc}^2-4R_{in}P_{bat}(k)}}{2R_{in}}$ into (45):

$$
\begin{aligned}
H(P_{bat}) &= a\cdot P_{bat}+b-p\cdot\frac{1}{C_{bat}}\cdot\frac{V_{oc}-\sqrt{V_{oc}^2-4R_{bat}P_{bat}}}{2R_{bat}} \\
&= -aR_{in}C_{bat}^2(SOC_k-SOC_{k-1})^2+(p-aC_{bat}V_{oc})\cdot(SOC_k-SOC_{k-1})-b_k \\
&= m_1\cdot SOC_k^2+m_2\cdot SOC_k+m_3
\end{aligned}
\tag{48}
$$

where m_1, m_2 and m_3 are coefficients only related to the battery state of charge at the last time step (SOC_{k-1}), which is known at the current time step k.

From (48), we can see that the Hamiltonian in this case is a convex quadratic function with respect to the current *SOC(k)*. The vertex of this parabola is always at a costant value as shown in (49):

$$P_{bat}^{*}(k) = \frac{V_{oc}^{2} - \left(\frac{p}{aC_{bat}} \right)^{2}}{4R_{in}} = const. \tag{49}$$

Thus, with the linear approximation of the fuel consumption curve, the minimization problem in (47) becomes a simple convex quadratic problem with bounded constraint ($P_{bat\_\min}(k) \le P_{bat}(k) \le P_{bat\_\min}(k)$). The solution point will be one of the following three cases:

1) at the constant vertex point shown in (49);

2) at the $P_{bat}(k)$ boundary point for the current time step k;

3) at the pure electric point.

The above result reduces the computation time of the proposed PMP algorithm, since only three points need to be evaluated at each time step. Fig 19 shows the simulation result over US06 driving cycle, where the blue parabola curves are all the Hamiltonian functions over different time steps and the black star points are the optimal points obtained by searching minimum for the minimization problem in (47) numerically at different time steps over US06. As can be seen from Fig 19, part of the optimal points reside at a constant value; part of them are at the pure electric points (red points); the rest are at the P_{bat} boundary points.

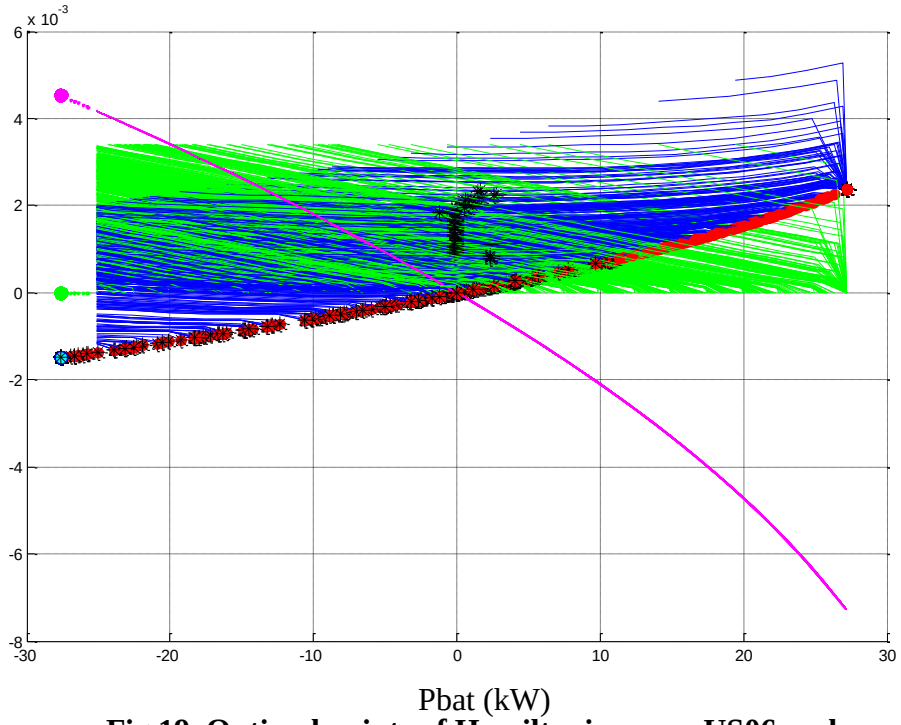

Fig 19. Optimal points of Hamiltonian over US06 cycle.

Constraint (29.b) is satisfied by tuning the value of the costate p such that $SOC(k=N)=SOC(k=1)$. The appropriate tuning of the p value is the key to ensure optimality of the resulting trajectory. In the case of HEV with constant V_{oc} and R_{in}, a constant p throughout the driving cycle is able to give the global optimal trajectory. However, for different driving cycles, the corresponding optimal p that gives initial and final SOC balance has different values.

Although the tuning of p in PMP needs the future driving cycle information, PMP computes the optimal $P_{bat}(k)$ value by Eq.(47) "dynamically"(time step by time step) in a forward-moving fashion, which gives it the potential for online(real-time) implementation.

Physical meaning of the constant costate can be interpreted as an equivalent ratio balancing fuel usage and electric energy consumption. The optimization is based on the power train operation over the total driving cycle instead of an instantaneous point, which means that the resulting energy consumption at an instant cannot be decided

separately without considering the upcoming energy consumption in the furture trip, rather it should be a trade off between the current control for a low consumption and the future undesirable high consumption event.

To take care of the state variable SOC boundary constraint (29), the cost function is modified where an additional item is added:

$$J = \sum_{k=1}^{N} \dot{m}_{fc}(k) = \sum_{k=1}^{N} \left[g(P_{bat}(k)) + \alpha \cdot \Gamma(SOC(k)) \right] \tag{50}$$

where $\Gamma(SOC(k))$ is a step function whose value is given by:

$$\Gamma(SOC(k)) = \begin{cases} 0 & \text{if } SOC_{\min} \le SOC(k) \le SOC_{\max} \\ 1 & \text{if } SOC(k) < SOC_{\min} \text{ or } SOC(k) > SOC_{\max} \end{cases} \tag{51}$$

If the battery SOC exceeds its boundary limit, the above additional item introduces extra cost, which as a result keeps the operating points away from the boundary. The value of the parameter $\alpha > 0$ is chosen such that the additional cost due to exceeding the state boundary limits can make the corresponding solution unacceptable[51], which is determined by a trial-and-error process.

Accordingly, we have the following augmented Hamiltonian function:

$$H(P_{bat}(k), k) = g(P_{bat}(k), k) + p(k) \cdot f(P_{bat}(k)) + \alpha \cdot \Gamma(SOC(k)) \tag{52}$$

Note that the introducing of the extra cost in (52) makes the costate to be discontinuous at the moment when the state variable hits its boundary limit. According to (44), the costate *p(k)* jumps when the state constraint is activated:

$$p(k+1)=\begin{cases} p(k)+\alpha & \text{at the moment when } SOC(k) \text{ hits its boundary limit (from inside out of the feasible range)} \\ p(k)-\alpha & \text{at the moment when } SOC(k) \text{ hits its boundary limit (from outside into the feasible range)} \\ p(k) & \text{elsewhere} \end{cases} \quad (53)$$

Fortunately, the costate *p(k)* never reaches beyond its boundary limits in most driving cycles for hybrid electric vehicles, which means that *p(k)* remains to be a constant in most cases. Moreover, the jump of the costate *p(k)* only occurs at the instant when it exceeds the boundary limit if happening, but it returns to its constant value once it goes back into its bounded feasible range. For example, if the costate *p(k)* hits its upper limit at time step *k*, its value jumps up to $p(k+1)=p(k)+\alpha$. Meanwhile, the additional cost in (52) is activated and so the solution point of the augmented Hamiltonian minimization problem will tend to be moved back into its bounded state feasible range, which will further cause a jump down of the costate value since $p(k+2)=p(k+1)-\alpha$.

2.4.2 On-Line (Real-Time) Practical Approach

For practical application, since the computational burden of applying PMP has been dramatically reduced due to the procedures taken in Section 2.2.2 and even more if using the convex quadratic approximation of the Hamiltonian described in Section 2.4.1, the only remaining issue is the tuning of costate *p* which relies on future cycle information. Essentially, it's impossible to achieve global optimal results for the optimal control problem presented in (29) without knowing the whole cycle information.

To overcome that, an adaptive approach based on SOC feedback is taken for practical use in this work to correct the value of *p*. A form of PI controller as shown in (54) is used as the feedback law to prevent *p* from drifting from the reference value.

$$p(k) = p_0 + K_p[SOC(k) - SOC_{ref}] + K_i \sum_{i=1}^{k} [SOC(i) - SOC_{ref}] \qquad (54)$$

where p_0 is the initial guess of the optimal costate p. K_p and K_i are the PI parameters. SOC_{ref} is the reference SOC value. The use of the PI-type SOC feedback correction in (54) takes care of the impact of both constraint (29.b) and (29.c). The adaptive costate is implemented in Simulink as shown in Fig 20.

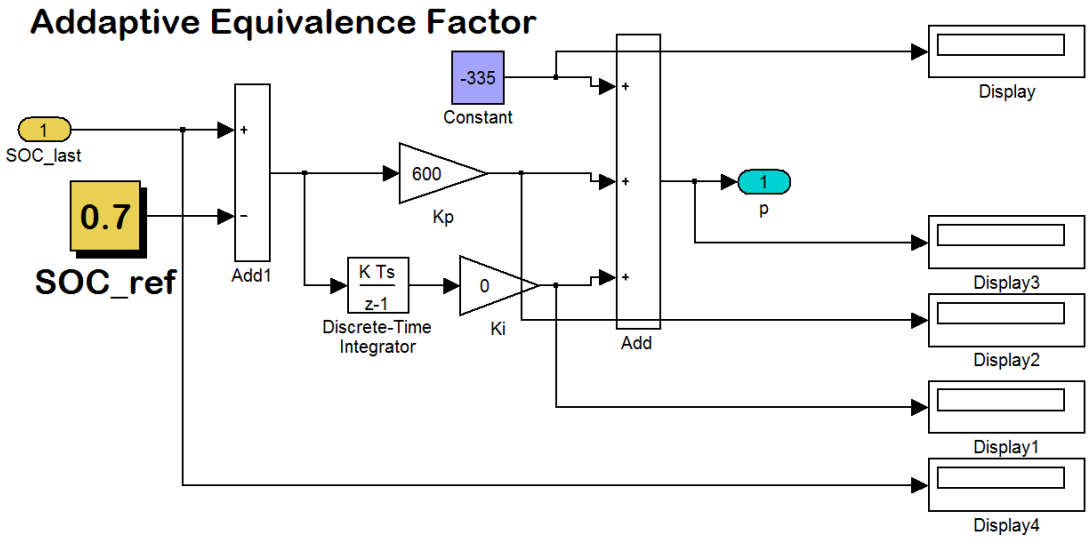

Fig 20. Adaptive costate in Simulink.

After the optimal $P_{bat}(k)$ is obtained using Eq.(47) at each time step, the corresponding engine operating point on the fuel minimum line described in the previous section is also fixed. All the other control variables are then determined based on this optimal engine operating point.

2.5 Supervisory Controller Implementation of the Proposed Optimal Control Algorithm

Using simulation models developed in a MATLAB-Simulink environment, the continuous behavior of the vehicle is approximated as a series of discrete steps. The controller inputs are the states of the vehicle at the current time step (as a feedback to

the controller) and the controller outputs are the torque requests as input to the plant model for the next time step. The topology of the forward-looking simulation model including both plant and controller model is shown in Fig 11.

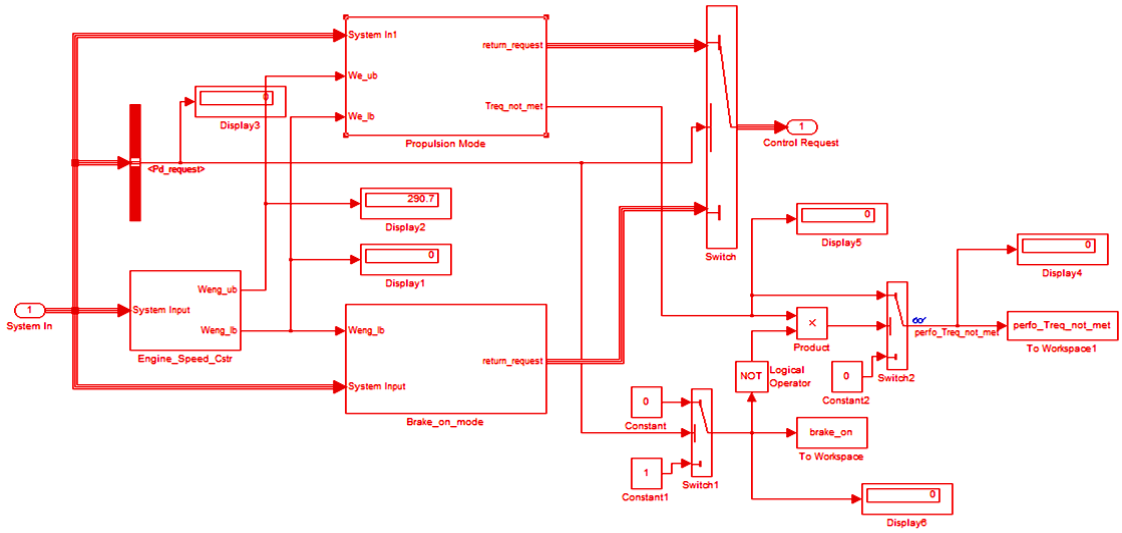

Fig 21. Supervisory controller model in MATLAB/Simulink.

The supervisory controller model is built by standard real-time compatible Simulink blocks and embedded MATLAB functions, as shown in Fig 21. The sampling time is 1s. Fig 22 shows the flow diagram of the controller logic.

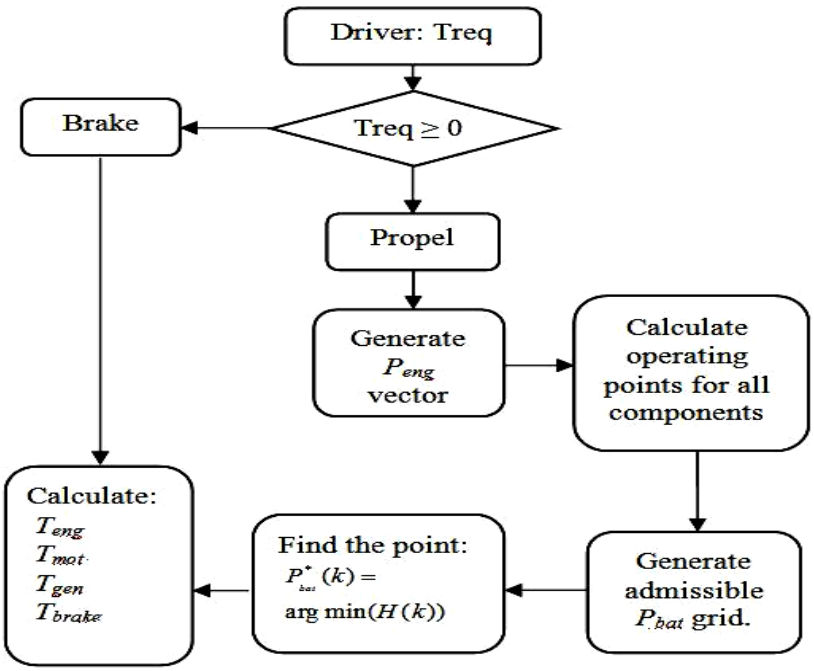

Fig 22. Flow diagram of the controller logic.

2.6 Hardware-In-the-Loop Real-time Validation of the Proposed Supervisory Control Algorithm

Ultimately, the supervisory control system will be implemented in embedded control hardware and run in real time. An efficient and effective way to test and validate the real-time performance of the embedded controller without connecting it to the "real plant" is needed.

Hardware-in-the-loop (HIL) is a powerful tool that enables a high level of controller validation even before the actual vehicle and/or components are available for testing. HIL is a technique for combining a mathematical simulation model of a system with actual physical hardware and run the simulation in real-time, such that the hardware controller performs as though it were integrated into the real system. The exact behavior of how the controller will function in the real vehicle can therefore be examined in the simulation environment. Ideally, a controller validated on a HIL system should be able to transition directly to in-vehicle testing without any modification.

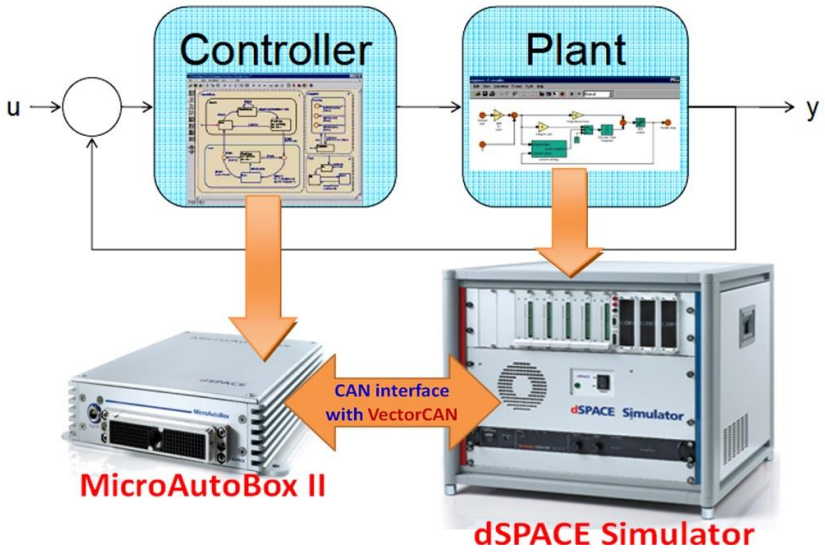

Fig 23. Hardware-in-the-loop test illustration.

In this study, rather than using an embedded ECU, we have compiled the

supervisory controller model into production C code by using MATLAB Coder™ (previously called Real Time Workshop) and downloaded the compiled code into MicroAutoBox II by using dSPACE ControlDesk software for HIL real-time test (shown in Fig 23), which is more convenient in terms of implementation for performing rapid control prototyping in fullpass and bypass scenario.

MicroAutoBox II is the 2nd generation of dSPACE's robust and compact stand-alone prototyping unit. It operates without user intervention, just like an ECU. Its comparison to other prototyping system is shown in Fig 24.

	AutoBox System	MicroAutoBox	ECU
Processor	Scalable, floating-point, high processing power	Floating-point, high processing power	Fixed-point or floating-point, target type, low processing power
Memory	Large, scalable	Large	Limited
I/O	Flexible, modular, scalable	Fixed[1)2)]	Application-specific, fixed
Signal conditioning	External, flexible, e.g. via RapidPro hardware	Built-in[2)], additional flexible signal conditioning e.g. via RapidPro hardware	Built-in, fixed, application-specific
Size	19.5 x 20 x 48 cm (7.7 x 7.9 x 18.9 in)	Small (see pp. 3-5)	Small
Operation	Stand-alone or PC	Stand-alone or PC	Stand-alone
Programming	Graphical, convenient, automatic implementation	Graphical, convenient, automatic implementation	Difficult, manual

Fig 24. Comparison between MicroAutobox with other prototyping system

At the same time, the plant model in Simulink was compiled into C code as well and downloaded to the dSPACE simulator through ControlDesk, as shown in Fig 23. The

specifications of the dSPACE mid-size simulator used in this study are shown in Table 4.

Table 4. Specifications for dSPACE Mid-Size Simulator

Processor	2.6 GHz Quad Core AMD Opteron
Memory	256 MB DDR-400
CAN channels	2 High Speed
Digital/PWM Outputs	16
Digital/PWM Inputs	38
Analog Outputs	20, 12-Bit Differential
Analog Inputs	16, 14-Bit Differential
Power Supply	33 V Max, 33 A Max, 1kW Max

Fig 25 shows the HIL test setup in the lab. A 12V power supply provides power for both the dSPACE simulator and MicroAutobox II. The MicroAutobox II communicated with the dSPACE simulator through CAN bus, which was configured by using VectorCAN software. The dSPACE real-time simulator, where the plant model is downloaded to, receives electrical signals from the hardware controller (in this case MicroAutobox II) as actuator commands to drive the plant, and converts these signals into the physical variables connected to the plant model. The plant model calculates the physical variables that represent the outputs of the plant, which are converted into electrical signals that represent the voltages produced by the sensors that feed back to the controller. All the variables in both the dSPACE simulator and MicroAutobox II can be monitored in real time through ControlDesk interface in desktop computer, as shown in Fig 25.

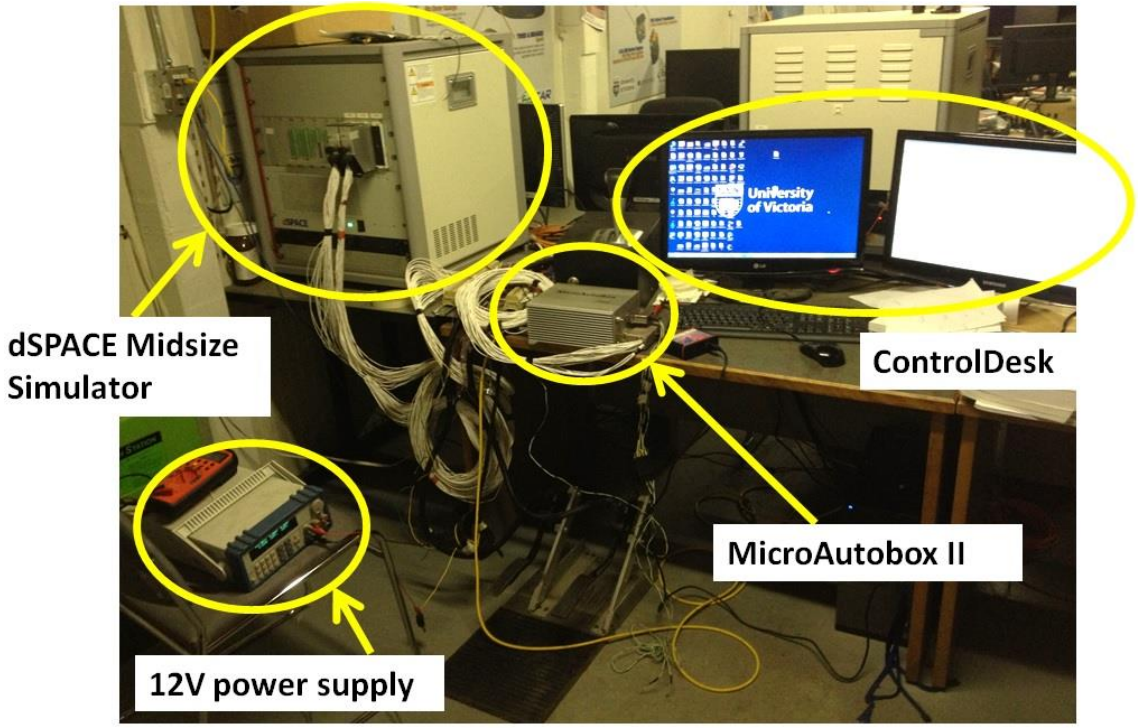

Fig 25. Hardware-in-the-loop test setup in the lab.

The HIL simulation results in ControlDesk over standard Urban Dynamometer Driving Schedule (UDDS) cycle (shown in Fig 26) shows that the proposed PMP algorithm is able to run in real time and track the predefined driving cycle very well. Close examination shows that there're slight difference between the HIL real-time simulation result and the MIL desktop non-realtime simulation result, as shown in Fig 27.

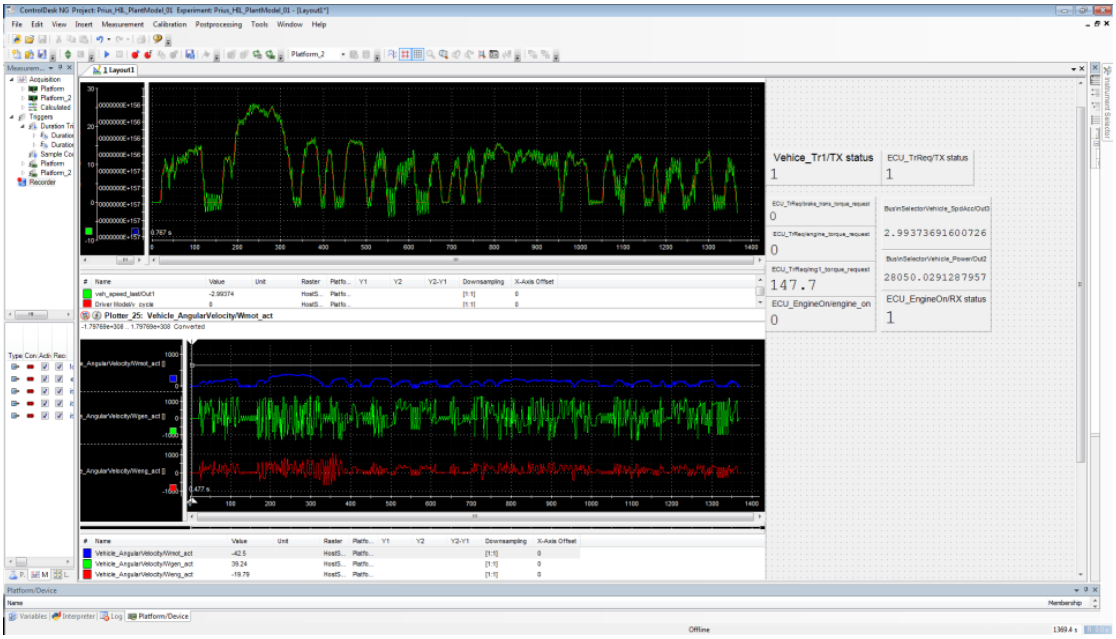

Fig 26. UDDS results in ControlDesk.

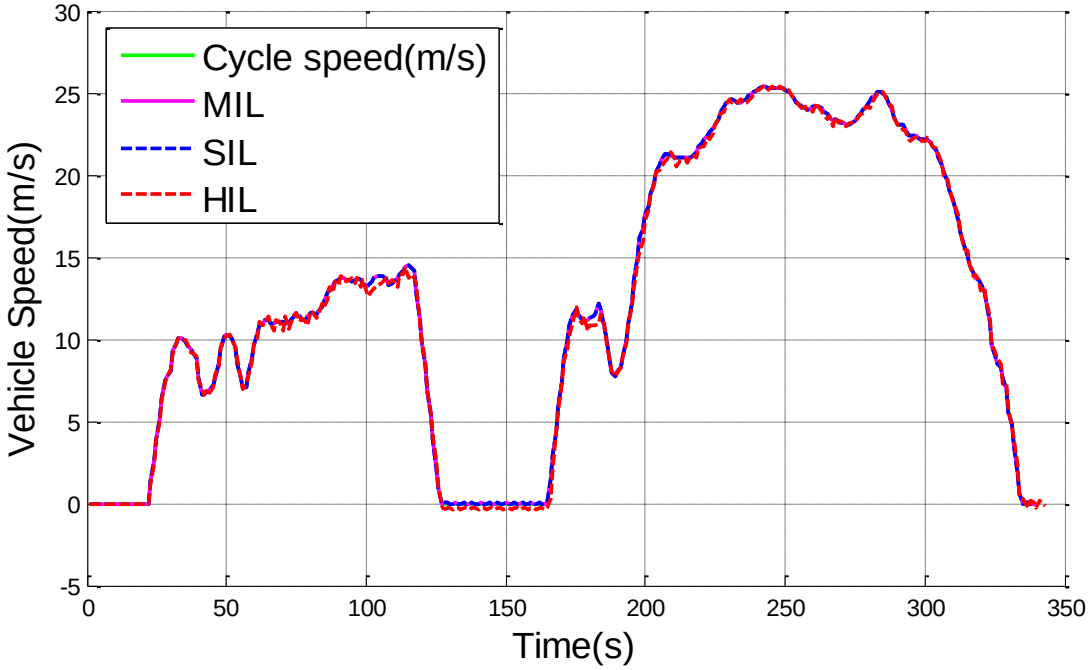

Fig 27. Comparison between desktop simulation and HIL real-time simulation result.

2.7 Results

The simulation has been carried out on several standard driving cycles (i.e., speed versus time driving schedules) to evaluate vehicle consumptions. Fig 28 shows the

speed profile of the Urban Dynamometer Driving Schedule (UDDS) cycle.

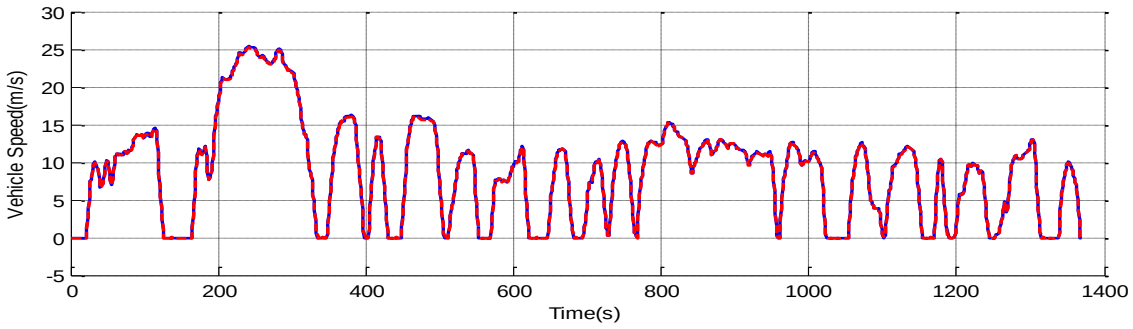

Fig 28. Vehicle speed output on the standard driving cycle (UDDS cycle).

Table 5 shows the simulation results of different control algorithms on the same UDDS cycle, where delta SOC is the difference between final SOC and the initial SOC. The initial SOC is set to 0.7. For online PMP algorithm with constant costate *p*, the value of *p* is tuned such that $SOC_{end} = SOC_{initial}$. For online PMP with adaptive costate *p*, the adaptive law in (54) was used. A rule-based controller model was developed and used as a baseline model to compare with. Fuel improvement is the percentage of fuel reduction compared to the baseline rule-based controller. Currently only the engine fuel consumption is considered in the cost function.

Table 5. Simulation results of different control algorithms for UDDS cycle

Controller*	**Fuel Economy (MPG)**	**Delta SOC**	**Fuel Improvement**	**Computation Time****
Online Rule-based	60.5153	-0.00717	(baseline)	10s
Online PMP with adaptive p	63.1692	0.60%	4.39 %	262.51s
Online PMP with constant p	64.3675	-0.06%	6.37%	275s
Offline QP	61.1419	0	1.04%	103.10s
Offline DP	65.1312	0	7.63%	22475.38s (6.24h)

* With same plant model and driver model

** On a 32GB, 4 core, 2.5GHz computer

From the results, we can see that among all the results, offline DP gives the best

fuel economy with absolute zero delta SOC, although it takes more than 6 hour to compute. Offline QP computes very fast, although the result gives worse fuel economy compared to DP even to online PMP, due to the fact that quadratic approximation in QP introduces inaccuracy. Both the online PMP algorithm with constant costate *p* and with adaptive *p* show significant improvement in fuel economy comparing to the baseline rule-based controller, and their computation time is fast enough for real time application, as validated in Section 2.6. Online PMP with constant costate p has a better fuel performance than the PMP with adaptive costate p, since the former is essentially a fine-tuned result based on a known driving cycle.

Fig 29 shows the resulted SOC trajectories for different control algorithms over the same UDDS cycle. As can be seen, the offline DP algorithm (in blue) and the online PMP with constant costate p (in green) have resulted in very close optimal SOC trajectory, while the result from online PMP with adaptive costate p (in red) is a little different from the above two.

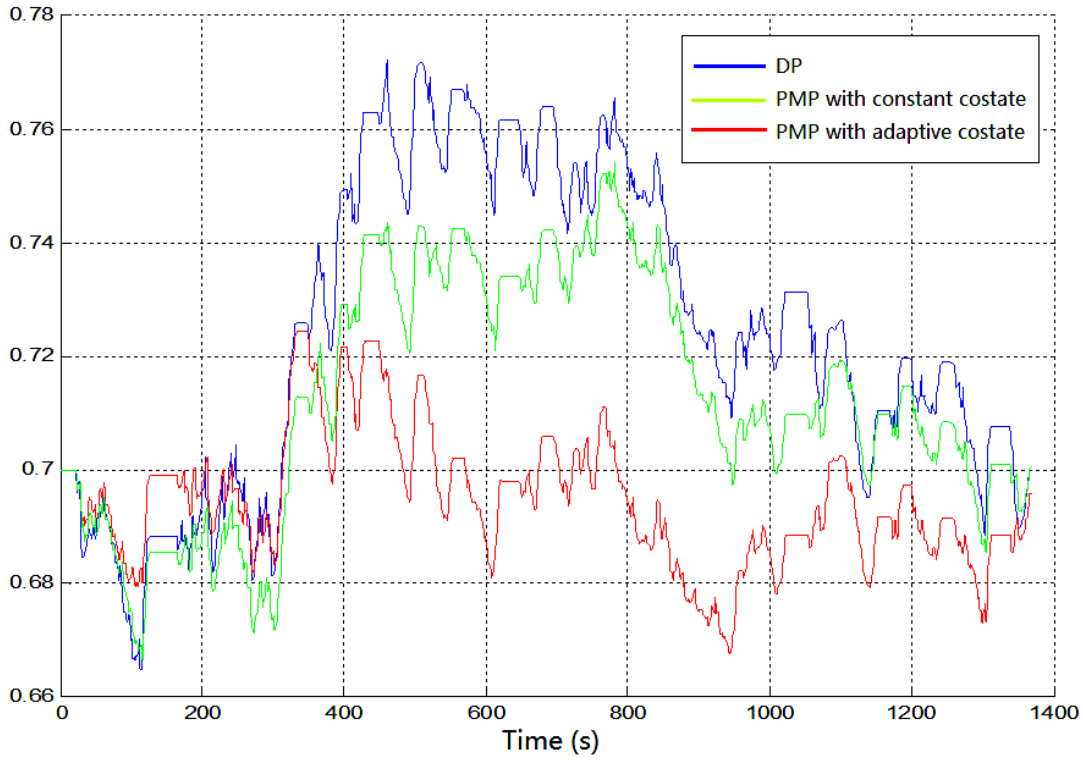

Fig 29. Resulted SOC trajectories for different control algorithm over

UDDS.

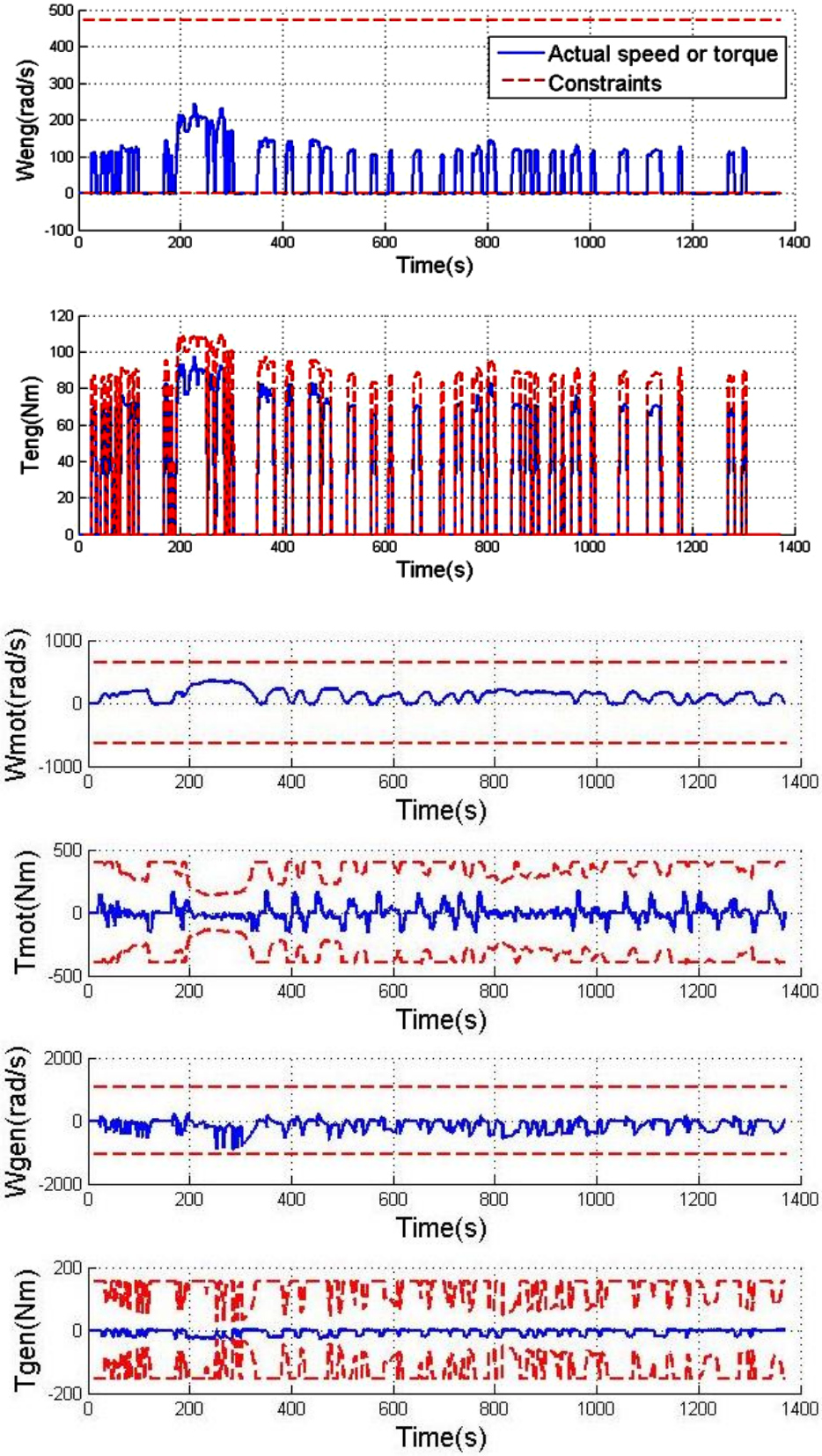

Fig 30. Simulation results on UDDS cycle.

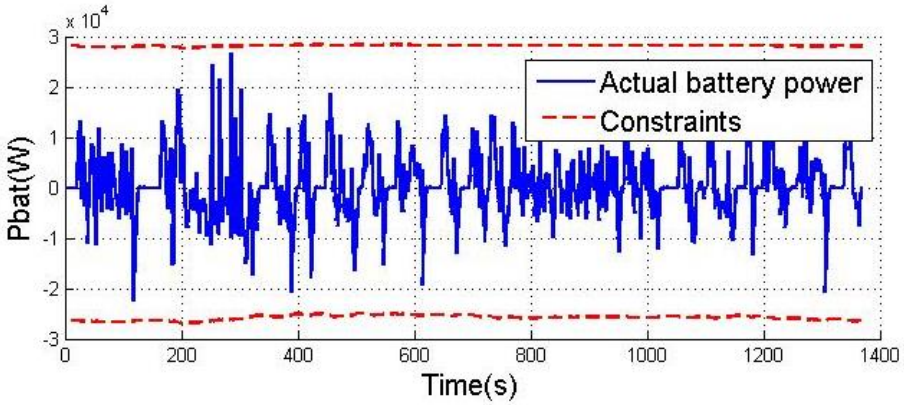

Fig 31. Battery power on UDDS cycle.

Fig 30 and Fig 31 show the results of each component's variables along with their constraints for the proposed online (real-time) implementable PMP with adaptive costate p under UDDS cycle. As can be seen, all the variables are within their constraints.

The simulation results on other different cycles are shown in Table 6. Results show that online PMP with adaptive p gives better fuel economy than the baseline rule-based control for different cycles.

Table 6. Simulation results on HWFET cycle.

	Fuel Economy (MPG)	***SOC*(t_f)**	**Improvement**
baseline	62.64	0.7080	/
online PMP with constant p	66.00	0.7054	5.36%
online PMP with adaptive p	64.51	0.7321	3%

Simulation results on US06 cycle

	Fuel Economy (MPG)	***SOC*(t_f)**	**Improvement**
baseline	40.70	0.6636	/
online PMP with constant p	43.22	0.6998	6.19%
online PMP with adaptive p	43.77	0.6647	7.54%

Simulation results on J1015 cycle

	Fuel Economy (MPG)	$SOC(t_f)$	Improvement
baseline	68.07	0.7074	/
online PMP with constant p	81.14	0.6999	19.20%
online PMP with adaptive p	76.93	0.7224	13.02%

To obtain the result in Table 6, the corresponding value of the control parameters, i.e. the costate p for the constant-costate PMP and the PI control parameters for the online adaptive PMP, are shown in Table 7. As can be seen, for the constant-costate PMP, the optimal p value for different driving cycles are very different, in which case an iterative process of tuning is needed. However, for the adaptive PMP, with the same initial guess of p_0, the algorithm works well to keep SOC from drifting from its reference value and the fuel economy results are relatively close to the solution produced by constant-costate PMP algorithm.

Table 7. Costate p for different cycles.

Cycle	ECE15	UDDS	HWFET	NEDC	J1015
Rule-Based Fuel Economy (MPG)	60.71	60.52	62.64	62.50	68.07
PMP with constant p	-342.3	-337.5	-338	-338.5	-332.5
Fuel Economy (MPG)	81.72	67.22	64.21	71.36	81.00
PMP with adaptive p	p_0 = -335, Kp = 600, Ki = 0				
Fuel Economy(MPG)	79.55	64.20	63.30	61.10	74.23

Additionally, from the simulation results, we observed that the value of costate p has an almost linear relationship with the final SOC or delta SOC, as shown in Fig 32. This linear relationship can be used to find the optimal costate p.

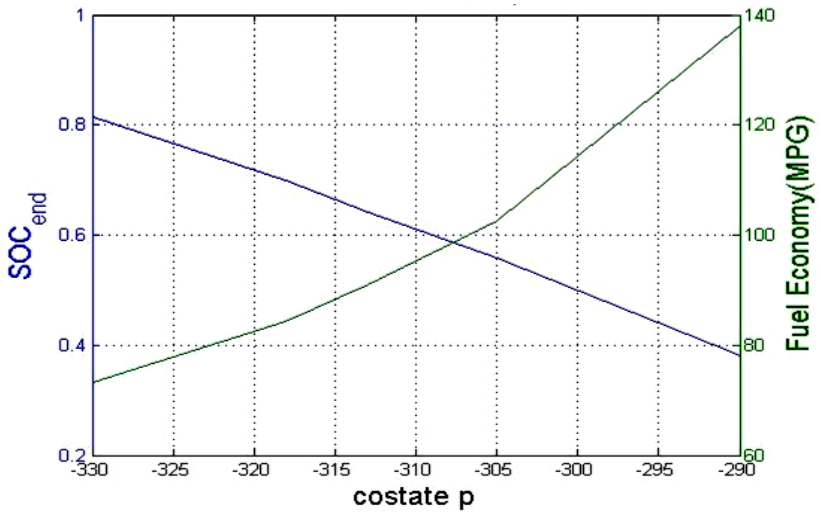

Fig 32. Optimal costate p for the same cycle.

Chapter 3. Modeling, Optimal Control and Its Real-Time Validation for PHEV: Case Study on UVic EcoCAR2 - A Multi-Regime PHEV

This chapter extends the work presented in the previous chapter on HEV to more advanced plug-in hybrid electric vehicle (PHEV) with 4WD and multi-regime capabilities. The work uses the University of Victoria (UVic) EcoCAR 2 competition and research vehicle as the research platform to carry out the study on the optimal control of advanced PHEVs.

As discussed in Chapter 1.2.4, comparing to a conventional HEV, due to the reason that most of the available electrical energy is supplied from the grid instead of on-board battery, additional challenge is introduced in the energy optimization problem for PHEV. Unlike HEV, the performance of PHEVs are significantly influenced by additional variables, such as the upstream marginal electricity generation mix, fuel choices, battery capacity and the resulting all-electric-range (AER), the consumer's interaction related information such as trip distance. These implications can be fully understood through a full cycle well-to-wheels (WTW) assessment of energy use and GHG emissions, as provided by this analysis, where the cost function was redefined for PHEV energy management. In addition, due to the complex powertrain architecture proposed by this work, additional degree of freedom in terms of control compared to the Prius HEV optimal control problem discussed in previous chapter was also introduced and handled for real time application. A few practical issues including controller integration and drivability was dealt with. Hardware-in-the-loop evaluation was also carried out to validate the proposed real-time optimal control algorithm.

3.1 Introduction of EcoCAR 2 and PHEV Design Process

EcoCAR2: Plugging into the Future was a 3-year university student competition which ran between 2011 and 2014. The program was sponsored by the U.S. Department of Energy (DOE) and administered by Argonne National Laboratory

(ANL), and is part of a longer series of Advanced Vehicle Technology Competitions (AVTCs). The competition was sponsored by a multitude of automotive industry sponsors, including General Motors (GM), dSPACE, Mathworks, among others. AVTCs enable unique research collaboration between government, industry, and university academic departments, with a focus on sustainable vehicle solutions.

EcoCAR2 had an overarching goal of reducing the overall environmental impact of a vehicle while maintaining consumer safety, performance, and comfort standards demanded by the domestic auto market. Each team integrated a custom developed plug-in hybrid electric vehicle (PHEV) powertrain into a 2013 Chevrolet Malibu. Vehicles were evaluated across multiple metrics in controlled test situations including fuel consumption, Wheel-To-Well (WTW) emissions, criteria emissions, total energy consumption, acceleration, braking, dynamic handling, ride comfort, Noise Vibration and Harshness (NVH) characteristics, and static consumer acceptability.

The 3-year vehicle development process follows a modified version (as shown in Fig 33) of the GM Vehicle Development Process (GM VDP) for advanced technology implementation. Development was broken into 3 streams (mechanical, electrical, controls) with the yearly plan objectives as follows:

Year 1: concept design and performance estimation modelling

Year 2: vehicle construction and model refinement

Year 3: vehicle refinement and controls optimization and robustness improvements

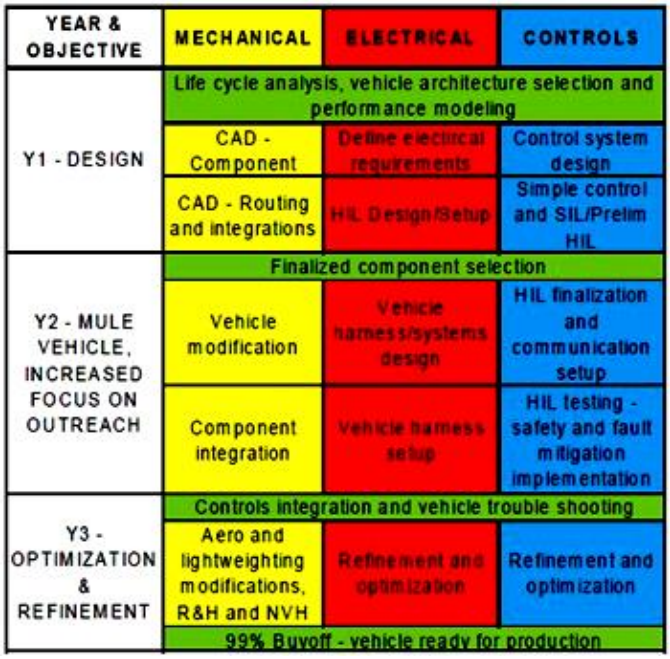

Fig 33. Three-year EcoCAR VDP

3.2 Modeling of the Proposed Multi-Regime PHEV Powertrain

3.2.1 Architecture Selection Process

A methodological process for architecture selection was employed for analyzing multiple vehicle options, which resulted in the selection of three final alternatives. The first step was a literature search, performed in order to evaluate past and current research and developments of hybrid powertrain designs and to provide a basis as to which architecture designs are the most applicable to this project. The process then involved vehicle configuration modeling and research, along with utilization of inputs from all team members to help determine the likely accuracy and relevance of the results.

While analyzing these alternative powertrain architectures, the appeal of using a plug-in enabled design was kept in mind due to the strong feedbacks of our local community through various communications and outreach activities, as well as the industrial trend. British Columbia and most parts of Canada have an abundance of

renewable, hydro-electric power that is clean and affordable. In addition, the city of Victoria, like many medium-sized North American cities, has relatively short commuting distances. Therefore, the concept of a hybrid plug-in design with substantial EV-only range was viewed as ideal from a non-technical standpoint in addition to its technical merits.

The fuel selection process was driven by use of the GREET and GHGenius models to combine the physical properties of fuels with their resulting emissions and petroleum use, along with the range-sensitive utility factor curve. It was determined that electrification of the vehicle substantially improved fuel consumption and petroleum use metrics, and had potential impact on GHG and CAC emissions. E85 was shown to have the best petroleum use and GHG reductions relative to the other liquid fuels available in the competition.

High-level calculations of a Malibu vehicle were performed using fundamental equations to determine the power and energy requirements at the wheels on various city, highway and aggressive drive cycles. The values for propulsion power and energy were determined regardless of vehicle architecture. Since the electric drive efficiency on different vehicles with similar weights is comparable, the fuel efficiency was analyzed in charge sustaining (CS) mode. The estimation of the tank to wheel efficiency for a range of different hybrid vehicles was made with empirical efficiency data for engines and electrical motors. More detailed quantitative calculations were then performed on the three most promising of the identified architectures, discussed in Appendix 0, to show the variation in fuel efficiencies. The three designs were modeled in both Autonomie and Simulink to obtain more accurate analysis of fuel economy and performance measures relative to the initial empirically-based calculations. Detailed component selection, packaging and vehicle integration was also performed alongside the performance modelling tasks, to ensure the architectures were physically feasible.

3.2.2 Architecture Overview

The proposed PHEV architecture is shown in Fig 34, which is a series-parallel multi-regime prototype PHEV built on a mid-size sedan platform. The UVic Series-Parallel architecture provides many substantial improvements over the production 2013 Malibu. These are accomplished by virtue of the tremendous flexibility the architecture is capable of providing. The powertrain includes a powerful motor coupled to the engine through a belt system functioning as a belt-alternator-starter (BAS) at the front wheel, as well as a rear traction motor (RTM) and large battery. The battery and RTM make this architecture a full hybrid, giving it a significant electric-only range. This configuration was identified as having several advantageous operating modes. With the transmission set in neutral, the vehicle could essentially function as a series EREV, with the ICE charging the batteries through the BAS system. When additional power is required, or when it is more efficient to do so, the ICE and transmission could be used to propel the vehicle. For high-performance driving situations, the BAS could provide a power-assist function to smooth out the torque curve of the ICE, and the RTM could add its power such that all available power sources propel the vehicle.

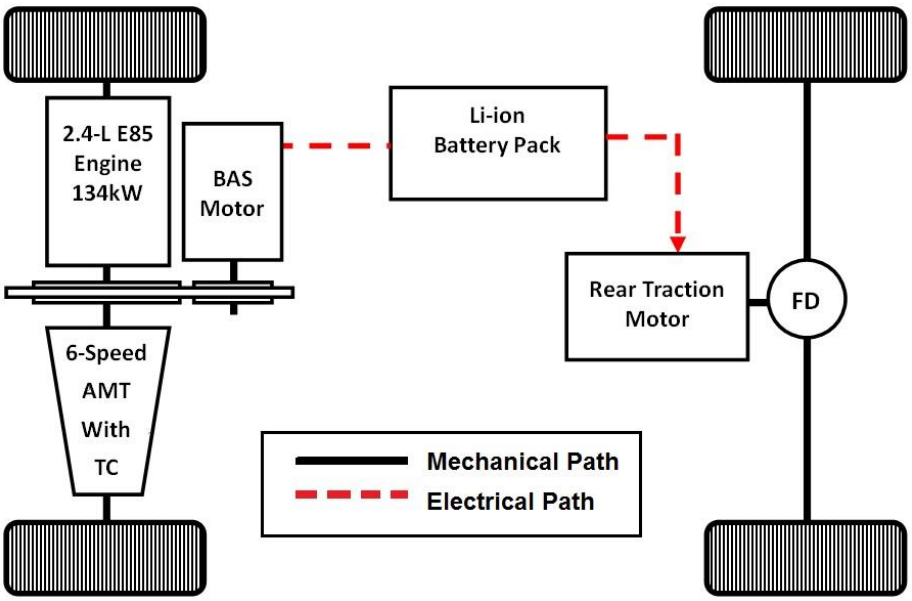

Fig 34. Proposed series-parallel multi-regime PHEV architecture.

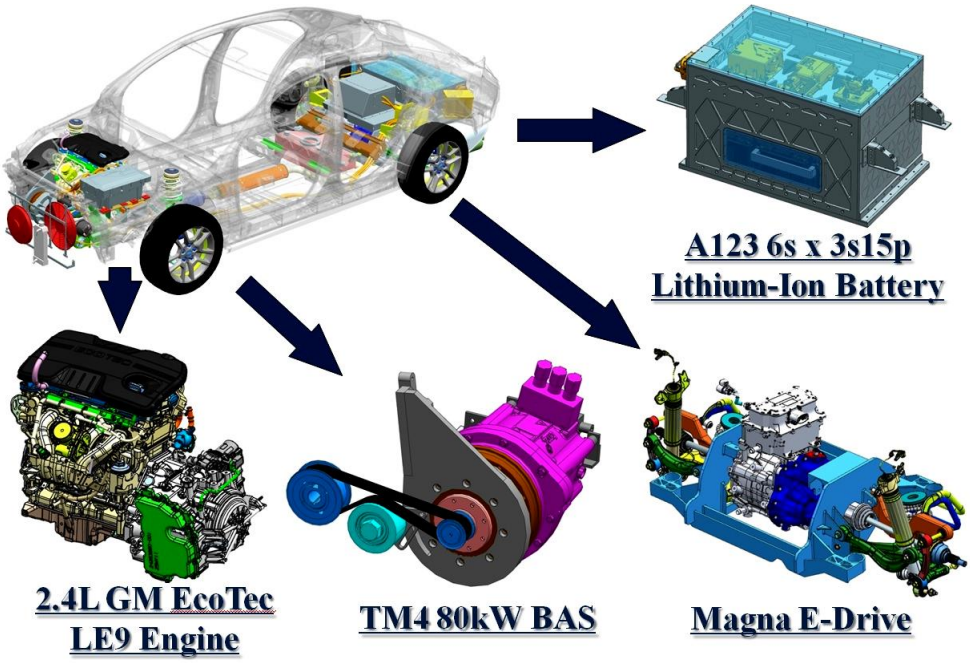

Fig 35. CAD model of the vehicle and its main components.

Fig 36. UVic's series-parallel PHEV in the garage.

3.2.3 Forward-oriented Simulation Model

In this work, following a model-based-design (MBD) process, two sets of powertrain models were developed: a simplified control-oriented model and a more

sophisticated implementation-oriented model.

The simplified Simulink/SimDriveline combined model (Fig 37) was developed first to allow conceptual validation of the proposed real-time optimal control strategy at the initial phase, since it computes faster and is easier to implement. The desktop simulation time step is set to 0.01s, which is lower than the response time of each powertrain component.

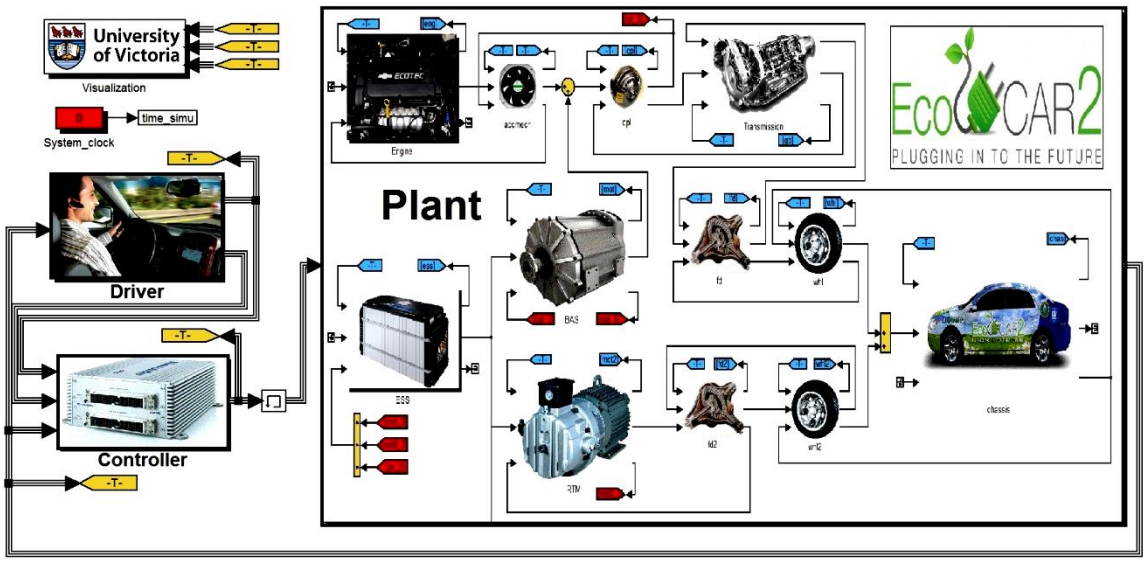

Fig 37. Forward-oriented vehicle model in MATLAB/Simulink/SimDriveline.

A more complex model was then developed by using dSPACE Automotive Simulation Models (ASM) (Fig 38), where I/O interface was exactly the same as in the real vehicle and low-level component Electronic Control Units (ECU) were also included in the plant model. The optimal control strategy was then migrated to the complex model and was integrated with other modules (such as subsystem diagnostic modules) in the rapid prototype controller (MicroAutobox II), where the sample time used was 0.001s.

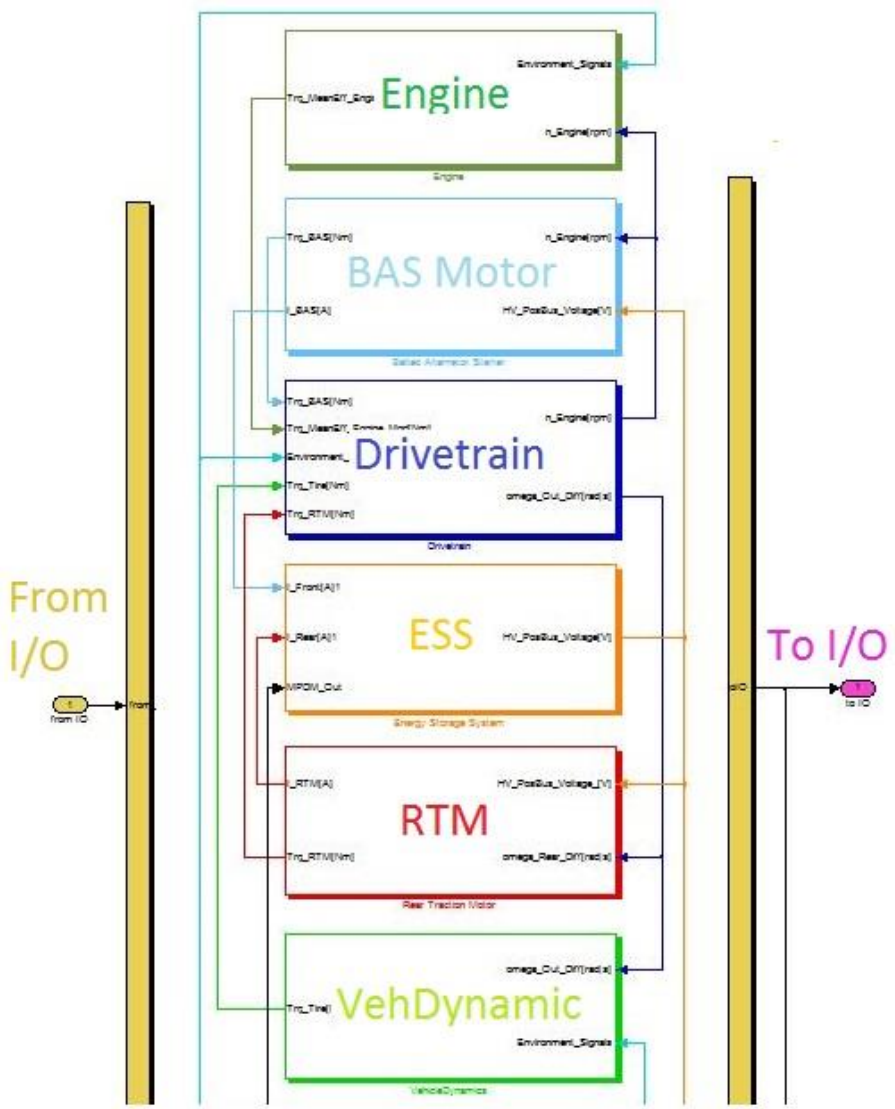

Fig 38. Vehicle model based on dSPACE Automotive Simulation Models (ASM)

Like for the HEV presented in Section 2.1, a forward approach is used to model the above PHEV powertrain in the MATLAB/Simulink environment based on AUTONOMIE. The fundamental assumptions described in Section 2.1 apply here for the PHEV as well. The components specification of the vehicle model is listed in Table 8, where all the data are provided by ANL and GM. Fig 35 shows the CAD model of the vehicle and its main components and Fig 36 shows the donated Malibu in the garage.

Table 8. Components specification of the PHEV model based on AUTONOMIE.

Component	Selection and Description
Engine	The GM LE9 4-cylinder internal combustion engine (ICE) was modeled by using the static fuel map given by GM and ANL with full power capabilities, where the fuel consumption data for engine speeds above 4000 RPM is extrapolated.
Mechanical Accessories	Constant mechanical power loss representing components such as A/C, water pump, power steering, etc. Set to 0.
Motor 1 (Front BAS motor)	To represent the additional motor/generator (TM4 Motive 80 electric motor) added to the stock BAS system, the PM motor (mot_plant_pm_35_70_escape_MG1) is selected and scaled to 80kW, as it has the closest operating curve to the TM4.
Clutch/Torque Converter	Default torque converter model (for over 150Nm: cpl_plant_clutch_1) in Autonomie was used.
Gearbox	6-speed 6T40 automatic transaxle with gear ratios 4.58, 2.96, 1.91, 1.45, 1.00, 0.75 and corresponding up/down shift and torque loss tables
Final Drive1(FWD)	2.89 ratio with torque loss table
Wheel Axle1(FWD)	17 inch wheel plant with rolling resistance based on coefficients supplied in the model
Chassis	Custom component by ANL representing the chassis of the 2013 Malibu and corresponding curve fit coefficients and data for aerodynamics and mass
Batteries	The donated A123 6x15s3p battery module system was modeled with corresponding voltage and power curves compared to state of charge and energy/power densities scaled at a pack capacity of 58.8Ah (16.2kWh).
Motor2(RTM)	Magna E-Drive with peak power at 90kW and continuous power at 45kW.
Final Drive2(RWD)	Ratio set at 7.82 with torque loss table
Wheel Axle2(RWD)	17 inch wheel plant with rolling resistance based on coefficients supplied in the model
Power Converter	Generic 12V power converter
Electrical Accessories	Constant electrical power loss representing components such as fans. Set to 200 W.
Driver	Normal PI-type driver with integral gain of 1000, proportional gain of 0.5

The detailed powertrain dynamics and component models are described as follows.

3.2.4 Vehicle Dynamics and Drivetrain Model

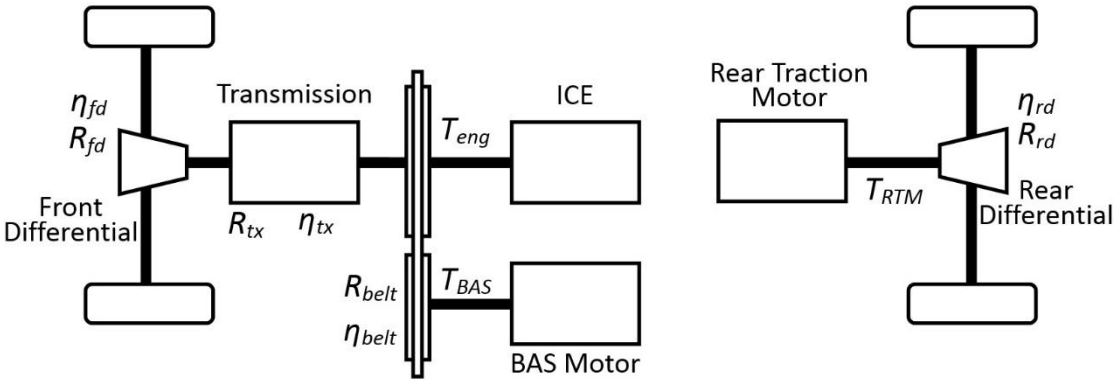

Fig 39. Drivetrian speed and torque.

The transmission and other driveline components, shown in Fig 39 are modeled as rigid bodies. We have the following speed and torque relationship at the front wheel side:

$$\begin{aligned} &(T_{eng} + T_{BAS} \cdot R_{belt}\eta_{belt}^{k}) \cdot R_{tx}\eta_{tx}R_{fd}\eta_{fd} + T_{RTM} \cdot R_{rd}\eta_{rd}^{k} = T_{req} \\ &P_{bat} = \eta_c^{\,m}(\eta_{BAS}T_{BAS}\omega_{BAS} + \eta_{RTM}T_{RTM}\omega_{RTM}) \end{aligned} \tag{55}$$

where ω_{BAS} is the speed of the BAS motor that coupled with the engine through the belted system. R_{belt} is the belt ratio between engine and BAS motor, which is equal to 1.68 in this work. The torque loss of the belted system is represented by a constant efficiency coefficient η_{belt} and k is equal to 1 when BAS motor is the driver and -1 when engine is the driver. The combined engine and BAS motor torque is transmitted through a torque converter and a six-speed automatic transmission. R_{tx} is the gear ratio of the transmission. Losses in the transmission, differential and belted system are accounted for through the definition of efficiency terms. The gear shifting strategy is determined by a simple scheduling controller based on the vehicle speed and the accelerator command (essentially vehicle torque demand).

At the rear wheel side, the RTM is coupled to the rear axle through a fixed gearbox, for which we have the following speed and torque relationship:

$$\begin{aligned} \omega_{RTM} &= \omega_{rd} \cdot R_{rd} \\ T_{RTM} \cdot R_{rd} \eta_{rd}^{k} &= T_{rd} \end{aligned} \tag{56}$$

Depending on the operational mode, the torque from front wheel together with the torque from rear wheel propels the vehicle. The overall vehicle dynamics is shown in (57). Only the longitudinal vehicle dynamics is considered in this work, neglecting all the other high-frequency dynamic effects.

$$\begin{aligned} T_{fd} + T_{rd} &= T_{req} = (mg\sin(\alpha) + mgC_{rr} + \tfrac{1}{2}\rho C_d A_f v^2 + m\frac{dv}{dt}) \cdot r \\ \omega_{fd} &= \omega_{rd} = \omega_{req} = \frac{v}{r} \end{aligned} \tag{57}$$

Equation (55)-(57) gives the drive train model, where the degree of freedom of the system is two.

3.2.5 Battery Dynamics

The energy storage system (ESS), which is the battery pack, was modeled as a charge reservoir and an equivalent circuit was used as if it were a perfect open-circuit voltage source in series with an internal resistance. The amount of charge that the ESS can hold is taken as constant, and the battery is subject to a power limit.

The required power of the battery can be calculated as:

$$P_{bat} = \eta_c^{\ m}(\eta_{BAS} T_{BAS} \omega_{BAS} + \eta_{RTM} T_{RTM} \omega_{RTM}) \tag{58}$$

where the efficiencies of BAS motor and RTM, η_{BAS} and η_{RTM}, are obtained based on motor efficiency maps of each motor, which include the motor and inverter losses, and η_c is the converter efficiency, where:

$$m = \begin{cases} 1, & when \quad charging : P_{bat} < 0 \\ -1, & when \quad discharging : P_{bat} \geq 0 \end{cases} \tag{59}$$

For each battery cell, we use the following zero-order model, neglecting the impact from the polarization current:

$$V_{bat\_out} = V_{oc} - I_{bat} \cdot R_{in} \tag{60}$$

$$(V_{bat\_out} = V_{oc} - I_{bat} \cdot R_{in} - I_{p1} \cdot R_{p1} - I_{p2} \cdot R_{p2})$$

$$SOC(t) = SOC_0 - \frac{1}{C_{bat}} \int_{t_0}^{t_f} I_{bat}(t) dt \tag{61}$$

where V_{bat_out} is the battery output voltage. I_{bat} is the battery current. V_{oc} is the open-circuit voltage. R_{in} is the internal resistance of the battery. C_{bat} is the battery capacity. SOC_0 is the initial battery SOC.

The time derivative of *SOC* (battery state of charge), $\dot{SOC}$, can be calculated from the battery power, which gives the following dynamic equation of the battery:

$$\begin{aligned} \dot{SOC} &= \frac{d(SOC)}{dt} = f(P_{bat}(t)) \\ &= -\frac{1}{C_{bat}} \cdot \frac{V_{oc}(SOC) - \sqrt{V_{oc}(SOC)^2 - 4R_{in}(SOC)P_{bat}}}{2R_{in}(SOC)} \end{aligned} \tag{62}$$

For PHEV, V_{oc} and R_{in} are functions of battery SOC (assume under normal temperature: 10-50 C^o), as shown in Fig 40. The discharging and charging power limit are also shown in Fig 40.

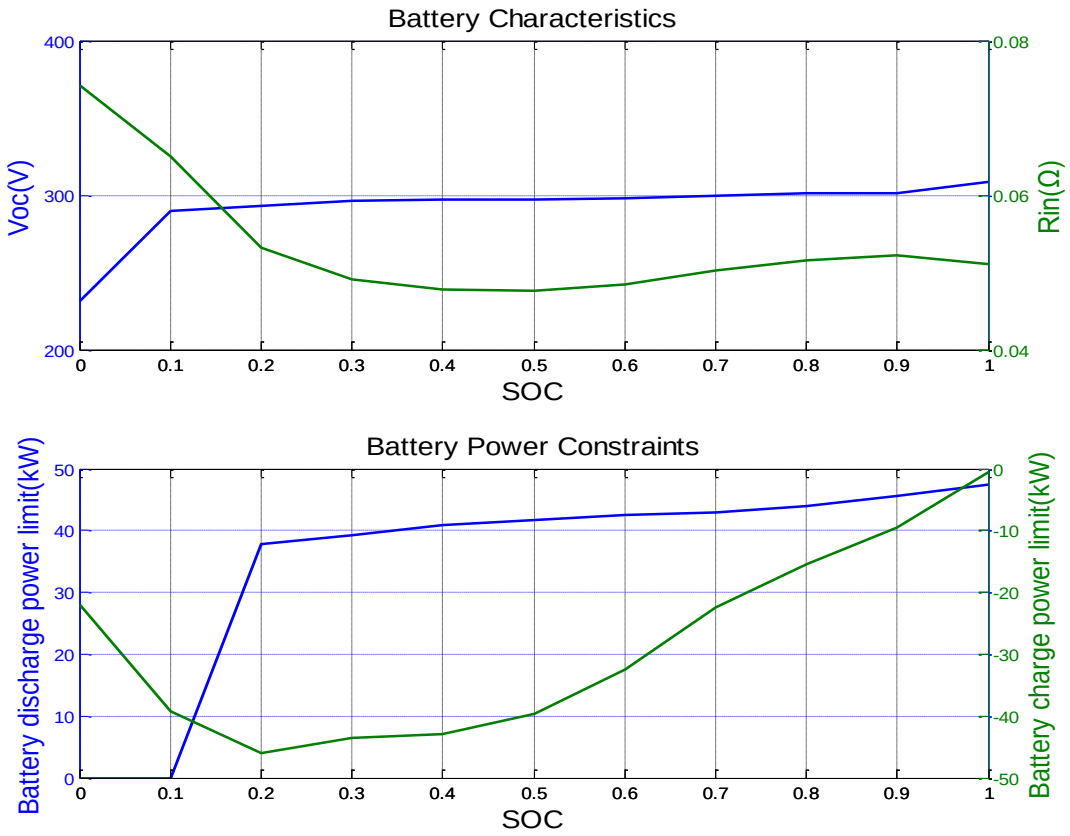

Fig 40. Battery characteristics and power constraints.

Other battery pack details are shown in Table 9.

Table 9. Battery pack details.

Manufacturer	A123	**Chemistry**	Li-ion Nanophosphate
Model	6x15s3p	**Nominal Voltage**	292VDC
Min Pack Energy (kWh)	16.2	**Cell Weight (kg)**	130

3.2.6 Engine and Electric Machines

The engine model is based on its steady-state fuel consumption map implemented in the simulator as a function of engine speed and input torque, along with a 0.3s engine time response to represent intake to power and intake to exhaust delays.

The engine fuel efficiency map with extra curves displaying fuel consumption rate is shown in Fig 41. The engine exhaust flow rate is zero if the engine is off and a positive

nonzero value if the engine is running.

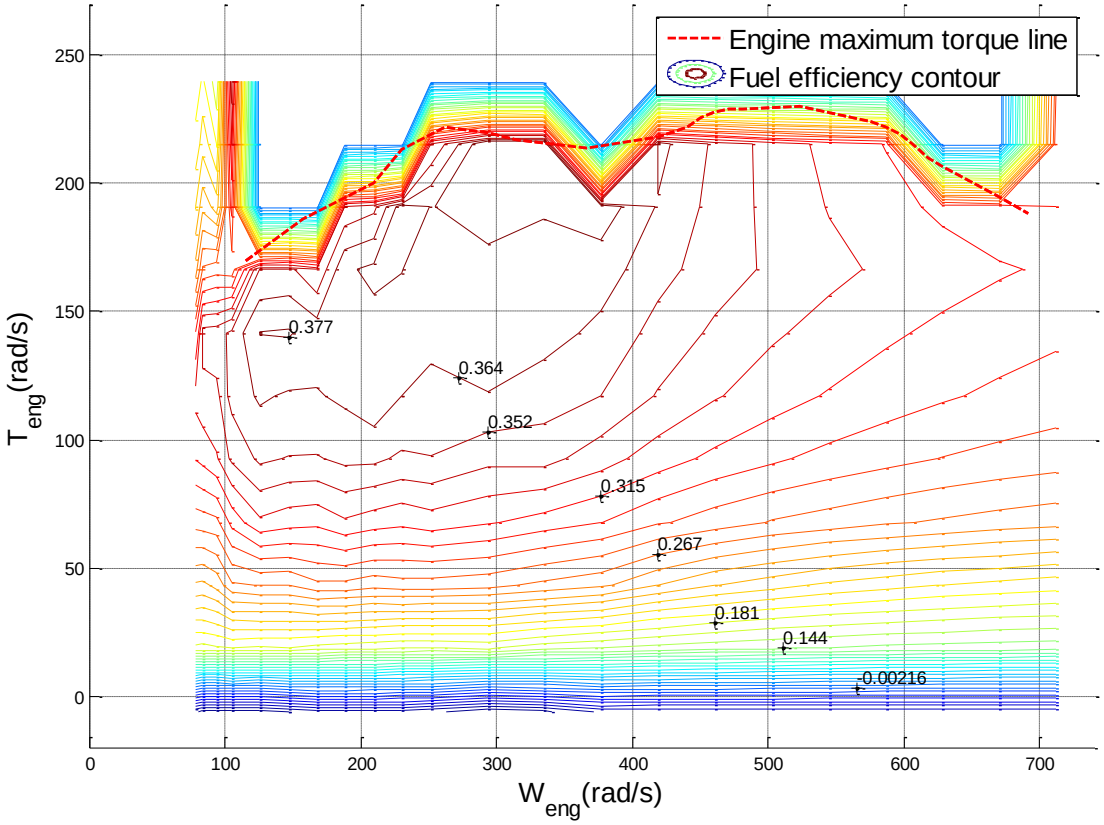

Fig 41. Engine fuel efficiency map.

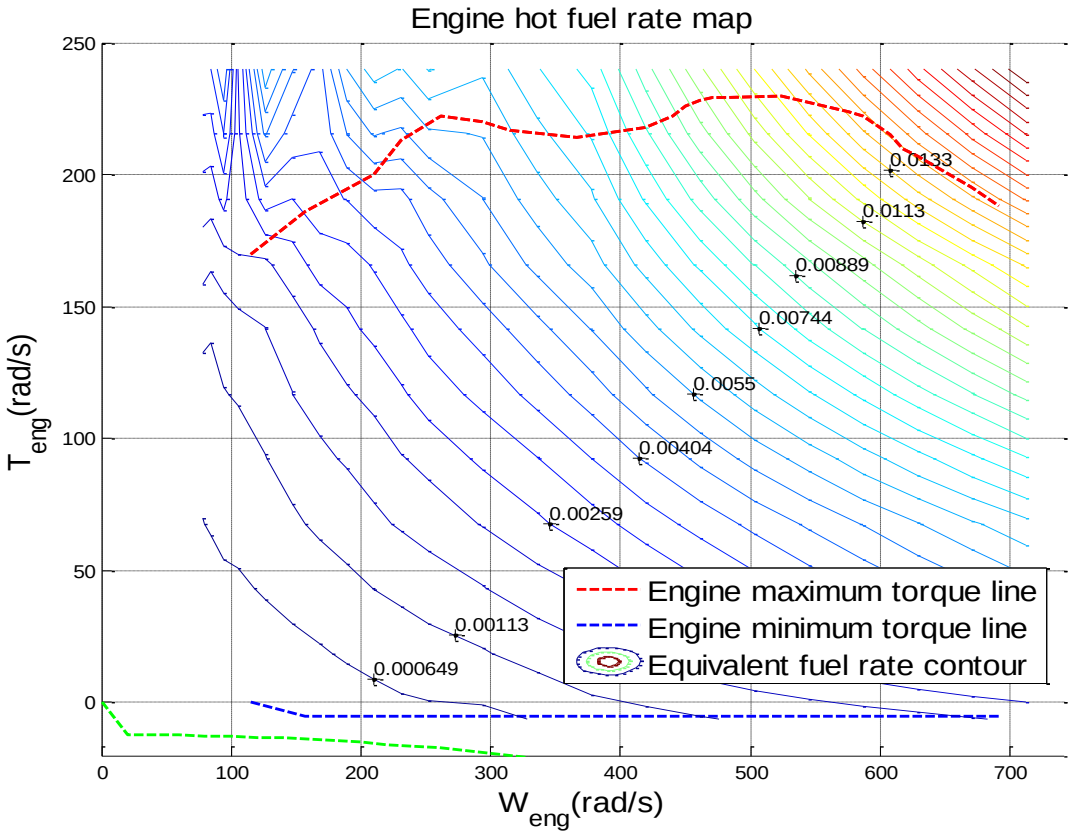

Fig 42. Engine hot fuel rate map.

Similarly, the electric machines are modeled as static elements with a 0.05s time response, wherein the efficiency is mapped as a function of their speed and input torque, as shown in Fig 43 and Fig 44.

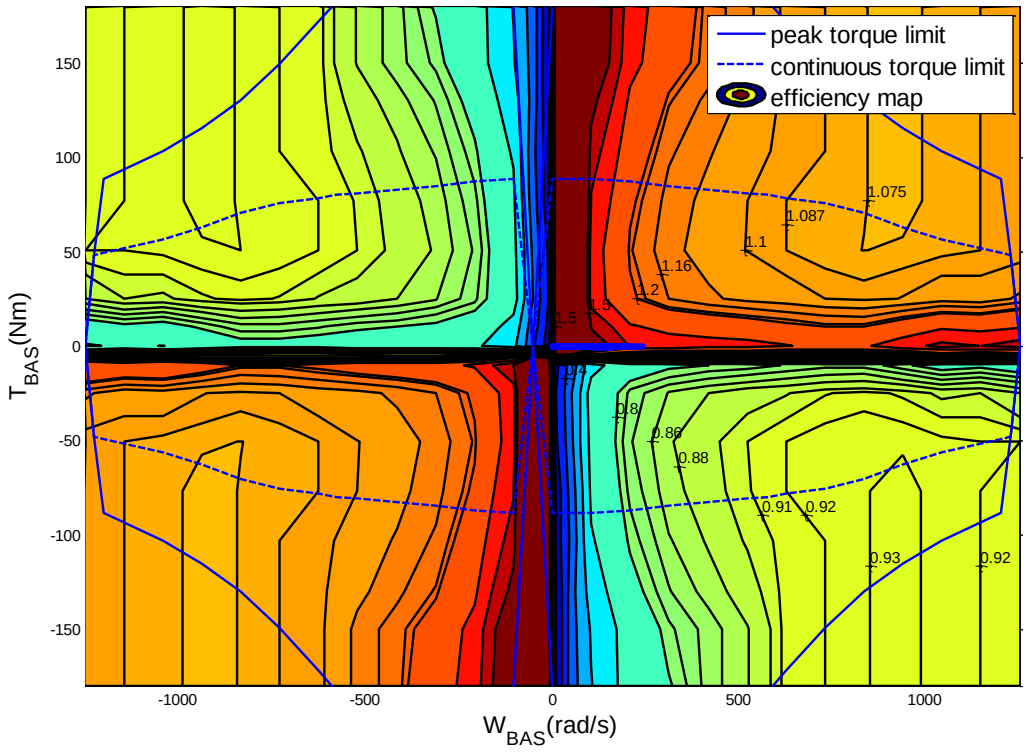

Fig 43. Front BAS motor efficiency map.

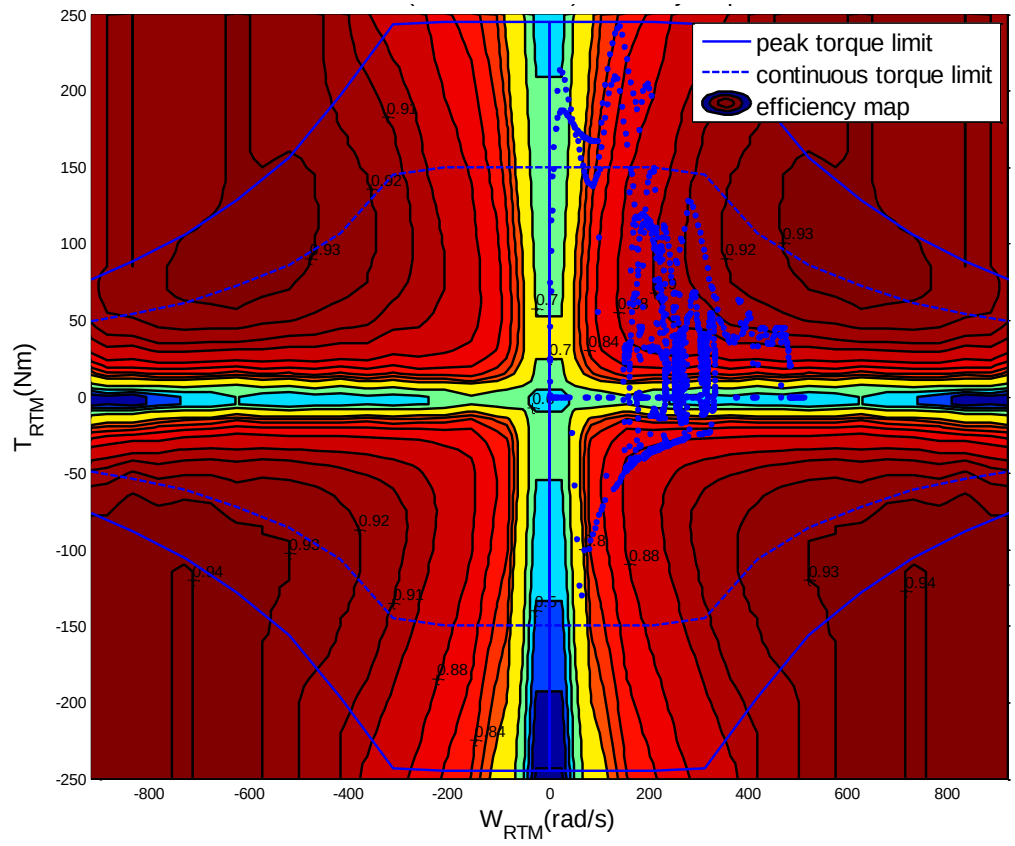

Fig 44. Rear traction motor (RTM) efficiency map.

Note that during engine start, the BAS motor in the front wheel will function as starter, where normal BAS motor torque request calculated from the energy management strategy will be overridden by maximum BAS motor torque to speed up the engine first until engine reaches a predefined target speed. After engine starts, the BAS motor torque request calculated from the energy management strategy will be used again.

3.3 Rule-Based Controller Design for the Proposed PHEV Powertrain

A deterministic rule-based controller is developed first for the proposed PHEV powertrain, which will also serve as the baseline controller for the optimization-based controller that will be developed later to compare with.

The deterministic rule-based controllers operate on a set of predefined event-triggered rules implemented prior to actual operation. They use state machine models (which are implemented using MATLAB/Stateflow as shown in Fig 45) to reflect various operating modes, where the transition between these modes are determined by predefined rules based on current operating conditions, i.e., instantaneous inputs for the decision-making process.

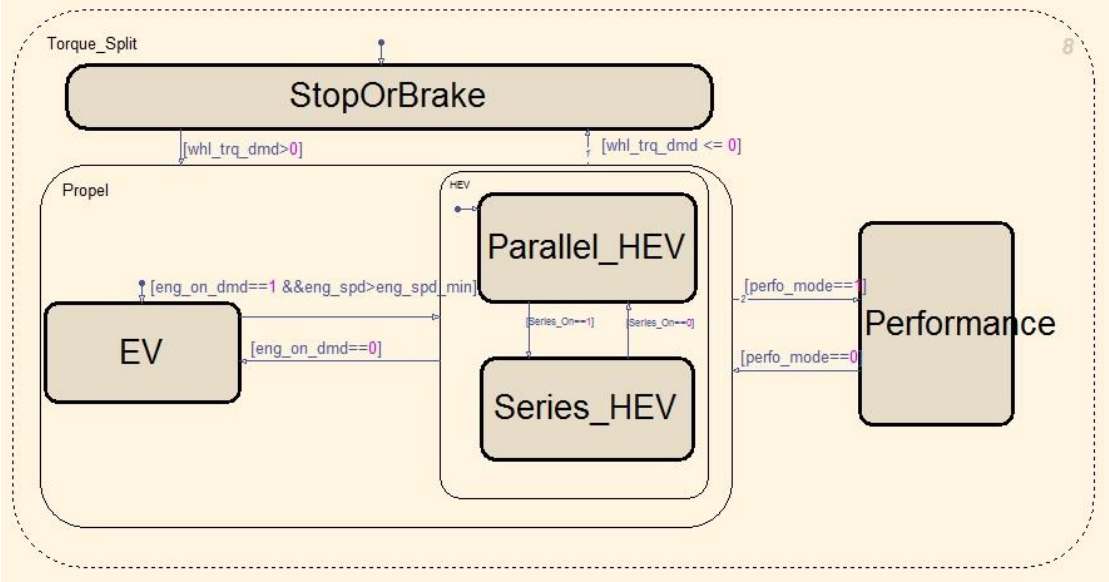

Fig 45. State-machine-based control logic in Simulink/Stateflow.

The several modes of operation considered in this study are listed as follows:

Table 10. Operating modes of the proposed PHEV.

Operating Modes	Mode Description
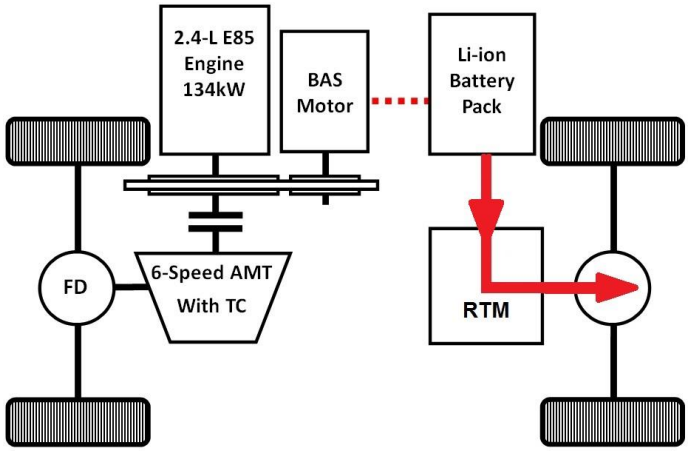 EV Only Mode	EV operation mode is the simplest regime from a controls perspective. In this mode, the ICE is off, and transmission is in neutral, with all drive power being supplied by the RTM. This regime is active in CD situations where the ESS has surplus charge to use for driving.
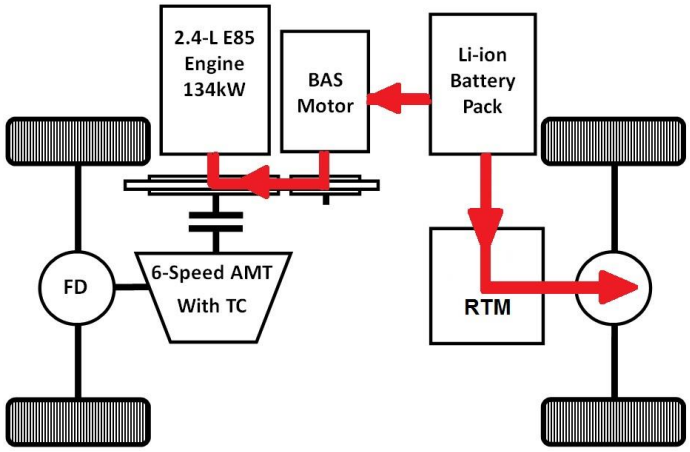 Engine Start Mode	Engine start mode is activated during engine start, where BAS motor in the front wheel supplies maximum torque to spin up the engine until it reaches a predefined threshold speed to allow engine start.

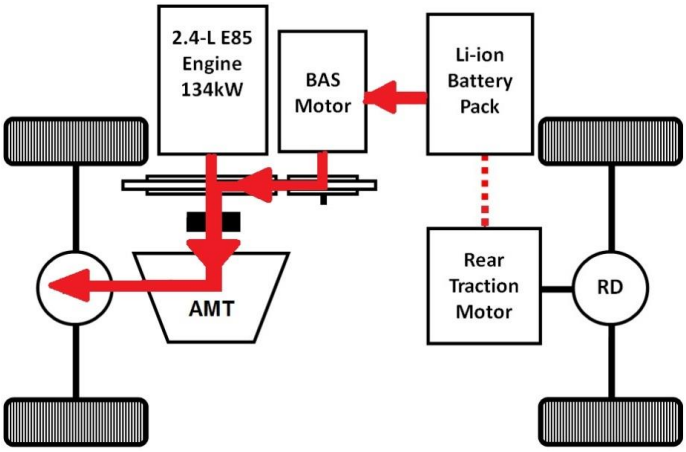 BAS Parallel Mode	Engine/BAS conventional hybrid operation is the fundamental regime during CS driving. It is split into two sub-modes: conventional ICE-only operation mode, and BAS operation mode. During conventional ICE-only mode only the ICE provides tractive power, with all electrified systems being inactive. During BAS operation, the BAS motor is engaged and it may add or subtract power to the ICE in powering the wheels, allowing for manipulation of the engine operation point and maintenance of average ESS SOC. In both sub-modes, the BAS is used to start and stop the engine as needed.
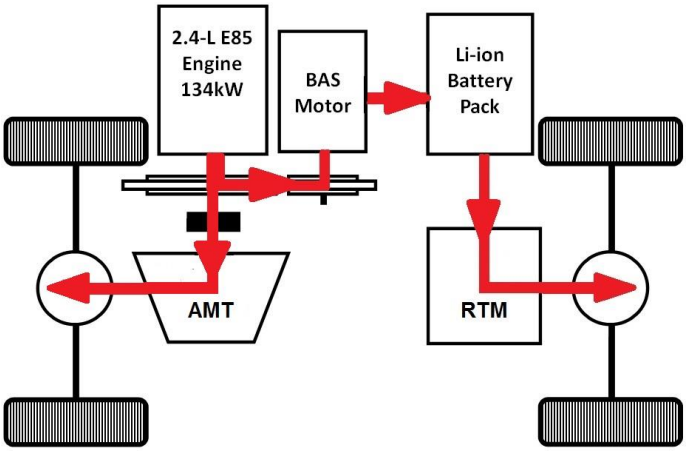 Series Parallel Mode	Series-Parallel hybrid operation is engaged by the vehicle controller logic. It can be active in either CD or CS driving as needed. During Series-Parallel high power operation, AWD functionality is realized through using both the ICE and RTM to power the drive axles. The BAS is also engaged, and may add or subtract torque from the ICE to improve efficiency and maintain ESS SOC. During series operation, the transmission is set to neutral and ICE torque is converted to electrical energy relayed over the high voltage (HV) bus. The RTM is the sole provider of tractive power. ICE power regeneration is set based on average driver power demand

	to maintain the ESS SOC. This sub-mode is beneficial during low power, traffic creeping situations during CS driving.
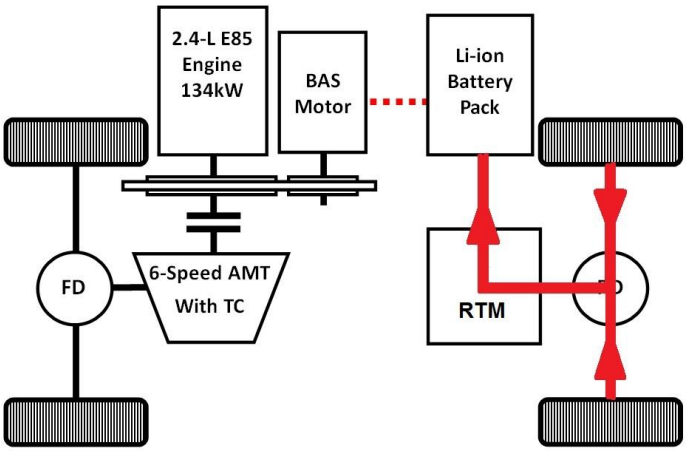 Regenerative Braking Mode	In all sub-modes discussed in the preceding sections, regenerative braking can be applied via the RTM when requirement dictates. Regenerative braking is applied with two criteria. The first is passive regenerative braking applied when the driver torque request is zero, occurring when the accelerator pedal is not pressed down. The second is active regenerative braking which is proportional to the brake pedal depression percentage and is applied on top of the mechanical hydraulic assist braking in the stock vehicle chassis.

Depending on different driving situations, the Charge Depleting-Charge Sustaining (CDCS) rule-based controller will operate the vehicle in one of the above modes of operation. CDCS strategy operates the vehicle first in CD mode, where battery is used exclusively (except during hard acceleration) to power the vehicle until its battery SOC is depleted to a predetermined low threshold level, and then the vehicle will operate in CS mode where engine will start to provide power along with battery and the battery SOC will be kept at a nominally constant value as in a conventional HEV.

The simulation results of the rule-based controller are shown below. The UDDS driving cycle with an iteration of 20 was used. The regenerative braking was set to be able to recover 10% of the braking power (the rest is consumed by the normal friction brake).

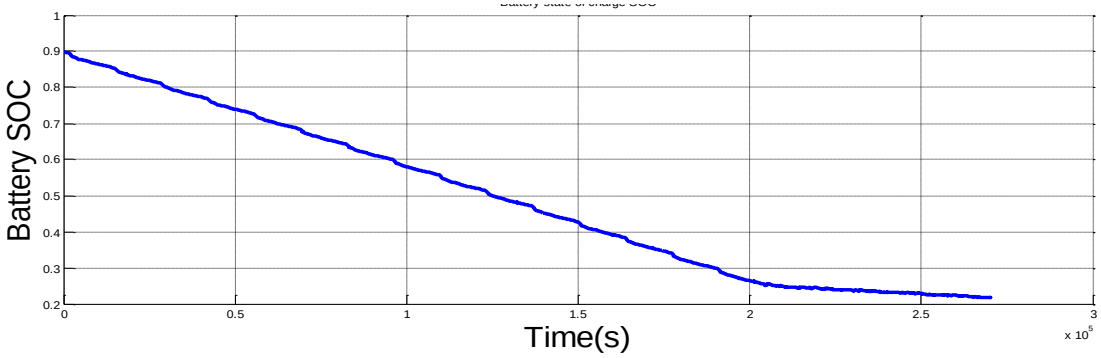

Fig 46. Battery SOC result over 20*UDDS.

An advantage of using rule-based controller is that consistency results in great reliability. The disadvantage of having this consistency is that it cannot adapt well to parameter changes in the vehicle's drive train. These changes are usually brought upon by changes in drive cycle, driving patterns, and driver behavior. The wear and tear of the vehicle and the simple fact that vehicles are not always utilized as they were designed add to these changes. Fixed control strategies cannot accommodate the many changes in driving conditions and patterns resulting in a non-optimized use of power, which leads to bad fuel economy.

3.4 Extension of the Proposed Fast Real-Time Implementable Optimal Control Algorithm

Compared with the optimal energy management problem formulated for HEV in (17), where the battery SOC is maintained around a nominally constant value during the whole driving cycle, the energy storage system in PHEV has much higher capacity and can deplete the battery to a pre-defined low threshold SOC and recharging it directly from the power grid. Therefore the constraint on final SOC defined in (17.c) and on the SOC upper and lower boundaries defined in (17. d) is no longer in existence for PHEV. Unlike HEV, most of the available electrical energy is supplied from the grid, which implies that the performance of PHEVs are not depending on fuel energy only, but are rather significantly influenced by additional variables, such as the

upstream marginal electricity generation mix, fuel choices, battery capacity and the resulting all-electric-range (AER), the consumer's interaction related information such as trip distance. The original cost function defined for HEV in (17) becomes incorrect and needs to be redefined for the case of PHEV, hence introducing the full-cycle well-to-wheel (WTW) assessment of energy use and GHG emissions into the energy optimization problem.

In this thesis, the objective is to minimize the full-cycle well-to-wheel petroleum energy use (PEU), where both the fuel and electric energy consumption is taken into account, as shown in the following:

$$PEU_{WTW} = E_{fuel} \cdot \eta_{PEU,\,fuel} + E_{elec} \cdot \eta_{PEU,elec} \tag{63}$$

where E_{fuel} and E_{elec} are the per-kilometer amounts of fuel and alternating current (AC) electric energy (kWh/km) used. The WTW PEU factor η_{PEU} is used to relate fuel (or electric) energy use to the well-to-wheel petroleum energy use based on the full-cycle life-cycle assessment (LCA) technique[52] considering both upstream and downstream (at the vehicle) environmental impacts associated with all the stages of a product's life. The WTW factors used in this study include the following 2 stages to cover the full life-cycle impact: upstream well-to-pump (WTP) and downstream pump-to-wheels (PTW) stage[53]. The upstream WTP stage starts with the fuel feedstock recovery, followed by fuel production, and ends with the fuel available at the pump, while the downstream PTW stage represents the vehicle's operation activities.

Alternatively, the objective can also be defined as to minimize the WTW greenhouse gas (GHG) emission, as shown in the following equation:

$$GHG_{WTW} = E_{fuel} \cdot \eta_{GHG,\,fuel} + E_{elec} \cdot \eta_{GHG,elec} \tag{64}$$

where the WTW GHG factor η_{GHG} is used to relate vehicle energy use to the well-to-

wheel amount of GHGs generated. The value of PEU factor and GHG factor can be found in Table 11[53]. Other cost criteria can also be taken into consideration such as daily or monthly running cost of the PHEV during the trip out of economic incentive, which essentially can be formalized by replacing the coefficients of the fuel and battery related item in the cost function.

Table 11. Well-to-Wheel Petroleum Energy Use (PEU) Factors (kWh of petroleum energy/kWh of fuel energy consumed) and Greenhouse Gas (GHG) Factors (g/kWh).

	E10	**E85**	**B20**	**Hydrogen**	**Electricity**
PEU factor η_{PEU} (kWh PE/kWh, WTW)	0.984	0.316	0.859	0.02	0.034
GHG factor η_{GHG} (g/kWh, WTW)	322	261	288	392	648

The cost function for PHEV optimal control is thus redefined as follows (taking PEU consumption as the cost function):

$$\min\left\{J=\int_{t_0}^{t_f}[\dot{m}_{fuel}(t)\cdot\eta_{FSE}\cdot\eta_{PEU,fuel}+P_{bat}(t)\cdot\eta_{PEU,elec}]dt\right\} \tag{65}$$

$$subject\quad to:$$

$$\begin{cases}
\dfrac{dSOC(t)}{dt}=f(P_{bat}(\mathrm{t}))=-\dfrac{1}{C_{bat}}\cdot\dfrac{V_{oc}-\sqrt{V_{oc}^2-4R_{in}P_{bat}(t)}}{2R_{in}}; & (65.a)\\
\dfrac{d\omega_{eng}(t)}{dt}=f(T_{eng}(\mathrm{t}),T_{mot}(\mathrm{t}),T_{gen}(\mathrm{t})); & (65.b)\\
SOC(t_0)=0.9 & (65.c)\\
SOC_{\min}\le SOC(t)\le SOC_{\max} & (65.d)\\
P_{bat_\min}\le P_{bat}(t)\le P_{bat_\max} & (65.e)\\
T_{eng_\min}(\omega_{eng}(t))\le T_{eng}(t)\le T_{eng_\max}(\omega_e(t)) & (65.f)\\
\omega_{eng_\min}\le\omega_{eng}(t)\le\omega_{eng_\max} & (65.g)\\
T_{BAS_\min}(\omega_{BAS}(t))\le T_{BAS}(t)\le T_{BAS_\max}(\omega_{BAS}(t)) & (65.h)\\
\omega_{BAS_\min}\le\omega_{BAS}(t)\le\omega_{BAS_\max} & (65.i)\\
T_{RTM_\min}(\omega_{RTM}(t))\le T_{RTM}(t)\le T_{RTN_\max}(\omega_{RTM}(t)) & (65.j)\\
\omega_{RTM_\min}\le\omega_{RTM}(t)\le\omega_{RTM_\max} & (65.k)
\end{cases}$$

where $\dot{m}_{fuel}$ is the fuel consumption rate (kg/s) and P_{bat} is the battery DC electric power (kW) used at each time step. η_{FSE} is the fuel-specific energy by mass (kWh/kg), the value of which can be found in Table 12. T_{BAS} refers to the torque of the front motor coupled with the BAS system and T_{RTM} refers to the torque of the rear traction motor.

Table 12. Fuel material properties[53].

	Gasoline	E10	E85	B20	Electricity	Hydrogen
Fuel-specific energy by mass η_{FSE} (kWh/kg)	11,.73	11.44	7.96	11.55	N/A	33.3
Fuel density (kg/L)	0.7583	0.746	0.7871	0.8552	N/A	/
Fuel energy density LHV_{fuel} by volume (kWh/L)	8.895	8.534	6.265	9.878	N/A	/
Fuel energy density by volume (kWh/gal)	33.7	32.3	23.7	37.4	N/A	/

Note that the cost metric defined in (65) has included both fuel and electric energy, taking the energy conversion efficiency of both engine and motors into account.

According to the Pontryagin's Minimum Principle, the original problem can be reduced to an instantaneous minimization problem in terms of battery power P_{bat} similar as in the case of HEV, subject to *SOC* dynamic equation (65.a) and the P_{bat} boundary constraint at each time step, while there is no end state constraint for PHEV.

The powertrain model described in 3.2 can be summarized as in the following two equations:

$$\begin{aligned} &(T_{eng} + T_{BAS} \cdot R_{belt}\eta_{belt}^{k}) \cdot R_{tx}\eta_{tx}R_{fd}\eta_{fd} + T_{RTM} \cdot R_{rd}\eta_{rd}^{k} = T_{req} \\ &P_{bat} = \eta_c^{\,m}(\eta_{BAS}T_{BAS}\omega_{BAS} + \eta_{RTM}T_{RTM}\omega_{RTM}) \end{aligned} \tag{66}$$

Unlike the case in Section 2 for the Prius powertrain, which has a degree of freedom of one in terms of control variables after simplification, the series-parallel powertrain in this section has a degree of freedom of two. In this study, we chose battery power P_{bat} and rear traction motor torque T_{rtm} as the two independent control variables. All the other variables can be determined by powertrain equations specified in 3.2.

To apply Pontryagin's Minimum Principle to the optimal control problem in (65), we first have the Hamiltonian as follows:

$$\begin{aligned} H(P_{bat}(t), T_{rtm}(t), t) = &\dot{m}_{fuel}(P_{bat}(t), T_{rtm}(t), t) \cdot \eta_{FSE} \cdot \eta_{PEU,\,fuel} \\ &+ P_{bat}(t) \cdot \eta_{PEU,elec} - p(t) \cdot \frac{V_{oc} - \sqrt{V_{oc}^2 - 4R_{in}P_{bat}(t)}}{2C_{bat}R_{in}} \end{aligned} \tag{67}$$

where *p(t)* is the costate (or can be treated as an equivalence factor), which is essentially the Lagrange multiplier of the Euler-Lagrange formulation of the optimal control problem. The dynamics of s are given by the necessary conditions of PMP.

The optimal control variables $\mathbf{u}^*(t) = [P_{bat}^*(t), T_{rtm}^*(t)]^T$ are determined such that the Hamiltonian is minimized at each time step:

$$\mathbf{u}^*(t) = [P_{bat}^*(t), T_{rtm}^*(t)]^T = \min_{\mathbf{u}(t)} H(\mathbf{u}(t), t) \tag{68}$$

For Prius, a 1D search has been conducted at each time step to get the optimal cost function (minimum Hamiltonian in this case), while for the powertrain in this section, essentially a 2D search (in terms of P_{bat} and T_{rtm}) for the optimal cost function has to be carried out at each time step.

Fig 47 shows the 2D search map for optimal cost function (Hamiltonian) at time step 35s of UDDS cycle. In this study, we used a grid size of 106 by 1 for battery power Pbat (with resolution of 891W) and a grid size of 50 by 1 for rear traction motor torque Trtm (with resolution of 5Nm). At each time step, the components constraints (such as battery power upper/lower limit, engine and motor maximum/minimum torque, and etc.) were calculated and those grid points exceeding the limits were set to NaN. In addition, the pure electric point was also calculated and its corresponding energy consumption was compared with the 2D cost map. The ultimate optimal point was the one that gave lowest cost (Hamiltonian) value.

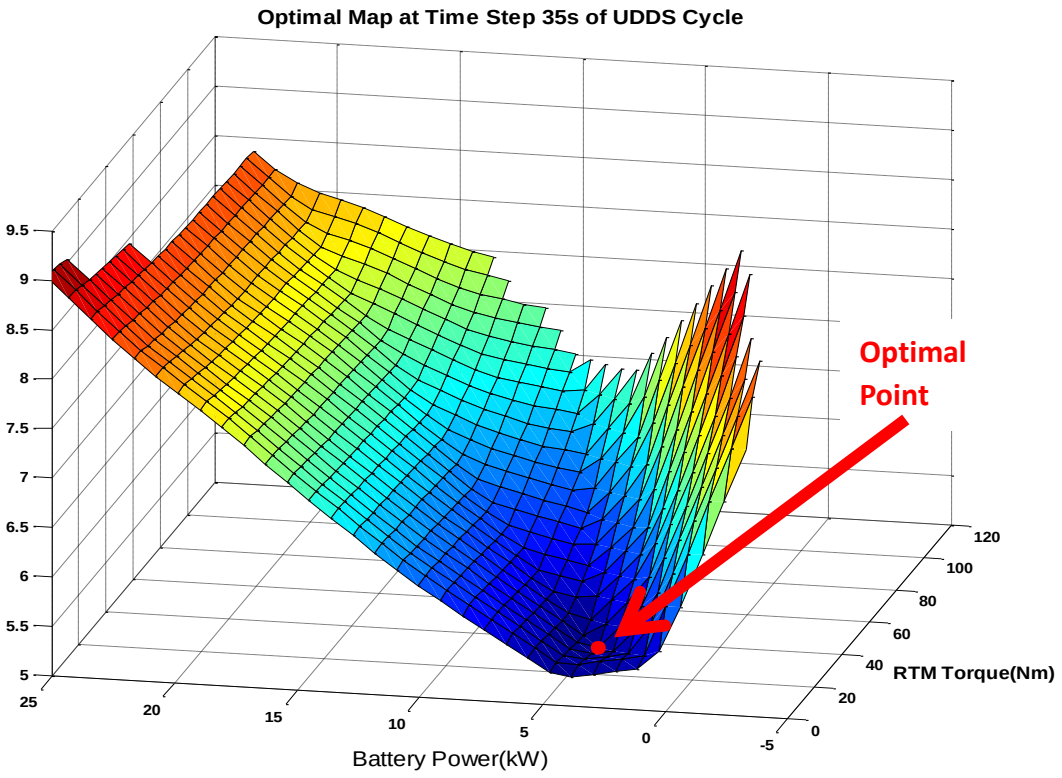

Fig 47. 2D search map for minimum cost function (Hamiltonian) at time step 35s of UDDS cycle.

For the proposed PHEV with the lithium-ion battery, the battery open circuit voltage V_{oc} and internal resistance R_{in} remains almost as constants within the operating SOC range of 0.2 to 0.9, as can be seen from Fig 40. In this case, we still have (69) same as for HEV shown in Section 2.4.1. As a result the optimal costate *p(t)* in (67) can be represented as a constant throughout the driving cycle.

$$\dot{p}(t) = -\frac{\partial H}{\partial SOC} = 0 \tag{69}$$

The value of the constant costate p that will result in optimal cost for a PHEV cannot be known in advance. In this work, we used a PI type of SOC tracker to tune the costate p based on estimated reference optimal SOC trajectory constructed prior to the trip for PHEV, where only the trip distance is needed.

With only the trip distance known in advance, the optimal value of the costate p

can be easily approximated according to the followings:

As can be observed from the simulation results shown in Fig 48 and Fig 49, which display the SOC trajectories under different costate p under UDDSx10 cycle, with a blended strategy that depletes the battery proportionally to the driving distance and the battery SOC reaches its depleted minimum value by the end of the trip, minimum cost (fuel economy, PEU consumption or GHG emission depending on which cost function is chosen) can be achieved. In other word, the optimal SOC trajectory versus trip distance is almost a linear line between its initial start point and its final point at the trip end. This has been also stated in various other studies[17, 29, 32, 40].

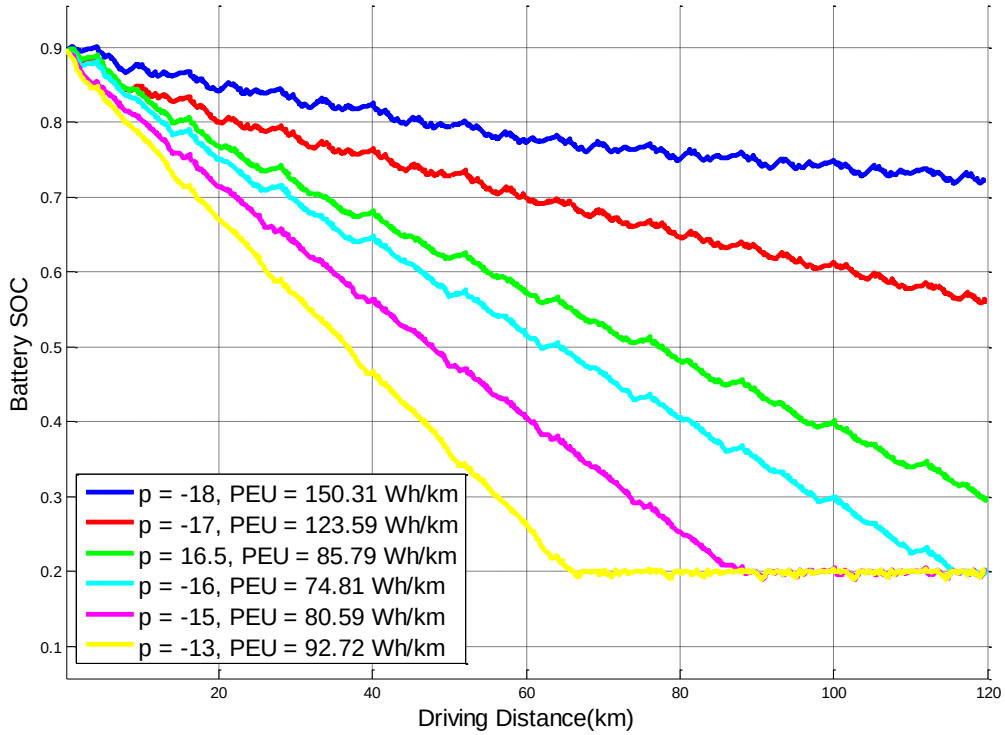

Fig 48. SOC trajectories and Well-to-Wheel Petroleum Energy Use (PEU) under different value of costate p for UDDSx10.

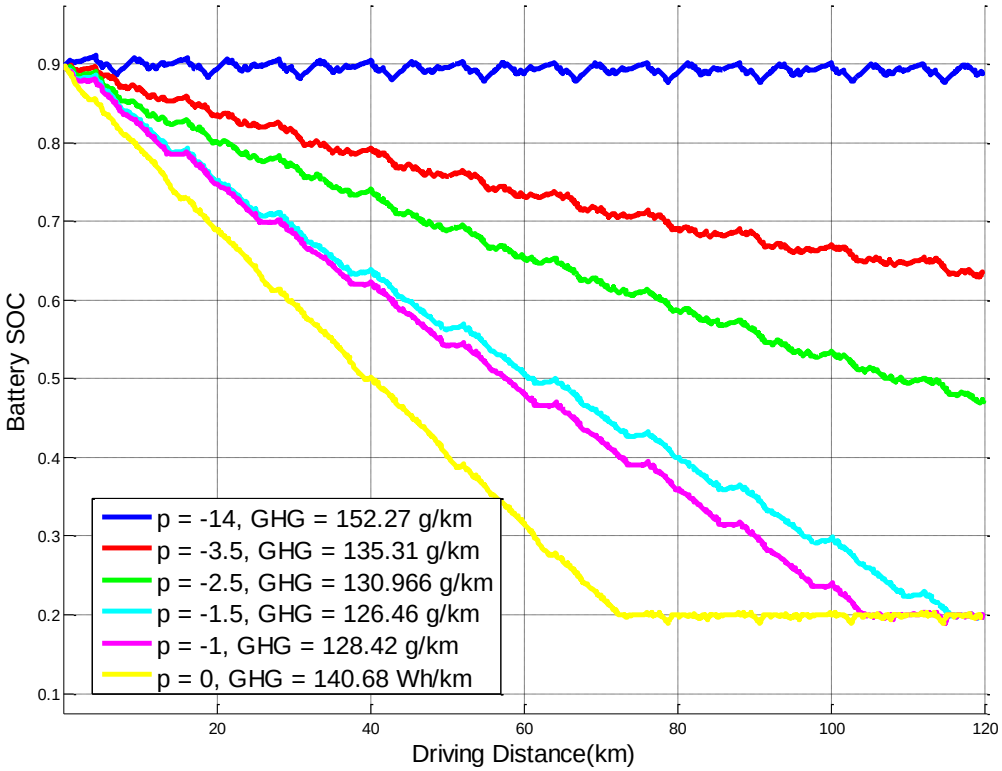

Fig 49. SOC trajectories and Well-to-Wheel Greenhouse Gas (GHG) emission under different value of costate p for UDDSx10.

Accordingly, in this study, an adaptive PI type of SOC tracker based on current driving distance was used to prevent SOC drifting away from this linear line:

$$p(k) = p_0 + K_p[SOC(k) - SOC_{ref}(k)] + K_i \sum_{i=1}^{k} [SOC(i) - SOC_{ref}(k)] \tag{70}$$

where p_0 is the initial guess of the optimal costate p. K_p and K_i are the PI parameters, which were manually tuned in this study. The value of initial guess p_0 was determined based on the average optimal value among all standard driving cycles used in the work. The value of K_p and K_i were basically tuned so that no oscillation of the requested torque of each component and no deviation from target SOC in CS mode were observed among all cycles. SOC_{ref} is the reference SOC value. where $SOC_{ref}(k)$ in this case is proportional to the current driving distance $D(k)$:

$$SOC_{ref}(k) = SOC_{init} - \frac{D(k)}{D_{trip\_total}} \cdot (SOC_{init} - SOC_{final}) \quad (71)$$

D_{tirp_total} is the total distance of the trip, which is the only information that's depending on the future cycle and can be easily obtained from the onboard GPS device assuming the driver enters his destination to the GPS at the beginning of the trip. A more reasonable definition of D_{trip_total} should be the total distance of the vehicle's driving trips during one particular day, since the optimal control should aim at minimizing the total fuel/emission cost of running the PHEV on a daily basis assuming battery energy is used up at daytime and charged fully at night. The total driving distance in one particular day can be predicted by using machine learning techniques based on past driving data, which is out of the scope of this thesis.

3.5 Fast Real-Time Optimal Control Algorithm Development for PHEV

Since the proposed series-parallel PHEV powertrain has a degree of freedom of two in terms of free control variables, a 2D search has to be conducted at each time step for the optimal point, which adds significant computational burden to the controller. To allow fast-computed control algorithm, in this section, the 2D search is converted into a 1D search based on some optimization techniques.

Let's recall the Hamiltonian defined in (67). At each time step, for each battery power $P_{bat}(t)$, the RTM torque $T_{rtm}(t)$ that leads to the minimum fuel rate $\dot{m}_{fuel}(P_{bat}(t), T_{rtm}(t), t)$ will be the candidate point under that specified $P_{bat}(t)$. This means that for each grid point $P_{bat}(k,t)$ in the battery power vector P_{bat}=[$P_{bat}(1,t)$ $P_{bat}(2,t)$…$P_{bat}(k,t)$…$P_{bat}(106,t)$], which was a 106x1 vector with a resolution of 861W in this study, a sub-level minimization problem needed to be solved as follows:

$$[T_{rtm}{}^{*}(t), T_{bas}{}^{*}(t)]^{T} = \min_{T_{rtm}(t)} \dot{m}_{fuel}(P_{bat}(k,t), T_{rtm}(t), T_{bas}(t), t) \tag{72}$$

According to the engine fuel rate map shown in Fig 42, the minimum engine fuel point happened when the engine was operated at its lowest allowable torque under the current engine speed, which was determined by the current wheel speed and drivetrain ratio. The minimization problem in (**72**) can thus be equal to the following problem:

$$[T_{rtm}{}^{*}(t), T_{bas}{}^{*}(t)]^{T} = \min_{T_{rtm}(t)} T_{eng}(P_{bat}(k,t), T_{rtm}(t), T_{bas}(t), t) \tag{73}$$

Based on the above minimization problem (73), the powertrain equations presented in (66) and the components defined in (65), we can further have the following minimization problem:

$$\min\left\{ J = T_{eng}(T_{bas}, T_{rtm}) = -a_1 \cdot T_{bas} - b_1 \cdot T_{rtm} + c_1 \right\} \tag{74}$$

subject to:

$$\begin{cases} a_2 \cdot T_{bas} + b_2 \cdot T_{rtm} = c_2 & \text{(74.a)} \\ d_1 \le T_{bas} \le d_2 & \text{(74.b)} \\ e_1 \le T_{rtm} \le e_2 & \text{(74.c)} \end{cases}$$

where $a_1>0$, $b_1>0$, $c_1>0$, $a_2>0$, $b_2>0$, c_2, d_1, d_2, e_1, e_2 are all constant known parameters, whose value can be calculated under the current driving conditions according to the followings:

$$\begin{array}{lll} a_1 = R_{belt}\eta_{belt}^{k} & b_1 = \dfrac{R_{rd}\eta_{rd}^{k}}{R_{tx}\eta_{tx}R_{fd}\eta_{fd}} & c_1 = \dfrac{T_{req}}{R_{tx}\eta_{tx}R_{fd}\eta_{fd}} \\ a_2 = \eta_c{}^{m}\eta_{bas}\omega_{bas} & b_2 = \eta_c{}^{m}\eta_{rtm}\omega_{rtm} & c_2 = P_{bat} \\ d_1 = T_{bas\_\min} & d_2 = T_{bas\_\max} & \\ e_1 = T_{rtm\_\min} & e_2 = T_{rtm\_\max} & \end{array} \tag{75}$$

According to optimization theory, the optimal point of problem (74) happens at the boundaries of the control variables $[T_{rtm}, T_{bas}]^{T}$. In other word, the optimal point is located at one of the following four points: lower and upper limits of T_{rtm} and lower and

upper limits of T_{bas}. This can be easily understood from the following diagrams in Fig 50. Note that the green dashed line represents the cost function (74), where the slope is a constant since a_1, b_1 and c_1 are all constants at a certain time step. The blue solid line represents constraint (74.a), where the slope is not a constant since the motor efficiency η_{bas} and η_{rtm} are both varying with motor torque (therefore a_2, b_2 and c_2 are varying with motor torque) at a certain time step. For the optimal point, engine torque T_{eng} needs to be as lower as possible, which means that the intercept of the green dashed line needs to be as higher as possible subject to the boundary limit.

As can be seen from Fig 50, taking all the possible cases when T_{eng} is the lowest into consideration, the optimal points take place at either the boundary limit of T_{bas} or T_{rtm}.

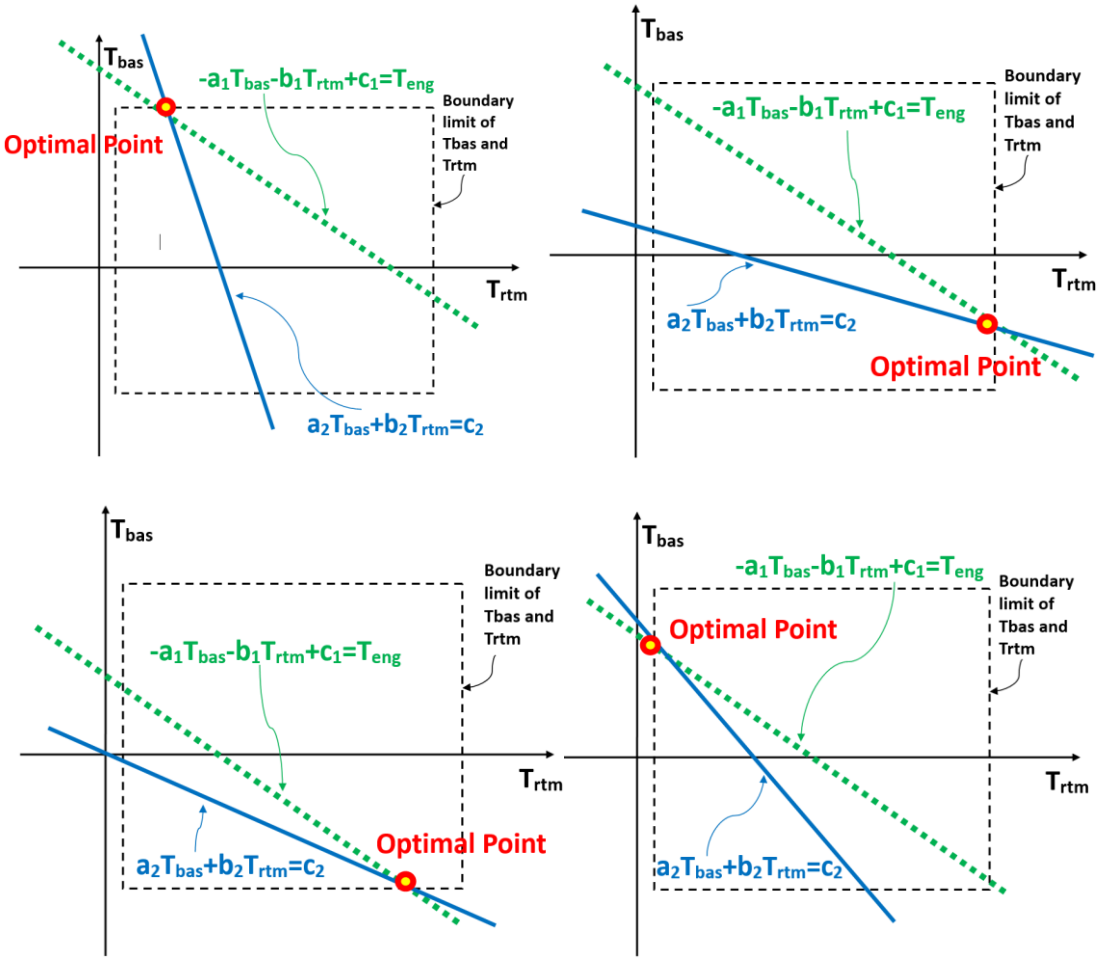

Fig 50. Optimal points on Tbas-Trtm map.

In this way, at each time step, for each P_{bat} grid, only 4 points were needed to be examined: lower and upper limits of T_{rtm} and lower and upper limits of $T_{bas.}$ The one that gave the lowest engine torque is the candidate point under that P_{bat} grid. Once T_{rtm} and T_{bas} are determined under that P_{bat} grid, engine torque T_{eng} can also be calculated.

The 2D search problem described in section 3.4 can thus be converted into a standard fixed final-time and fixed final-state optimal control problem with a single control variable (battery power P_{bat}) in discrete time format, which is essentially a 1D search algorithm. The only system state is the battery state of charge *SOC*:

$$\begin{aligned}
&\min\left\{ J = \sum_{k=1}^{N} \dot{m}_{fc}(k) = \sum_{k=1}^{N} g(P_{bat}(k)) \right\} \\
&subject \quad to: \\
&\begin{cases}
\Delta SOC(k) = SOC(k+1) - SOC(k) \\
\qquad\qquad = -\dfrac{1}{C_{bat}} \cdot \dfrac{V_{oc} - \sqrt{V_{oc}^2 - 4R_{in}P_{bat}(k)}}{2R_{in}} \\
SOC(k=1) = SOC_init = 0.9 \\
SOC_{\min} \le SOC(k) \le SOC_{\max} \\
P_{bat}(k) \in \{P_{bat_feasible}(k)\}
\end{cases}
\end{aligned} \tag{76}$$

The optimal P_{bat} is the one that gives minimum Hamiltonian at each time step (as shown in Fig 51), based on Pontryagin's Minimum Principle, similar to the case of Prius HEV presented in Section 2:

$$P_{bat}^{*}(k) = \arg\min(H(k))$$
$$subject \quad to: \qquad (77)$$
$$P_{bat}(k) \in \{P_{bat\_feasible}(k)\}$$

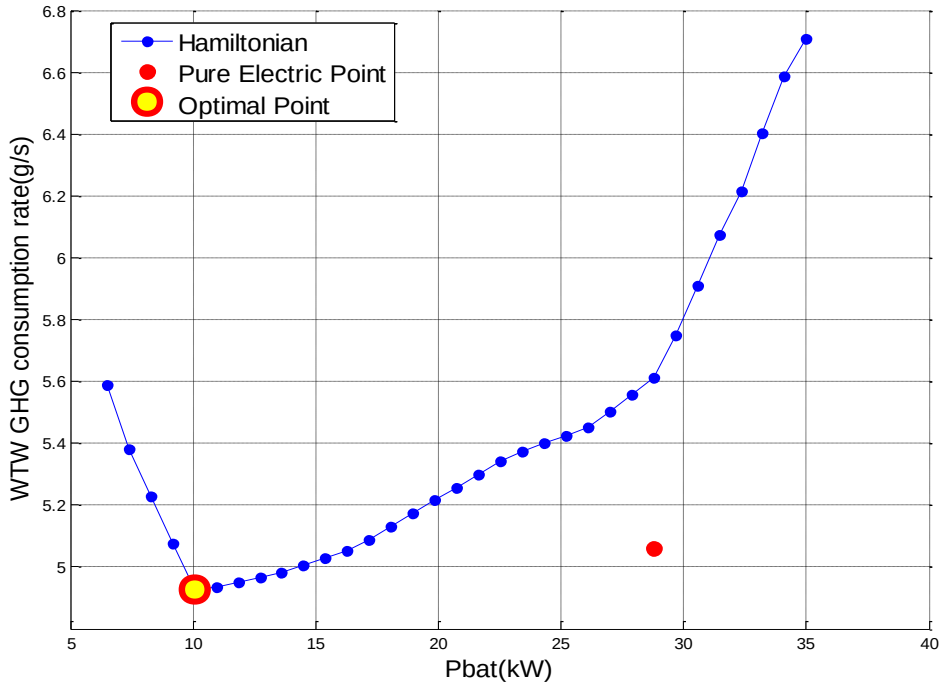

Fig 51. Hamiltonian at time step=60s for UDDS cycle.

As can be seen from Fig 52, the 2D and 1D search algorithm give very close Hamiltonians.

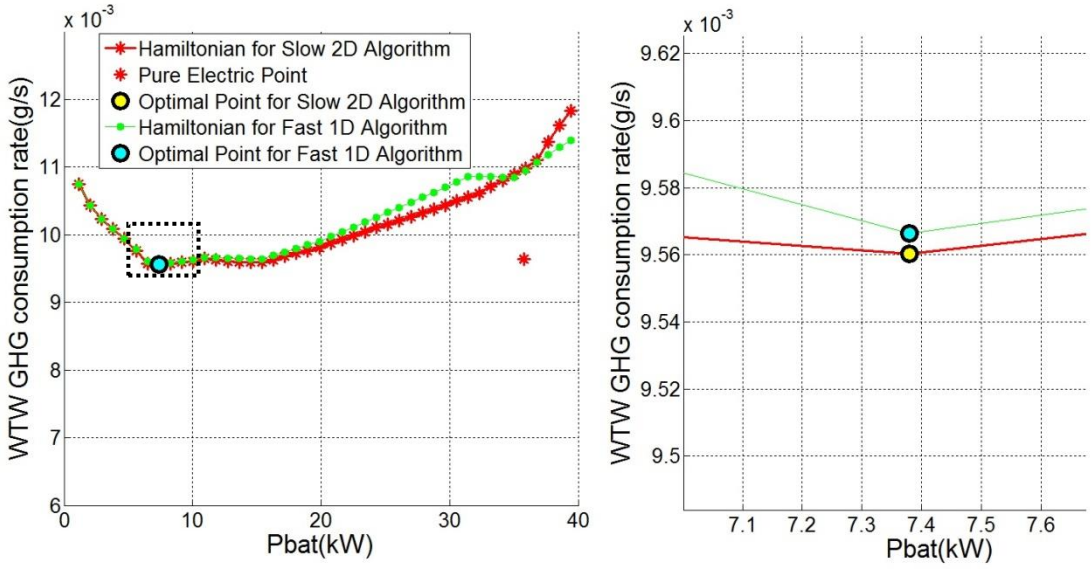

Fig 52. Comparison of the slow 2D algorithm and the fast 1D algorithm at

time t=171s under UDDS cycle.

By reducing the search map from 2D to 1D, the computational time has been significantly shortened, while the simulation results are very close between 2D and 1D algorithm, as can be seen from the simulation results shown in Table 13.

In those cases where engine map can be quadratic approximated, further computation reduction can be conducted as shown in 2.4.1, where the above presented 1D search can be reduced into a quadratic solution.

3.6 Practical Issues for Implementing the Optimal Controller

To implement the above-presented optimal control strategy into the supervisory controller used in the real vehicle, a few practical issues are going to be addressed in this section.

3.6.1 Controller Integration

The above optimal control strategy is causal and hence can be directly implementable in a real-time control architecture. The control architecture used in the vehicle is shown in Fig 53, where 3 hierarchical levels were implemented: energy management, system implementation, and sub-component control.

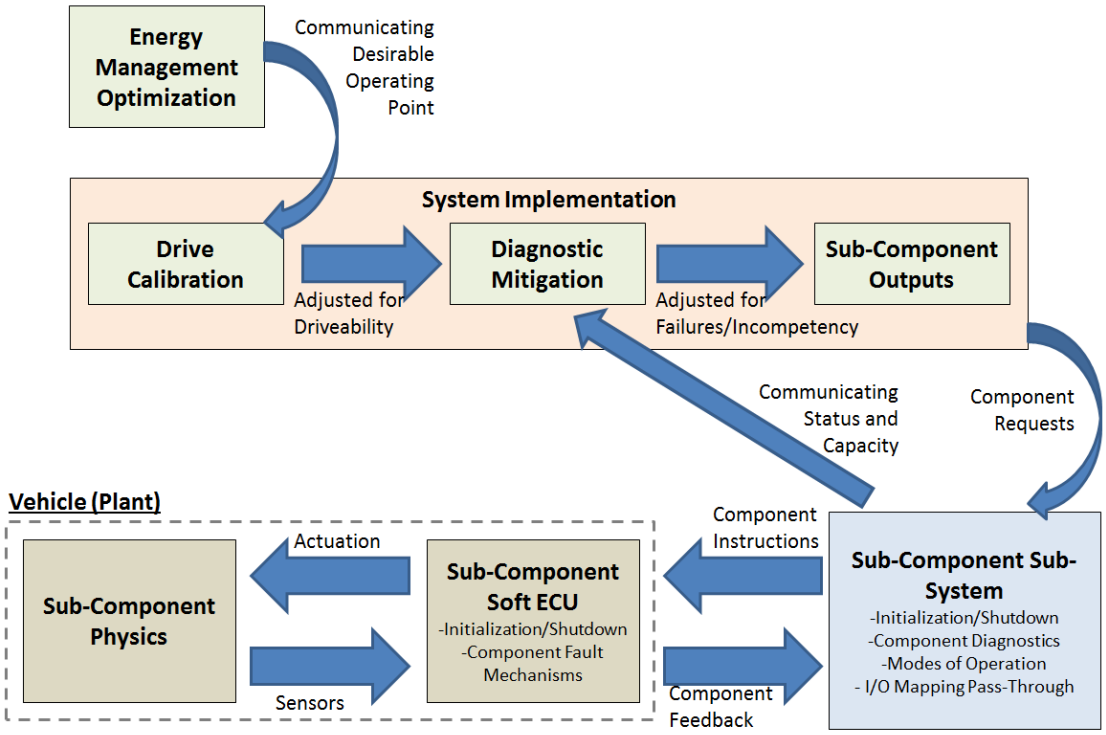

Fig 53. Optimal energy management strategy integrated in the control architecture.

The optimal control algorithm presented in the previous sections was implemented in the highest energy management level of the control system, where feedback real-time data from various vehicle system states, including ESS SOC, vehicle speed, and user torque request were sent to this level. The outputs of this level are desired torque requests for each component (confined to wheel torque level) as well as a definition of operation mode type to allow for downstream drivability filtering and mode transitioning.

The system implementation level of the control system receives primary torque requests from the energy management level and applies drivability filtering and manipulations before passing final requests down to the sub-component control level. Feedback from component level control includes instantaneous component torque limits and operational status of each component. These are used to impose constraints and overrides on the energy management level torque request outputs and transfer

commanded torque burden accordingly. Overall, these functions allow coordination between energy management level commands and sub-component level constraints. Additionally, non-strategic torque requests such as engine-start, regenerative braking and creep torque are overlaid on top of the strategic component torque requests.

The sub-component level of the control system is responsible for all low-level interaction between the supervisory controller and the individual sub-component ECU. This includes start-up and shutdown algorithms and handshaking, as well as failure detection. Real-time operational data is translated to functional values to be passed up through the logic hierarchy for decision making. In addition, low level diagnostic mitigation is invoked to accomplish actions such as switching on cooling systems or limiting component torque.

3.6.2 Drivability Restriction

In reality, drivability concerns need to be taken into consideration as crucial as energy consumption goals for the controller design. Applying the optimal control algorithm developed in the previous chapters directly to the hybrid electric vehicles might result in drivability issues such as engine frequent on/off and abrupt torque change due to mode transition, which is unacceptable in real life due to additional energy use and components wear-out as well as uncomfortable driving experience. Note that in this work, only drivability issues due to control strategy discontinuities are examined. Other drivability issues caused by driveline dynamics (such as gear change backlash) that are also present in conventional vehicle are not in the scope of this work.

For engine frequent on/off, as an example, Fig 58 shows that at some point of the UDDS driving cycle oscillation of engine on/off occurs when applying the above optimal control algorithm. Close investigation of the resulting control algorithm has indicated that engine on/off oscillation was mainly due to the selection between pure-electric point and engine-on point for consecutive operating points. This can be

explained by examining the Hamiltonian of the two consecutive operating points for UDDSx10 cycle, as shown in Fig 54, where the pure electric point happens to have a very close value compared to the lowest point of the Hamiltonian curve. This has caused the frequent switch between the pure electric point and the Hamiltonian bottom point for the consecutive operating points due to small changes of the vehicle state, and hence frequent engine on and off.

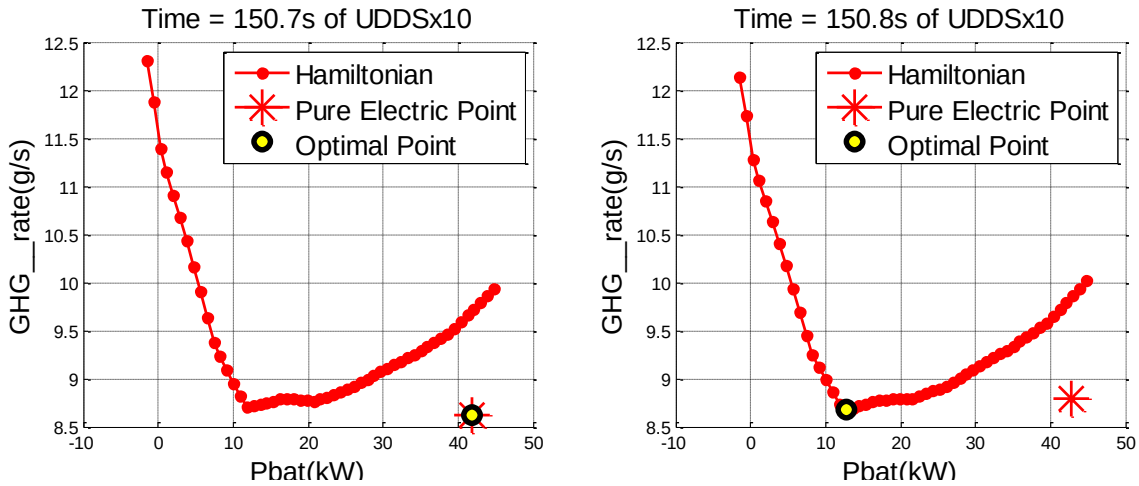

Fig 54. Hamiltonian of two consecutive operating points of UDDSx10 cycle.

To overcome the above engine frequent on/off issue, two approaches have been investigated to amend the original optimal control algorithm.

A. Applying an engine-on hysteresis filter to the computed torque request.

A first attempt to address the engine frequent on/off issue was to apply an engine-on hysteresis filter in the controller. In control systems, hysteresis can be used to filter signals to avoid frequent switch of the output, by taking recent history into account[7].

In this work, the engine-on hysteresis filter was implemented as follows: After engine is turned on, it will be able to turn off only after a pre-defined amount of time. Similarly, after engine is turned off, there will be a minimum 'engine-stay-off' time for it to be turned on. This time hysteresis filter was applied to the engine-on command generated from the original optimal controller described previously.

Fig 55 shows the resulting engine-on command after the hysteresis filter during the UDDS cycle, where 'engine-stay-on' and 'engine-stay-off' minimum time are both set to 2 seconds in this work, which is determined by a trial-and-error process. As can be seen, the frequent switches between engine on/off at around time=182-186 second are eliminated. Note that when the engine is forced to keep off, the torque initially assigned to engine needs to be re-assigned to the motors so that the driver request can still be satisfied.

However, a major drawback of applying the above hysteresis filter for engine-on command is that the 'spike' (for example, at time = 177s of UDDS as shown in Fig 55 and at time = 210s as shown in Fig 58) cannot be eliminated in this way.

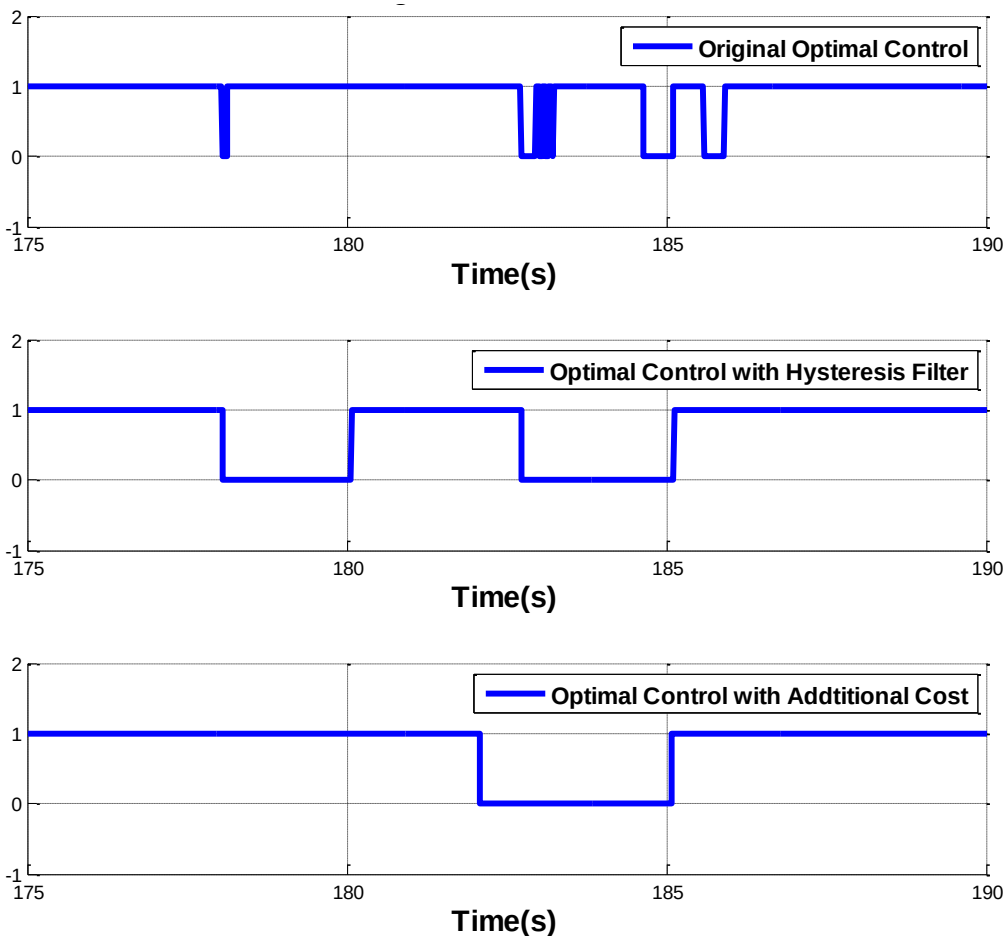

Fig 55. Engine-ON command generated by different control algorithms during UDDS cycle.

B. Assigning additional fuel cost due to engines on/off to the cost function (Hamiltonian in this case).

In this approach, an additional fuel cost item is added to the cost function defined in (78). This additional cost will be assigned a value when either engine-switch-on or engine-switch-off event is detected based on the current engine-on command generated by the optimal controller and the engine-on state in the last time step.

$$J = \int_{t_0}^{t_f} [(\dot{m}_{fuel}(t) + \dot{m}_{engOn}(t)) \cdot \eta_{FSE} \cdot \eta_{PEU,fuel} + P_{bat}(t) \cdot \eta_{PEU,elec}]dt$$
$$\dot{m}_{engOn}(t) = \begin{cases} 0.6 \text{ kg/s} & \text{when engine turns ON} \\ 0.3 \text{ kg/s} & \text{when engine turns OFF} \end{cases} \quad \textbf{(78)}$$

Fig 56 shows the Simulink model used to implement this additional cost item and Fig 57 shows the truth table used for determining the additional fuel cost.

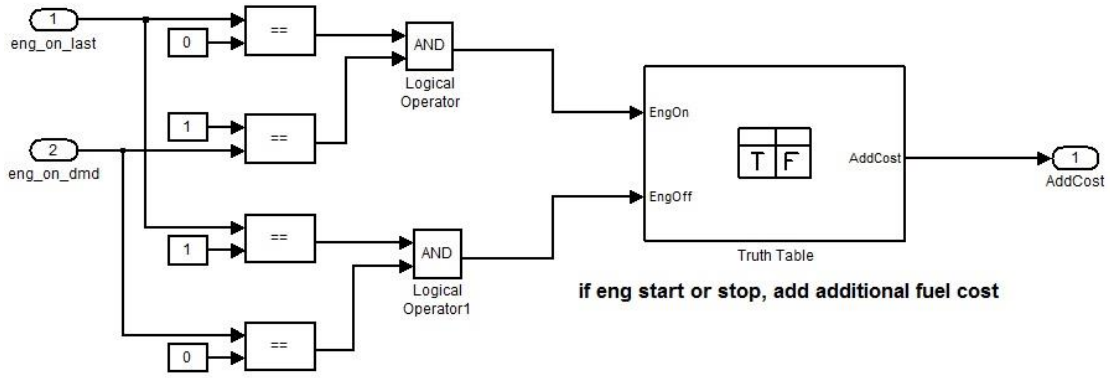

Fig 56. Additional fuel cost in the Simulink model.

Condition Table

	Description	Condition	D1	D2	D3	D4
1	Engine switch to ON	EngOn == 1	T	F	T	F
2	Engine switch to OFF	EngOff == 1	T	T	F	F
		Actions: Specify a row from the Action Table	1	2	3	4

Action Table

#	Description	Action
1	error	AddCost = NaN;
2	Engine switch to OFF	AddCost = 0.0006;
3	Engine switch to ON	AddCost = 0.0003;
4	Engine remains in its previous state	AddCost = 0;

Fig 57. Truth table for the additional fuel cost item.

According to the logic shown in Fig 56, an engine-switch-on event is detected when engine-on state in the last time step is OFF and the current engine-on demand is ON. An additional fuel cost will be added to the non-pure-electric points in the Hamiltonian curve shown in Fig 54, which means that the non-pure-electric curve will be translated up for a predefined value making it 'harder' for engine to switch on. Similarly, an engine-switch-off event is detected when engine-on state in the last time step is ON and the current engine-on demand is OFF, and an additional fuel cost will be added to the pure-electric point shown in Fig 54. The value of the additional cost (as shown in Fig 57) was determined such that the Hamiltonian in Fig 54 can be significantly impacted in terms of selecting between the bottom point of the non-electric Hamiltonian curve (which is engine-on case) and the pure-electric point (engine-off case).

As a result, Fig 55 and Fig 58 shows that engine operation on UDDS cycle. As can be seen, the engine on/off oscillation has been eliminated. Compared to the engine-on hysteresis filter approach, those individual spikes (for example, at time = 210s as shown in Fig 58) are also eliminated.

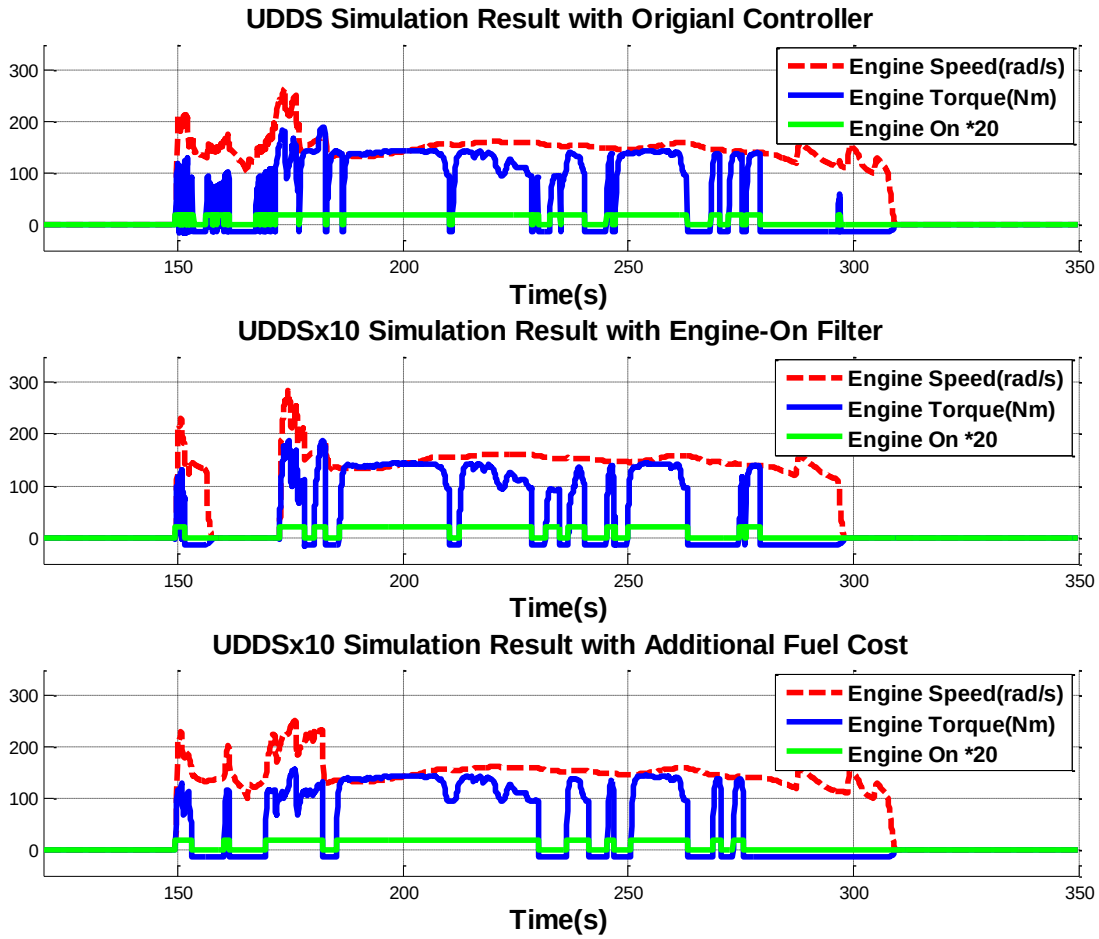

Fig 58. Engine Speed and Torque on UDDSx10 cycle.

Another drivability issue was found during mode transition especially when the vehicle switches between engine/BAS motor parallel mode (transmission in gear) and EV-only mode (transmission in neutral). Such mode transition if using original target torque request generated directly from the optimal control strategy without additional control mechanism could cause unacceptable driveline jerks due to abrupt change in components' commanded torques, as can be observed in Fig 59.

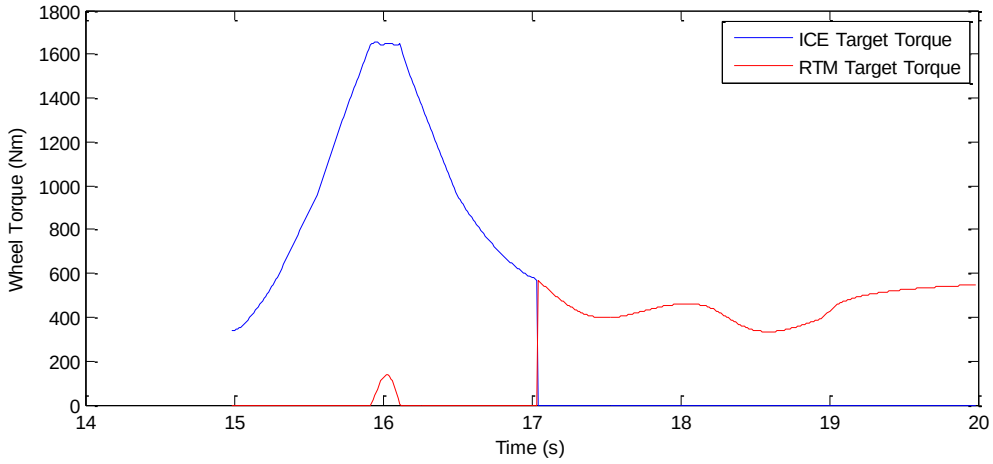

Fig 59. Target torque request during mode transition from series-parallel to EV-only mode.

To allow for a smooth torque change during mode transition, a hyperbolic tangent function (shown in Fig 60) was used to generate smooth transition torques to override the original torque requests. This was implemented in the 'drive calibration' module shown in Fig 53. When there is a mode transition signal detected, the original target torque request generated from the optimal energy management module will be overridden by the smooth torques resulted from the hyperbolic tangent function during the mode transition period, as shown in Fig 61.

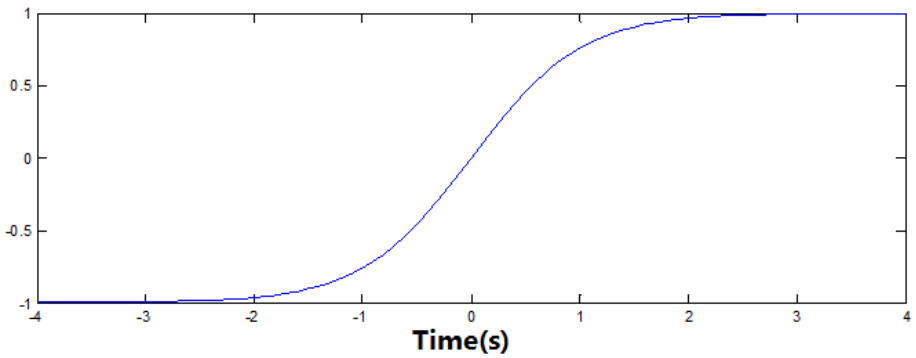

Fig 60. Hyperbolic tangent function used for smooth mode transition.

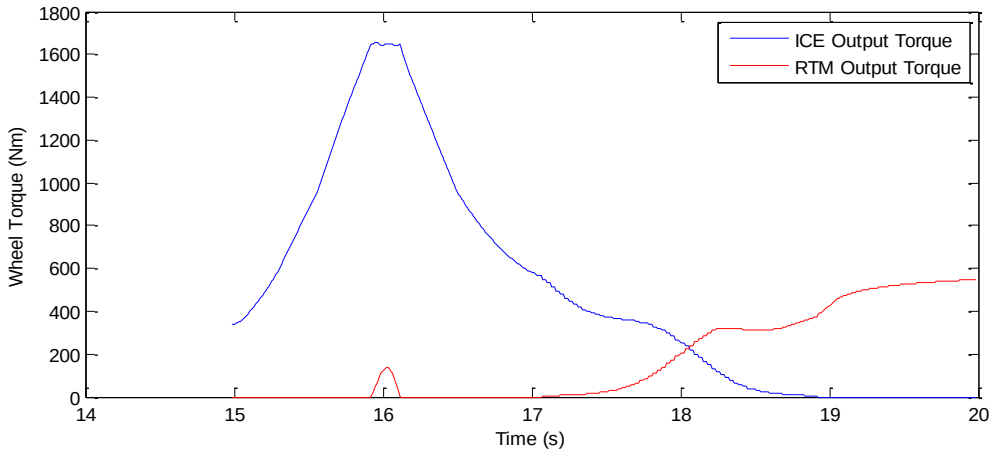

Fig 61. Overridding torque request during mode transition from series-parallel to EV-only mode.

3.7 Simulation Results of the PHEV Optimal Control Algorithm

Based on the powertrain model described in Section 3.2, various control algorithms have been tested in the simulation environment. The simulation time step was set to 0.01s, which was short enough to catch individual component's dynamic response time. The vehicle use E85 fuel and all energy consumption were calculated based on E85 fuel specification.

The control strategy first used a constant value for the costate p and after the battery SOC reaches its charge sustaining set point (0.2 in this study), a PI type of controller was activated to adapt the value of p preventing SOC drifting away from its CS level.

Table 13 shows the fuel energy consumption for different control algorithms (all used WTW GHG as the cost function) and their computation time on the same UDDSx10 cycle. As can be seen, the PMP algorithms have improved the WTW GHG by 3-5%. The slow PMP algorithm, which took 2D search at each time steps, gave the best WTW GHG improvement, while its computational burden was the heaviest. Among all algorithms, the fast PMP with adaptive costate p was the best one that has balanced energy consumption, computation efficiency, drivability, as well as the ability

for practical implementation, since only driving distance was needed for this algorithm.

Table 13. WTW GHG emissions for different control strategies on the same UDDSx10 cycle.

	Fuel Economy MPG	WTW GHG (g CO2/km)	CO2 Emission Improvement*	Computation Time** (Sample Time=0.01s)
Mild-hybrid: Production Malibu	26.64	774	/	/
PHEV: Rule-based	50.31	140.38	(baseline)	10min
PHEV: Slow PMP with fixed p	73.59	122.40	13.12%	6h
PHEV: Fast PMP with fixed p	67.22	126.46	9.92%	20min
PHEV: Fast PMP with adaptive p	63.89	129.33	7.87%	20min

* Compared to the baseline model.

** For 1 iteration, with same plant model and driver model, on a 32GB, 4 core, 2.5GHz computer.

Fig 62 shows the well-to-wheel Petroleum Energy Use (PEU) consumptions (Wh PE/km) for the fast PMP control strategy (where constant costate p was used and the cost function was set to minimize WTW PEU) proposed in 3.5 on UDDSx10 cycle (distance=119.5km). As can be seen, the lowest PEU consumption is obtained when battery SOC is just depleted at the end of the trip. Note that after SOC reaches 0.2, SOC is kept around its CS level by the PI controller (such as the case when p = -13 and -15 in Fig 62). According to PMP theory, with the same final SOC at 0.2, the optimal SOC trajectory is resulted from the constant costate p used over the whole driving cycle, which is the one that depletes battery almost linearly with distance until the end of the trip.

The algorithm with adaptive p results in a SOC trajectory (as well as the value of

PEU consumption) very close to the one with constant p that depletes SOC at the trip end. In comparison, the rule-based algorithm adopted a CD-CS strategy and the WTW PEU is 18% higher.

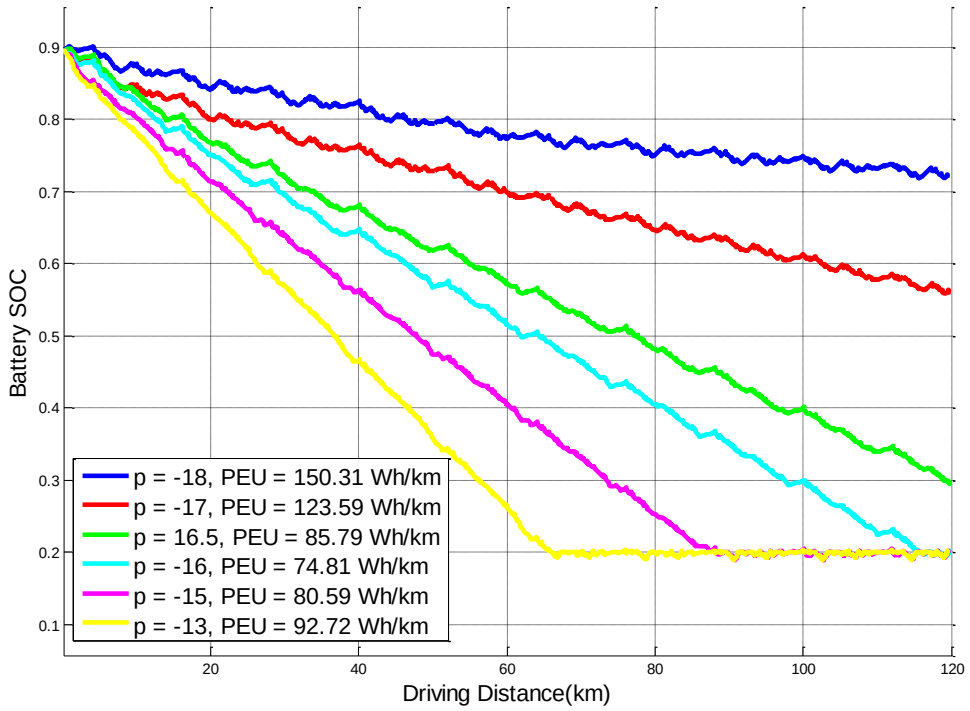

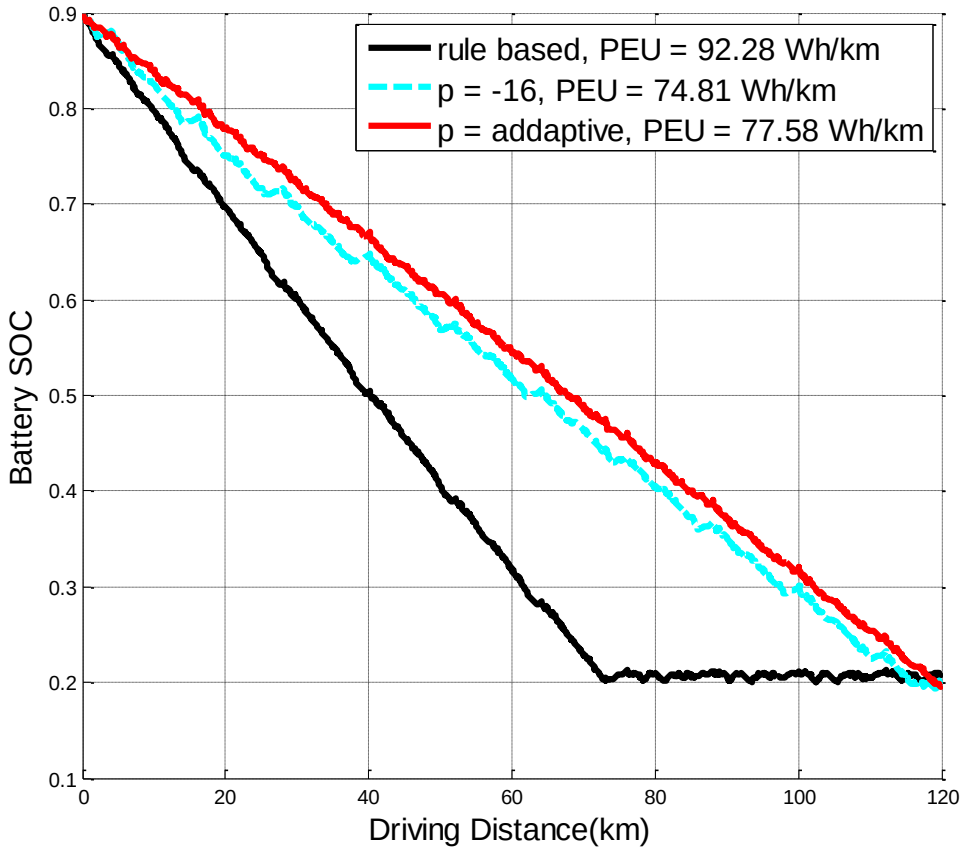

Fig 62. SOC trajectories and Well-to-Wheel Petroleum Energy Use (PEU) under different value of costate p for UDDSx10.

Fig 63 shows very similar results for WTW GHG emission when using the fast PMP algorithm (where the cost function was set to minimize WTW GHG) as the case for WTW PEU.

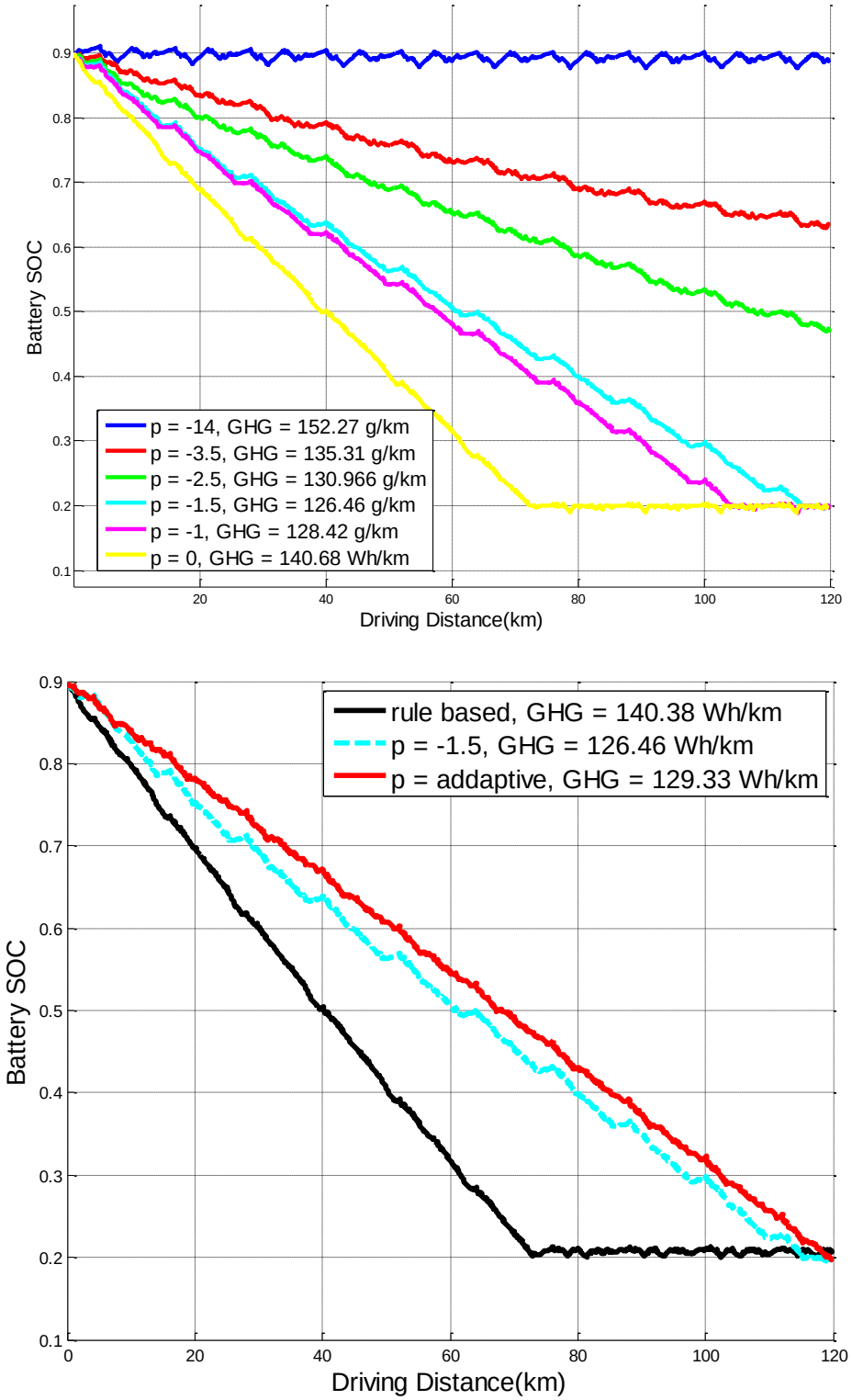

Fig 63. SOC trajectories and Well-to-Wheel Greenhouse Gas (GHG) emission under different value of costate p for UDDSx10.

Close investigation on various driving cycles (Fig 64 - Fig 65) has shown that

lowest WTW PEU and MPG have been always achieved when SOC was just depleted at the end of the trip, no matter using WTW PEU or using WTW GHG as the cost function.

While for WTW GHG, when using WTW GHG as the cost function, with the same final SOC, the lowest GHG was always achieved at trip end (that means a constant co-state was used instead of a varying co-state), which is consistent with the optimal control theory. While for those aggressive highway cycles (HWFETx8, INRETS_HWYx3), even lower WTW GHG was observed when final SOC was higher than its charge sustaining level (0.2). This was due to the fact that the GHG factor value (shown in Table 11) for electricity is much higher than for E85 fuel and aggressive highway cycles usually consume more electricity than city cycles, which has caused the optimal point to shift towards the situation with higher final SOC(when less electricity was used). But since lowest PEU and MPG always happens when SOC was just depleted at the end of the trip, taking all three factors (PEU, MPG and GHG) into consideration would make the proposed distance-dependent optimal strategy (which depletes SOC at the trip end) still a good solution.

In addition, when using WTW PEU as the cost function, even with the same final SOC, the lowest WTW GHG was not achieved at the trip end for those aggressive highway cycles (HWFETx8, INRETS_HWYx3, US06x10). This was further due to the reason that the cost function was set to optimize PEU in this case, and therefore GHG was not optimized.

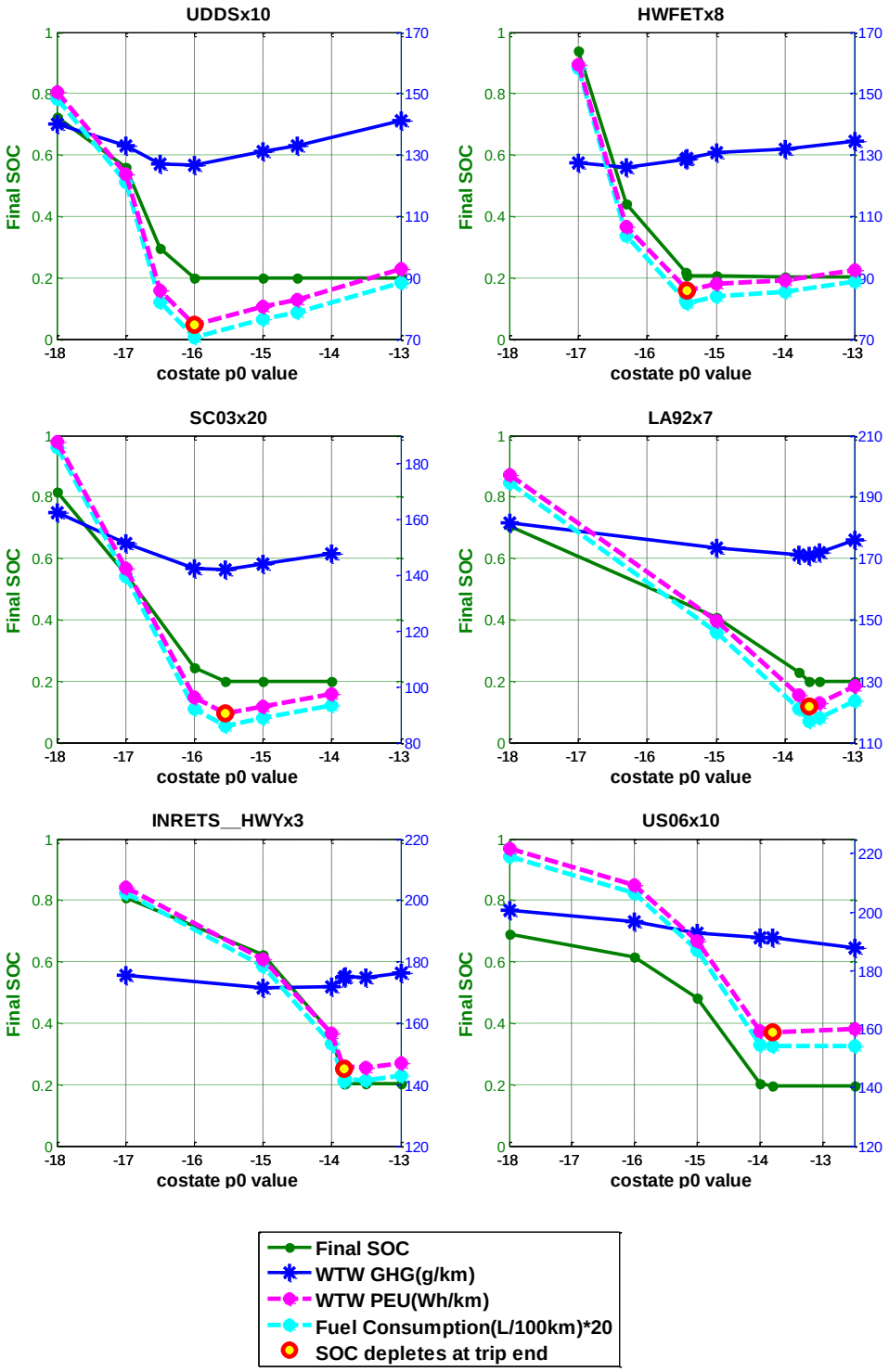

Fig 64. Sensitivity study of the costate p0 for different driving cycles when using WTW PEU as the cost function.

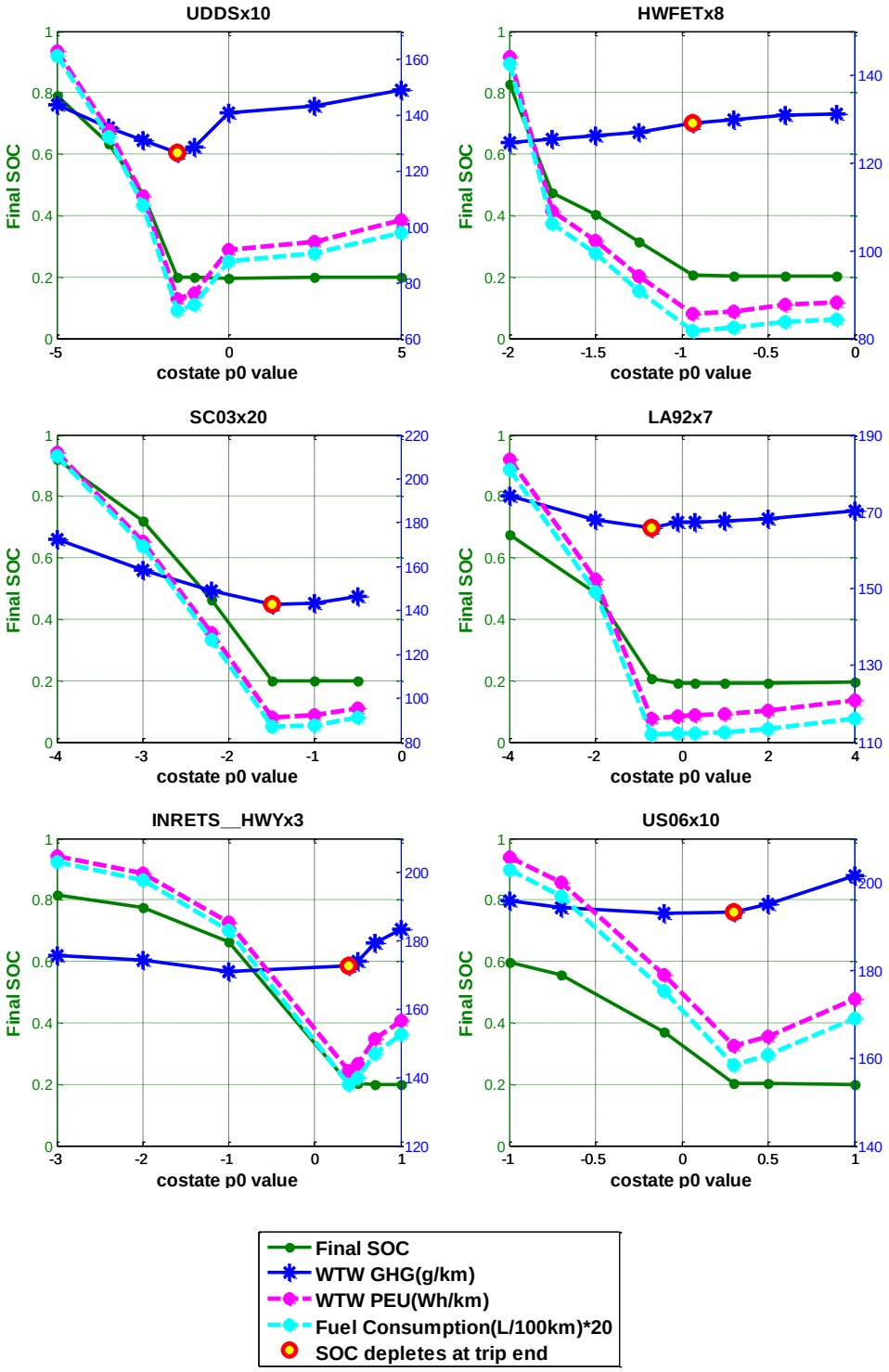

Fig 65. Sensitivity study of the costate p0 for different driving cycles when using WTW GHG as the cost function.

Table 14 shows the well-to-wheel PEU consumptions (Wh PE/km) of the proposed control strategies on various driving cycles. As can be seen, the WTW PEU consumption has been significantly improved by using the fast PMP algorithm on all driving cycles. While for WTW GHG (as shown in Table 15), the improvement is less significant comparing to the case for WTW PEU.

Table 14. WTW PEU(Wh PE/km) for different control strategies on various driving cycles

	UDDS x10	**HWFET x8**	**SC03 x20**	**INRETS_ HWYx3**	**LA92 x7**	**US06 x10**
Rule-based	92.28	100.06	108.03	153.95	129.80	169.12
Fast PMP with fixed p	74.81	85.67	90.30	145.23	121.69	158.71
Fast PMP with adaptive p	77.58	85.25	93.24	145.02	124.29	161.77
Improvement*	15.93%	14.80%	13.69%	5.8%	4.24%	4.35%

* Fast PMP with adaptive p with eng-on filter compared to the baseline model in terms of WTW PEU consumption.

Table 15. WTW GHG(g CO2/km) for different control strategies on various driving cycles

	UDDS x10	**HWFET x8**	**SC03 x20**	**INRETS_ HWYx3**	**LA92 x7**	**US06 x10**
Rule-based	140.38	135.2	149.68	176.621	169.55	192.08
Fast PMP with fixed p	126.46	129.15	142.48	172.706	165.64	193.6
Fast PMP with adaptive p	129.33	128.35	144.57	174.977	166.1	196.11
Improvement*	7.87%	5.07%	3.41%	0.93%	2.03%	-2.09%

* Fast PMP with adaptive p with eng-on filter compared to the baseline model in terms of WTW GHG emission.

3.8 HIL Validation of the PHEV Optimal Control Algorithm

In this study, following the model-based-design (MBD) process, two sets of plant

model were developed: a simplified control-oriented plant model to allow initial conceptual validation of the optimal control algorithm and a more sophisticated implementation-oriented plant model based on dSPACE Automotive Simulation Models (ASM) tool, where I/O interface was exactly the same as in the real vehicle.

After the proposed fast PMP algorithm was validated in MIL environment using the simplified simulation model, it was then migrated to the more complex model and integrated with other system modules (such as subsystem diagnostic modules) in the rapid prototype controller (MicroAutobox II). Ultimately, the supervisory control system will be implemented in embedded control hardware and run in real time. An efficient and effective way to test and validate the real-time performance of the embedded controller without connecting it to the "real plant" is needed. Controller HIL is a powerful tool that enables a high level of controller validation even before the actual vehicle and/or components are available for testing. The exact behavior of how the controller will function in the real vehicle can therefore be determined.

In this study, rather than using an embedded ECU, the compiled code of the supervisory controller was downloaded into MicroAutoBox II for HIL real-time test, which is more convenient in terms of implementation for performing rapid control prototyping in fullpass and bypass scenario.

As shown in Fig 23, the supervisory controller model was compiled into production C code by using MATLAB Coder^{TM} and downloaded the compiled code into MicroAutobox II by using dSPACE ControlDesk software for HIL real-time test (shown in Fig 23). At the same time, the plant model in Simulink was compiled into C code as well and downloaded to the dSPACE simulator through ControlDesk.

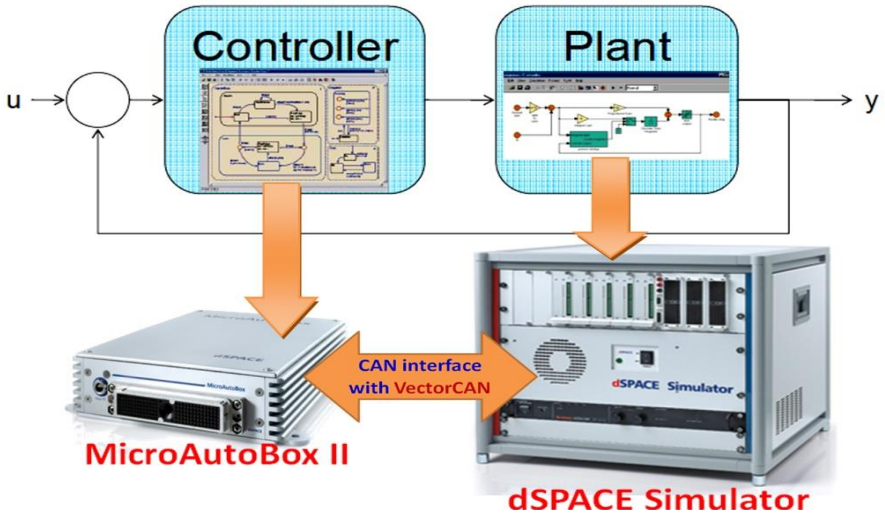

Fig 66. Hardware-in-the-loop test illustration.

Fig 67 shows the HIL test setup in the lab. A 12V power supply provides power for both the dSPACE simulator and MicroAutobox II. The MicroAutobox II communicated with the dSPACE simulator through CAN bus configured by using VectorCAN software. The dSPACE real-time simulator, where the plant model is downloaded to, receives electrical signals from the hardware controller (in this case MicroAutobox II) as actuator commands to drive the plant, and converts these signals into the physical variables connected to the plant model. The plant model calculates the physical variables that represent the outputs of the plant, which are converted into electrical signals that represent the voltages produced by the sensors that feed back to the controller. All the variables in both the dSPACE simulator and MicroAutobox II can be monitored in real time through ControlDesk interface in desktop computer, as shown in Fig 67.

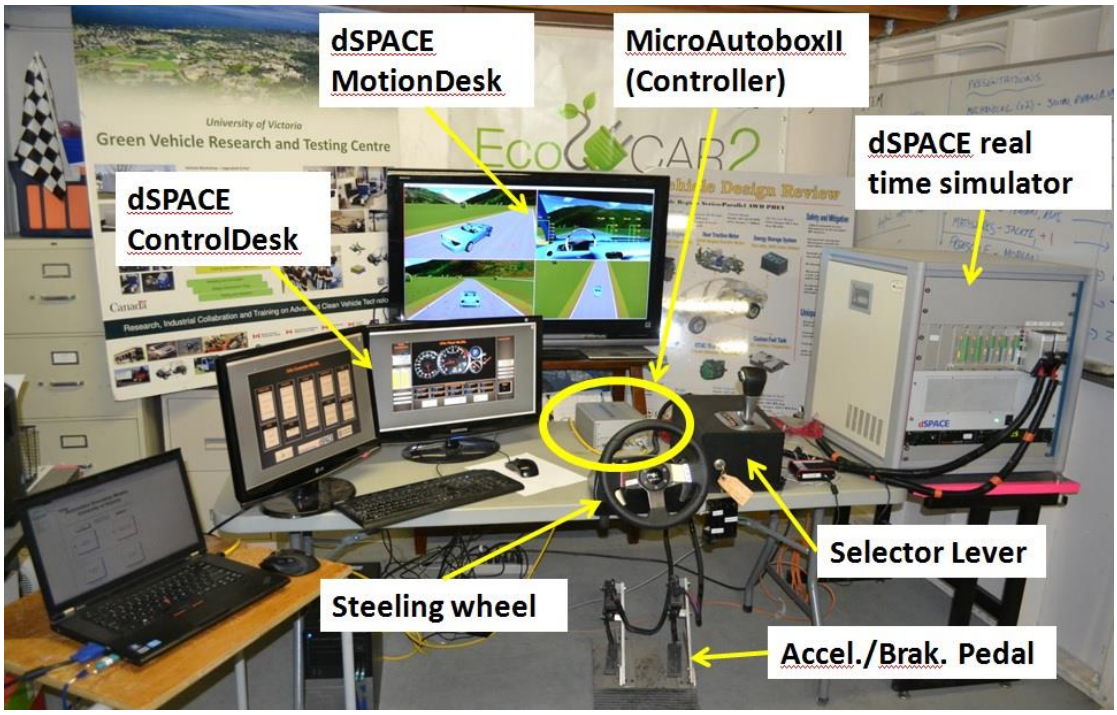

Fig 67. Driver-in-the-loop HIL setup.

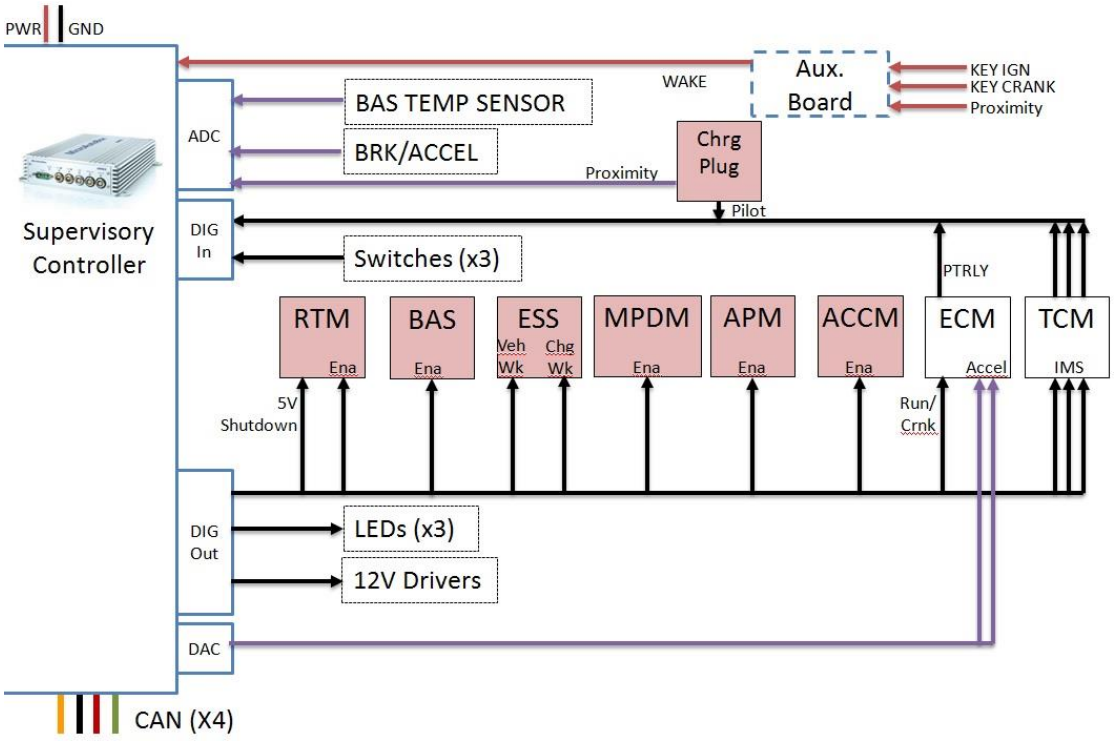

Fig 68. Supervisory controller connections.

Fig 68 shows the supervisory controller's connections to various sub-systems in the vehicle.

The HIL simulation results in ControlDesk over standard Urban Dynamometer Driving Schedule (UDDS) cycle (shown in Fig 69) shows that the proposed PMP algorithm is able to run fast enough in real time and track the predefined driving cycle very well.

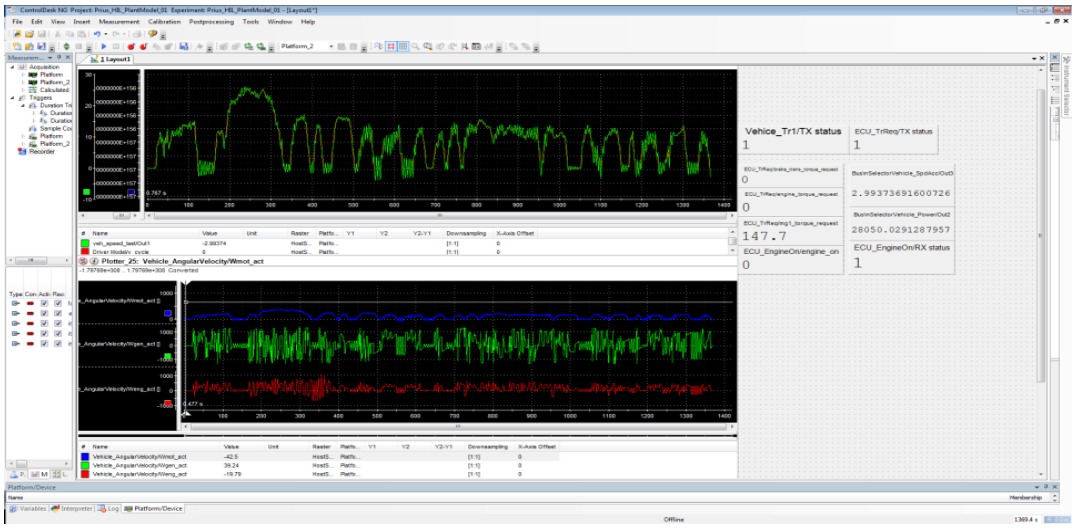

Fig 69. UDDS results in ControlDesk.

Other than HIL test and validation, a Vehicle-in-the-loop (VIL) test was also conducted. This was realized by using the bypass rapid prototyping as shown in Fig 70, where code is generated from the developed controller model via ControlDesk and was then cross-compiled and downloaded to the high-speed, floating-point, rapid-prototyping computer (in this case MicroAutobox II) where it executed in real time. The controller parameters are tweaked “on-the-fly” during test drives or in the lab involving the actual plant (e.g. engine, electric motor) and allowing for the insertion of new code to bypass existing ECU code. Success is declared when performance requirements are met, proving that the new algorithm is feasible.

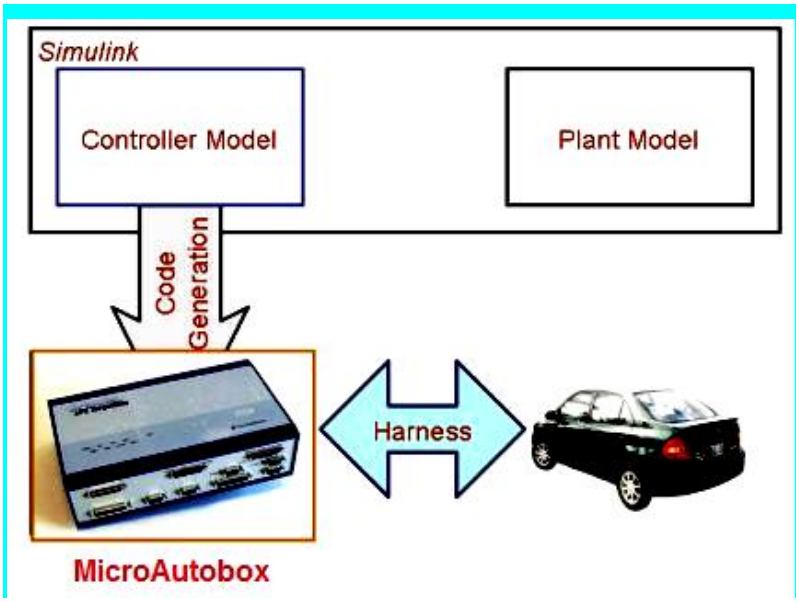

Fig 70. Bypass rapid prototyping

Chapter 4. Conclusions and Future Work

4.1 Summary

In this work, a systematic methodology for solving HEV and PHEV optimal energy management problem was presented. Two case studies have been used for developing online energy management strategy for both hybrid electric vehicle and plug-in hybrid electric vehicle.

The well-known Toyota Prius power-split hybrid powertrain was first used as a case study for developing online energy management strategy for hybrid electric vehicle, which is the representative of the power-split (input-split) hybrid powertrain systems. An analytical formalization of the optimal control problem for HEV associated with both offline and online (real-time) solution for the energy management problem, as well as the HIL real-time validation of the proposed control algorithm was presented. Both offline optimal control solution (based on DP, QP and PMP with constant costate) and a close-to-optimal online solution (based on PMP with adaptive costate) was developed, which is online implementable with fast computation speed and is applicable to general hybrid electric powertrains.

The second case study focusing on PHEV optimal control was an extended study based on the EcoCAR2 project, where a 2013 GM Chevrolet Malibu was retrofitted into a PHEV to improve energy efficiency, reduce emissions while retaining and increasing performance. Following the model-based-design (MBD) process, two sets of plant model were developed: a simplified control-oriented plant model to allow initial conceptual validation of the optimal control algorithm and a more sophisticated implementation-oriented plant model based on dSPACE Automotive Simulation Models (ASM) tool, where I/O interface was exactly the same as in the real vehicle.

Based on the above vehicle model, a real-time optimal control algorithm was developed, which identifies the optimal operational mode and the corresponding torque

split among each components at each time step. The control objective in this study was to minimize the well-to-wheel energy use (PEU and GHG), where both the fuel and electric energy consumption was taken into account. The optimal torque split was computed based on Pontryagin's Minimum Principle. Since the powertrain system has a degree of freedom of two in terms of free control variables, a 2D search algorithm were initially developed to find the optimal point. To reduce the computational burden, the 2D search algorithm was further converted into a 1D search algorithm based on optimization techniques. For practical implementation, an adaptive technique was utilized to update the equivalence factor based on battery SOC and current driving distance.

The proposed fast PMP algorithm was first investigated through Model-in-the-loop (MIL) simulation tests by using the simplified vehicle model. Simulation results have shown that the PMP algorithms have improved the PEU consumption by 3-5% when comparing to the baseline rule-based controller and the lowest PEU consumption was obtained when battery SOC is just depleted at the end of the trip. Among all algorithms, the fast PMP with adaptive costate p was the best one that has balanced both energy consumption and computation efficiency, as well as the ability for practical implementation, since only driving distance was needed for this algorithm.

After the control algorithm was validated in the MIL environment, it was then migrated to the more complex model and integrated with other system modules (such as subsystem diagnostic modules) in the rapid prototype controller (MicroAutobox II). The real-time performance of the developed controller was investigated through the rapid-prototyping controller HIL platform, where plant model was uploaded into dSPACE midsize real-time simulator and the controller model was uploaded into MicroAutobox II. HIL simulation has proved that the proposed control algorithm is able to run in real time and can track the driving cycle very well.

4.2 Outlook

Since HEV and especially PHEV optimal control is highly trip dependent, future research can be focused on predicting the future trip to facilitate the optimal energy management for hybrid vehicles. With the rapid development of intelligent transportation systems (ITS), geographical information systems (GIS), global positioning systems (GPS), vehicle-to-vehicle (V2V) and vehicle-to-infrastructure (V2I) interactions, drive cycle modeling and prediction becomes possible based on trip data accessed in real-time. Machine learning techniques can also be applied to learn the historical and current traffic patterns so as to better adapt to different driving cycle and driver's style.

Further research could also look at applying predictive control using a receding prediction horizon once the drive cycle modeling and prediction becomes available. The proposed fast-computing QP algorithm in this study can be applied within a Model Predictive Control (MPC) structure using a moving finite prediction time-horizon to make it real-time implementable.

Moreover, in real applications, energy management strategies have to take further into account other objectives such as emissions, the battery state of health, industry standard drivability and etc.

Bibliography

1. Simpson, A., "Cost-Benefit Analysis of Plug-In Hybrid Electric Vehicle Technology," in *22nd International Battery, Hybrid and Fuel Cell Electric Vehicle Symposium and Exhibition (EVS-22)* 2006: Yokohama, Japan.
2. *U.S. Regular Gasoline Prices*. 2014, U.S. Energy Information Administration |.
3. *The Electric Power Monthly*. 2013, U.S. Energy Information Administration.
4. Wikipedia. *Plug-in hybrid*. 2013; Available from: http://en.wikipedia.org/wiki/Plug-in_hybrid.
5. Dong, J., Z.Dong, and C. Crawford. "Review of Continuously Variable Transmission Powertrain System For Hybrid Electric Vehicles," in *ASME 2011 International Mechanical Engineering Congress & Exposition*. 2011. Denver, Colorado, USA.
6. Keith, B.W., "ADVISOR 2.1: a user-friendly advanced powertrain simulation using a combined backward/forward approach," *IEEE Transactions on Vehicular Technology*, **48** (6), 1999.
7. Ganesh Mohan, F.A., Stefano Longo, *Comparative analysis of forward-facing models vs backward-facing models in powertrain component sizing*, in *IET 4th Hybrid and Electric Vehicles Conference (HEVC13), 2013*. 2013.
8. Rousseau, A., Sharer, P., and Pasquier, M., *Validation Process of a Hev System Analysis Model: PSAT*. SAE Paper 2001-01-0953, 2001.
9. V.Gopal, R. and A.P. Rousseau, *System Analysis Using Multiple Expert Tools*, in *SAE 2011 World Congress & Exhibition*. 2011: Detroit, MI, USA.
10. Namdoo Kim, R.C., Forrest Jehlik and Aymeric Rousseau, *GM Tahoe HEV Model Development in PSAT*. SAE 2009-01-1307, World Congress, April 2009.
11. Salmasi, F.R., *Control Strategies for Hybrid Electric Vehicles: Evolution, Classification, Comparison, and Future Trends.* Vehicular Technology, IEEE Transactions on, 2007. **56**(5): p. 2393-2404.
12. Lee, H.D.a.S., S.K.,, *Fuzzy-Logic-Based Torque Control Strategy for Parallel-Type Hybrid Electric Vehicle.* IEEE Transactions on Industrial Electronics, **45** (4), 1998.
13. Schouten, N., Salman, M., Kheir, N.,, *Fuzzy Logic Control for Parallel Hybrid Vehicle. IEEE Transactions on Control Systems Technology* 2002. **Vol. 10, No. 3**.
14. Chan-Chiao, L., et al., *Power management strategy for a parallel hybrid electric truck.* Control Systems Technology, IEEE Transactions on, 2003. **11**(6): p. 839-849.
15. Delprat, S., et al., *Control of a parallel hybrid powertrain: optimal control.* Vehicular Technology, IEEE Transactions on, 2004. **53**(3): p. 872-881.
16. Jinming, L. and P. Huei, *Modeling and Control of a Power-Split Hybrid Vehicle.* Control Systems Technology, IEEE Transactions on, 2008. **16**(6): p. 1242-1251.
17. Tulpule, P., V. Marano, and G. Rizzoni. *Effects of different PHEV control*

strategies on vehicle performance. in *American Control Conference, 2009. ACC '09.* 2009.

18. Chan-Chiao Lin, H.P., J. W. Grizzle, Jason Liu and Matt Busdiecker, *Control System Development for an Advanced-Technology Medium-Duty Hybrid Electric Truck.* SAE Paper 2003-01-3369, 2003: p.
19. Bellman, R.E., *Dynamic Programming*. 1957, Princeton: NJ: Princeton, University Press.
20. Magnus Neuman, H.S., Bo Wahlberg, *Rule-Based Control of Series HEVs Derived from Deterministic Dynamic Programming*. 2008, Royal Institute of Technology, Stockholm, Sweden.: http://www.diva-portal.org/smash/get/diva2:472116/FULLTEXT01.pdf.
21. T. Leroy, F.V.-N., P. Tona, *Stochastic Dynamic Programming based Energy Management of HEV's: an Experimental Validation*, in *19th World Congress The International Federation of Automatic Control (IFAC), August 24-29, 2014*. 2014: Cape Town, South Africa.
22. Tate, E.D., J.W. Grizzle, and H. Peng, *Shortest path stochastic control for hybrid electric vehicles.* International Journal of Robust and Nonlinear Control, 2008. **18**(14): p. 1409-1429.
23. Borhan, H., et al., *MPC-Based Energy Management of a Power-Split Hybrid Electric Vehicle.* Control Systems Technology, IEEE Transactions on, 2011. **PP**(99): p. 1-11.
24. Wang, W., et al. *Model predictive control-based controller design for a power-split hybrid electric vehicle*. in *Modelling, Identification & Control (ICMIC), 2014 Proceedings of the 6th International Conference on*. 2014.
25. Borhan, H.A., et al. *Predictive energy management of a power-split hybrid electric vehicle*. in *2009 American Control Conference*. 2009.
26. Prokhorov, D. *Toyota Prius HEV neurocontrol*. in *Neural Networks, 2007. IJCNN 2007. International Joint Conference on*. 2007.
27. Murphey, Y.L., et al., *Intelligent Hybrid Vehicle Power Control—Part I: Machine Learning of Optimal Vehicle Power.* IEEE Transactions on Vehicular Technology, 2012. **61**(8): p. 3519-3530.
28. Murphey, Y.L., et al., *Intelligent Hybrid Vehicle Power Control—Part II: Online Intelligent Energy Management.* IEEE Transactions on Vehicular Technology, 2013. **62**(1): p. 69-79.
29. Wirasingha, S.G. and A. Emadi, *Classification and Review of Control Strategies for Plug-In Hybrid Electric Vehicles.* Vehicular Technology, IEEE Transactions on, 2011. **60**(1): p. 111-122.
30. Amgad Elgowainy, A.B., Michael Wang, John Molburg, and Aymeric Rousseau, *Well-To-Wheels Energy Use and Greenhouse Gas Emissions of Plug-in Hybrid Electric Vehicles.* SAE Int. J. Fuels Lubr. , 2009: p. 2(1):627-644.
31. Rui, W. and S.M. Lukic. *Dynamic programming technique in hybrid electric vehicle optimization*. in *Electric Vehicle Conference (IEVC), 2012 IEEE International*. 2012.

32. Chen, Z. and A. Vahidi, *Route Preview in Energy Management of Plug-in Hybrid Vehicles.* Control Systems Technology, IEEE Transactions on, 2012. **20**(2): p. 546-553.

33. Langari, R. and W. Jong-Seob, *Intelligent energy management agent for a parallel hybrid vehicle-part I: system architecture and design of the driving situation identification process.* Vehicular Technology, IEEE Transactions on, 2005. **54**(3): p. 925-934.

34. Phillip B. Sharer, A.R., Dominik Karbowski, Sylvain Pagerit, *Plug-in Hybrid Electric Vehicle Control Strategy: Comparison between EV and Charge-Depleting Options.* SAE Technical Paper 2008-01-0460, 2008.

35. R. Edwards, J.-F.L., J-C. Beziat, *Well-to-wheels Analysis of Future Automotive Fuels and Powertrains in the European Context*. 2011, European Commission Joint Research Centre, Institute for Energy.

36. Bovee, K., et al. *Well-to-wheel analysis and measurement of energy use and greenhouse gas and criteria emissions in a Plug-in Hybrid Vehicle: the EcoCAR 2 case study*. in *Electric Vehicle Conference (IEVC), 2014 IEEE International*. 2014.

37. Banvait, H., S. Anwar, and C. Yaobin. *A rule-based energy management strategy for Plug-in Hybrid Electric Vehicle (PHEV)*. in *American Control Conference, 2009. ACC '09.* 2009.

38. Alipour, H. and B. Asaei. *A heuristic power management strategy for plug-in hybrid electric vehicles*. in *Electric Power and Energy Conversion Systems (EPECS), 2011 2nd International Conference on*. 2011.

39. Overington, S. and S. Rajakaruna. *Review of PHEV and HEV operation and control research for future direction*. in *Power Electronics for Distributed Generation Systems (PEDG), 2012 3rd IEEE International Symposium on*. 2012.

40. Stockar, S., et al., *Energy-Optimal Control of Plug-in Hybrid Electric Vehicles for Real-World Driving Cycles.* Vehicular Technology, IEEE Transactions on, 2011. **60**(7): p. 2949-2962.

41. Lee, H., Y.i. Park, and S.W. Cha. *Power management strategy of hybrid electric vehicle using power split ratio line control strategy based on dynamic programming*. in *Control, Automation and Systems (ICCAS), 2015 15th International Conference on*. 2015.

42. Reedy, J.a.L., S., *Model Based Design Accelerates the Development of Mechanical Locomotive Controls.* SAE Technical Paper 2010-01-1999, 2010, 2010.

43. S. Kaban, J.N., Z Dong, Jian Dong, *An Innovative 4WD PHEV Utilizing a Series-Parallel Multiple-Regime Architecture.* SAE International Journal of Alternative Power. 1(2):419-437, 2012, 2012.

44. Jian Dong, R.C., Z. Dong, Curran Crawford. *Fast Online-Implementable Optimal Energy Management for a Power-Split Hybrid Electric Vehicle*. in *ASME 2013 International Design Engineering Technical Conferences (IDETC) and Computers and Information in Engineering Conference (CIE), 2013, Portland, Oregon, USA*. 2013.

45. Laboratory, A.N. *The Greenhouse Gases, Regulated Emissions, and Energy Use*

in Transportation Model. 2013; Available from: http://greet.es.anl.gov/.

46. A. Rousseau, J.K., P. Sharer, S. Pagerit, M. Duoba, *Integrating Data, Performing Quality Assurance, and Validating the Vehicle Model for the 2004 Prius Using PSAT*. SAE Technical Paper, 2006. **2006-01-0667**.
47. Lino Guzzella, A.S., *Vehicle Propulsion Systems*. 2005: Spriner.
48. Qiuming, G., L. Yaoyu, and P. Zhong-Ren, *Trip-Based Optimal Power Management of Plug-in Hybrid Electric Vehicles*. Vehicular Technology, IEEE Transactions on, 2008. **57**(6): p. 3393-3401.
49. Sturm, J.F., *Using SeDuMi 1.02, a MATLAB toolbox for optimization over symmetric cones*. Optimization Methods & Software, 1999(11-2(1-4)): p. 625-653.
50. Koot, M.W.T., *Energy management for vehicular electric power systems*, in *Department of Mechanical Engineering*. 2006, Eindhoven University of Technology.
51. Serrao, L., *A Comparative Analysis of Energy Management Strategies for Hybrid Electric Vehicles*, in *Mechanical Engineering*. 2009, The Ohio State University.
52. Agency, U.E.P. *Defining Life Cycle Assessment (LCA)*. 2010 [cited 2010 17 October].
53. Laboratory, A.N., *EcoCAR2: Non-Year-Specific Rules*. 2012.
54. Sharer, P.R., A.; Nelson, P.; and Pagerit, S., *Vehicle Simulation Results for Plug-in HEV Battery Requirements*, in *EVS23*. 2006: Japan.

Appendix.A Parameters for QP Algorithm

The original time horizon optimal control problem can be converted into the following convex Quadratic Programming (QP) problem with both linear equality and linear inequality constraints:

$$\min_{\mathbf{u}} J = \sum_{k=1}^{N} \dot{m}_{fc}(k) = \frac{1}{2}\mathbf{u}^T\mathbf{H}\mathbf{u} + \mathbf{u}^T\mathbf{h} \tag{79}$$

$$\begin{aligned} subject \quad to: \quad & \mathbf{A}\mathbf{u} \geq \mathbf{b} \\ & \mathbf{c}^T\mathbf{u} = 0 \end{aligned}$$

where for the linear inequality constraints: $\mathbf{A}\mathbf{u} \geq \mathbf{b}$, **A** is a *4N-by-N* constant matrix, and **b** is a 4N-by-1 vector. The elements of **A** and **b** are given as follows.

$$\mathbf{A} = \begin{bmatrix} 1 & 0 & \cdots & \cdots & 0 \\ -1 & 0 & & & \vdots \\ 0 & 1 & & & \vdots \\ \vdots & -1 & & & \vdots \\ \vdots & & \ddots & & \vdots \\ \vdots & & \ddots & & \vdots \\ \vdots & & & 1 & 0 \\ \vdots & & & -1 & 0 \\ \vdots & & & 0 & 1 \\ 0 & \cdots & \cdots & 0 & -1 \\ & & & & \\ 1 & 0 & \cdots & \cdots & 0 \\ -1 & 0 & & & \vdots \\ 1 & 1 & & & \vdots \\ -1 & -1 & & & \vdots \\ \vdots & & \ddots & & \vdots \\ \vdots & & \ddots & & \vdots \\ \vdots & & & 1 & 0 \\ \vdots & & & -1 & 0 \\ 1 & 1 & \cdots & 1 & 1 \\ -1 & -1 & \cdots & -1 & -1 \end{bmatrix}_{4N \times N} \qquad \mathbf{b} = \begin{bmatrix} \frac{\sqrt{V_{oc}^2 - 4R_{in}P_{n\_bmax}(1)} - V_{oc}}{2C_{bat}R_{in}} \\ -\frac{\sqrt{V_{oc}^2 - 4R_{in}P_{n\_bmin}(1)} - V_{oc}}{2C_{bat}R_{in}} \\ \vdots \\ \vdots \\ \frac{\sqrt{V_{oc}^2 - 4R_{in}P_{n\_bmax}(k)} - V_{oc}}{2C_{bat}R_{in}} \\ -\frac{\sqrt{V_{oc}^2 - 4R_{in}P_{n\_bmin}(k)} - V_{oc}}{2C_{bat}R_{in}} \\ \vdots \\ \vdots \\ \frac{\sqrt{V_{oc}^2 - 4R_{in}P_{n\_bmax}(N)} - V_{oc}}{2C_{bat}R_{in}} \\ -\frac{\sqrt{V_{oc}^2 - 4R_{in}P_{n\_bmin}(N)} - V_{oc}}{2C_{bat}R_{in}} \\ \\ SOC_{\min} - x(1) \\ -(SOC_{\max} - x(1)) \\ \vdots \\ SOC_{\min} - x(1) \\ -(SOC_{\max} - x(1)) \end{bmatrix}_{4N \times 1}$$

Appendix.B Power and Energy Requirements Analysis for a PHEV

To determine power and energy requirements of a glider based on the 2013 Malibu Eco, a standard physical analysis of the vehicle was performed. This glider evaluation and analysis is important when selecting architectures and components to ensure competition standards and performance metrics are met. There are a multitude of forces acting on a moving vehicle and the forces considered in the analysis were those due to acceleration, rolling resistance, braking, aerodynamic losses, and degree of inclination as shown in Fig 71.

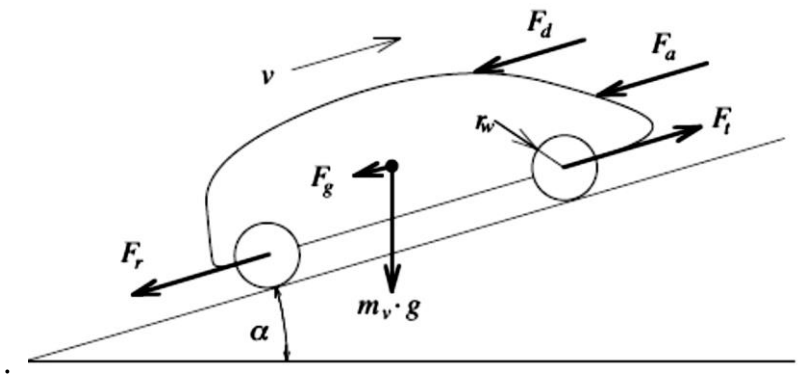

Fig 71. Free Body Diagram of a Glider [47]

The vehicle parameters (typical of a midsize sedan) were defined and provided by the competition organizers are shown in Table 16.

Table 16. Dynamic Vehicle Model Characteristics of 2013 Malibu Eco

Parameters	Value
Vehicle Equiv. Test Weight (EPA inertial weight class)	1589.6 kg
Gross Vehicle Weight Rating (GVWR)	< 2,260 kg
Road Load Coefficients for Equivalent Test Weight	F_0 = 126 N F_1 = 3.6 N/(m/s) F_2 = 0.42N/(m/s)^2
Drag Coefficient C_d	0.29
Front Area A_f	2.295
Coefficient of rolling resistance C_{rr}	0.01

The vehicle modeling and computation was performed in the MATLAB/Simulink environment. As can be seen in Equation (80), vehicle road load consists of four major forces: inertial force ($F_{inertial}$), incline force due to gravity ($F_{incline}$), aerodynamic resistant force (F_{drag}), and rolling resistant force (F_{rr}). These forces are calculated using either the curve fitting functions (81) and (82), or the empirical equation (83). The solutions based on the two functions sets are virtually identical.

$$F_{Tr} = F_{inertial} + F_{incline} + F_{drag} + F_{rr} \tag{80}$$

$$F_{Tr} = F_0 + F_1 v + F_2 v^2 + F_{inertial} \tag{81}$$

$$F_{inertial} = ma \tag{82}$$

$$F_{Tr} = ma + mg\sin(\alpha) + \tfrac{1}{2}\rho C_d A_f v^2 + mgC_{rr} \tag{83}$$

where the vehicle road load F_{Tr} is the tractive effort force at the wheels (N), v is the vehicle speed (m/s), m is the vehicle inertial mass (kg), a is the vehicle acceleration (m/s^2), $F_{inertial}$ is the inertial force due to acceleration (N), α is the grade, C_{rr} is the rolling resistance, ρ is the density of air (1.2kg/m^3), C_d is the drag coefficient and A_f is the front area.

B1. Power Demand for Driving Cycles

The model above was implemented in Simulink to estimate power demand at the wheels for following the UDDS (city), HWFET (highway), US06 City and US06 Highway drive cycles. A vehicle equivalent test weight of 1700kg, roughly equivalent to the base Malibu weight with minimal occupants/cargo, and 2000kg, roughly equivalent to the predicted final mass of the modified hybrid Malibu. Using these two values will result in a range of power, giving the team a good idea of power

requirements to achieve team goals. Average and peak propulsive/braking power can be found in Table 17 and Table 18, and histograms of the power demand are found in Fig 72.

Table 17: Power Demand for Different Driving Cycles (m = 1700kg)

	Average / Peak Propulsion Power (kW) (At the Wheels)	Average / Peak Braking Power (kW) (At the Wheels)
UDDS	7.29 / 37.62	-7.18 / -29.89
HWFET	10.30 / 30.66	-8.99 / -41.74
US06 City	21.57 / 91.35	-19.18 / -65.38
US06 Hwy	19.85 / 90.25	-18.22 / -64.62

Table 18: Power Demand for Different Driving Cycles (m = 2000kg)

	Average / Peak Propulsion Power(kW) (At the Wheels)	Average / Peak Braking Power(kW) (At the Wheels)
UDDS	8.48 / 44.02	-8.37 / -35.36
HWFET	11.39 / 35.79	-10.40 / -49.59
US06 City	24.25 / 105.38	-22.56 / -77.07
US06 Hwy	21.92 / 103.61	-21.24 / -76.18

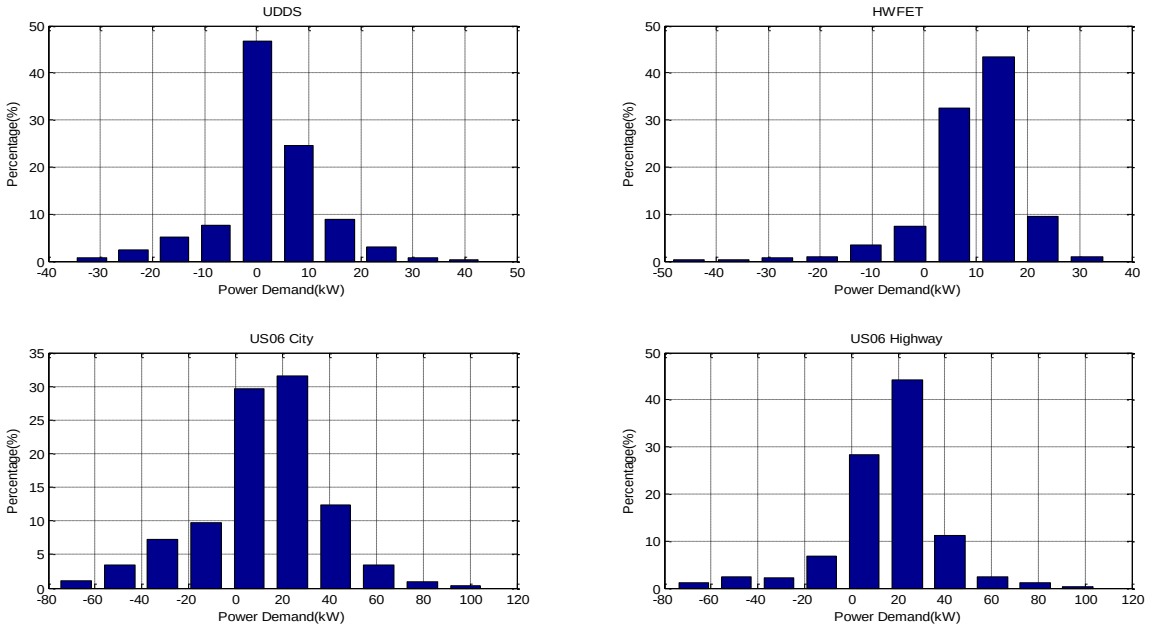

Fig 72. Wheel Power Demand Distribution

The vehicle power demand at the wheels was calculated by multiplying the traction force with vehicle speed, while the positive and negative propulsive energy requirements were calculated by integration of positive and negative propulsive power. Average power was calculated only for non-zero periods for the various drive cycles (assuming 0% grade for the drive schedule). The above results are essential in determining the peak and average power requirements of the propulsion system.

B2. Energy Demand for Driving Cycles

The mechanical energy demanded at the wheels without regenerative braking energy taken into account is defined as the propulsive energy. An approximation of the propulsive energy demand can be derived as:

$$W_{prop} = \sum_{i \in trac} \overline{F_{Tr}}(i) \cdot \bar{v}(i) \cdot \Delta t \tag{84}$$

where $i \in trac$ is the set of all time intervals where $F_{Tr}(i) > 0$ (the sections of the cycle in which the vehicle drives in traction mode [47]). The total traction force includes contributions from three different effects and is approximated by Equation (85). The average speed and average acceleration is approximated by Equation (86) and (87).

$$\overline{F_{Tr}}(i) = \overline{F_{inertial}}(i) + \overline{F_{drag}}(i) + \overline{F_{rr}}(i) = m \cdot \bar{a}(i) + \frac{1}{2} \rho C_d A_f \overline{v^2}(i) + mgC_{rr} \tag{85}$$

$$\bar{v}(i) = \frac{v(i+1) + v(i)}{2} \tag{86}$$

$$\bar{a}(i) = \frac{v(i+1) - v(i)}{\Delta t} \tag{87}$$

The propulsive energy is mainly consumed by three losses (assuming 0% grade): aerodynamics (drag resistance), rolling resistance and acceleration resistance. The distribution of propulsive energy required by the UDDS and HWFET driving cycles in

shown in Fig 73. It can be observed that a much higher percentage of energy goes to aerodynamic losses on the highway cycle than during the city cycle.

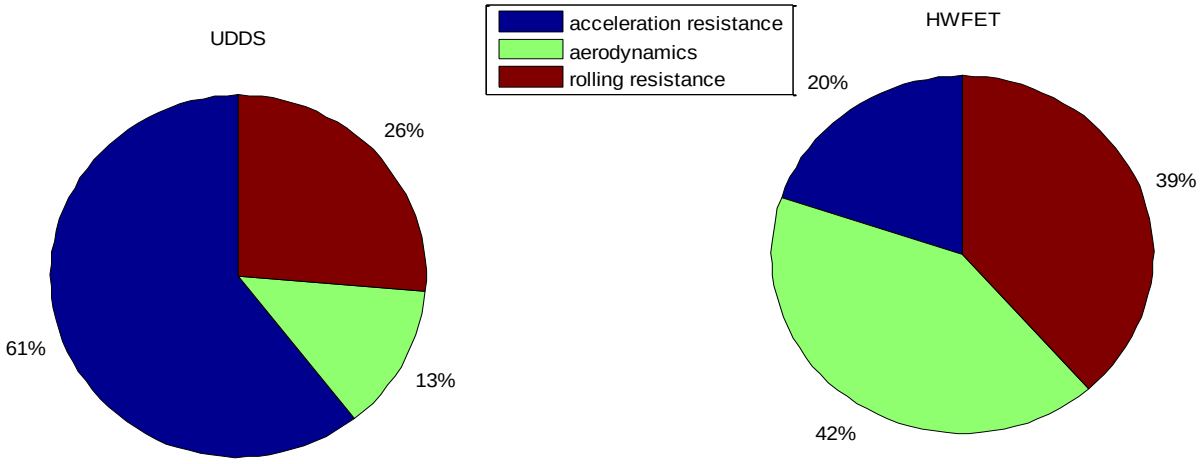

Fig 73. UDDS and HWFET Energy Consumption

The propulsive energy demand for the 2 vehicle masses over the 4 driving cycles was calculated and the results are summarized in Table 19 and Table 20.

Table 19. Propulsive Energy Consumption of Different Drive Cycles

(m = 1700kg)

Cycles	Distance (km)	Accel. (kJ)	Aero. (kJ)	Rolling. (kJ)	Overall	
					(kJ / kWh)	(Wh/km)
UDDS	11.99	3,299	846	1,466	5,611 / 1.559	130
HWFET	16.5	1,269	3,168	2,498	6,936 / 1.927	117
US06 City	12.89	3,860	3,337	1,724	8,920 / 2.478	192
US06 Hwy	9.98	1,603	2,985	1,447	6,034 / 1.676	168

Table 20. Propulsive Energy Consumption of Different Drive Cycles

(m = 2000kg)

Cycles	Distance (km)	Accel. (kJ)	Aero. (kJ)	Rolling. (kJ)	Overall	
					(kJ / kWh)	(Wh/km)
UDDS	11.99	3,922	832	1,701	6,455 / 1.793	150
HWFET	16.5	1,551	3,146	2,913	7,610 / 2.114	128
US06 City	12.89	4,620	3,295	2,001	9,916 / 2.754	214
US06 Hwy	9.98	1,960	2,944	1,678	6,582 / 1.828	183

B3. Power Demand for Performance and Drivability

Performance and drivability are very important characteristics of a vehicle; however, they are not easily defined or measured. In this study, three quantifiable factors were addressed which will be used to evaluate performance and driveability: top speed, gradeability, and 0-100 km/h acceleration time. The calculation details are discussed in sections below.

Top Speed Performance

The top speed performance is mainly determined by the available power and the aerodynamic resistance (Note: at top speed, the power consumed to overcome rolling friction is typically one order of magnitude smaller than the power dissipated by the aerodynamic friction and will therefore be neglected). Neglecting all other losses, the maximum speed is obtained by solving the following power balance:

$$P_{\max} \approx \tfrac{1}{2} \rho C_d A_f \cdot v_{\max}^3 \tag{88}$$

where $P_{\max}$ is the maximum traction power available at the wheels and this power demand depends on the vehicle speed cubed. Based on Equation (88), the power demand for different top speeds is calculated and the results are listed in Table 21 below.

Table 21. Power Demand for Different Top Speeds

Top Speed (mph)	100	110	120	130	140	150
Power Demand at the Wheels (kW)	43.37	56.00	71.00	88.59	108.97	132.38

Gradeability

The relationship between $P_{\max}$ and the maximum gradient angle $\alpha_{\max}$ is obtained by neglecting all the resistance forces in Equation (**80**) other than $F_{incline}$:

$$P_{\max} \approx m \cdot v_{\min} \cdot g \cdot \sin(\alpha_{\max}) \tag{89}$$

where $v_{\min}$ is the desired uphill speed. The power demand for gradeability was then calculated by using Equation (83). The results are useful when calculating the max gradient angle the vehicle can climb at a certain speed. The values are shown in Table 22 below. The Malibu GVWR of 2250kg was used to account for a maximum possible vehicle weight (the 2013 Malibu base vehicle equivalent test weight is 1589.6 kg).

Table 22. Power Demand for Gradeability

GVWR(kg)	Power Demand at the Wheel to Climb at 60 mph at GVWR (kW)	
	3.5% Grade	10% Grade
2250	34.54	73.14

Acceleration Performance

The acceleration performance, the time necessary to accelerate the vehicle from 0 to 60 mph (100km/h), is one of the most important quantifiable drivability factors, from a consumer standpoint. If all the resistance forces are neglected, the energy produced by the engine should be equal to the kinetic energy of the vehicle. Since the engine does not run at peak power throughout the acceleration, the average power was set as $\bar{P} = \frac{1}{2} P_{\max}$. A simple relation between the acceleration time and the maximum power of the vehicle is given by the following expression [47]:

$$t_0 \approx \frac{v_0^2 \cdot m}{P_{\max}} \tag{90}$$

where t_0 is the time available for the acceleration. According to the equations above, the results for power demand at various acceleration times are given as follows in Table 23.

Table 23. Power Demand for Acceleration Performance

Power Demand at the Wheels (kW)	0-60mph Time (s)		
	8	**9.5***	11.5
m =1700kg	153.5	129.3	106.8
m=1800kg	162.6	136.9	113.1
m=2000kg	180.6	152.1	125.7

* Competition Design Target.

B4. Summary of Power and Energy Demand

From the previous analyses, the power and energy demand are summarized in Table 24, assuming a vehicle weight of 1700 kg.

Table 24. Summary of Power and Energy Demand (vehicle weight = 1700kg)

Power Demand at the Wheel			
Average/Peak Propulsive Power to Follow the Drive Cycles	UDDS		7.29 / 37.62 kW
	HWFET		10.30 / 30.66 kW
	US06 City		21.57 / 91.35 kW
	US06 Hwy		19.85 / 90.25 kW
	EcoCAR Combined 4-Cycle		8.70 / 45.39 kW
Average / Peak Braking Power to Follow the Drive Cycles	UDDS		-7.18 / -29.89 kW
	HWFET		-8.99 / -41.74 kW
	US06 City		-19.18 / -65.38 kW
	US06 Hwy		-18.22 / -64.62 kW
	EcoCAR Combined 4-Cycle		-9.51 / -43.27 kW
Power Demand for Performance and Drivability	Top Speed: 140 mph		108.97 kW
	Gradeability: @60mph @GVWR(2260kg)	3.5%	34.54 kW
		10%	73.14 kW
	0-60mph Acceleration Time:	11.5s	106.8 kW
		9.5s	129.3 kW
		8s	153.5 kW
Energy Demand at the Wheel			
Energy to Follow the Drive Cycles	UDDS		130 Wh/km
	HWFET		117 Wh/km
	US06 City		192 Wh/km
	US06 Hwy		168 Wh/km
Energy for AER (All Electric Range)	10 miles		3.10 kWh
	20 miles		6.19 kWh

on US06	30 miles	9.29 kWh
	40 miles	12.39 kWh

In order to determine the component sizes and requirements of the powertrain, a sizing process was developed according to reference [54]. While engine power is the only variable for conventional vehicles, HEVs have two variables due to an additional electric machine providing power. PHEVs add yet another degree of freedom with the battery energy. The peak electric machine mechanical power is defined as the peak mechanical power required for the vehicle to follow the US06 cycle, assuming that power is only derived from an electric machine. This value will be used to size any traction motors, which will in turn allow the vehicle to follow the most aggressive drive cycle in an EV-only mode, resulting in reduced emissions and better fuel economy. The battery peak discharge power is defined as the electrical power that the motor requires to produce the peak mechanical power, following the required drive cycles. The engine was then subsequently sized to achieve the gradeability and performance requirements of the vehicle.

The results indicate the following requirements on the vehicle components, assuming a vehicle weight of 1700kg.

- The front and/or rear wheel traction motors need to provide a combined peak mechanical power of more than 105 kW, allowing the vehicle to follow the most aggressive US06 cycle in EV mode, assuming the efficiency from motor to the wheel is approximately 90%.
- In order to satisfy the acceleration requirements according to the competition design targets (0-60mph within 9.5 seconds), the available power at the wheels needs to be higher than 130 kW. For a series design, this means that the front and/or rear wheel traction motors need to be able to provide together a peak mechanical

power higher than 145 kW, assuming the efficiency from motor to the wheel is at 90%.

- For a parallel design, in order to achieve the gradeability requirement of the vehicle according to the competition design targets, the engine needs to be sized at a power higher than 45 kW for 3.5% grade at 60mph, or 90 kW for a 10% grade at 60mph, assuming the transmission efficiency from engine to wheels is 85%.
- In order to satisfy AER targets on US06, the energy capacity of the battery pack needs to be higher than 11.62 kWh for 30 miles EV only, or 15.50 kWh for 40 miles EV only. This assumes an efficiency of 80% when converting the electrical energy into mechanical energy at the wheels and that all the power is consumed from the battery pack.
- Since the popular version of a series hybrid has a small engine operating at constant output, providing the average power needed over the driving cycle along with a battery providing additional power as required (such as for acceleration or hill-climbing), the engine power need to be higher than 30 kW to be able to follow the average power demand for the most aggressive US06 cycle.

There are several things that should be noted through analysis. First, as shown in Table 17, Table 18 and Table 23, the average propulsive power necessary to drive each driving cycle is much smaller than the power necessary to satisfy the drivability requirements. For instance, a vehicle of 1700kg only requires at most 21 kW to follow the four cycles. However, it requires 129.3 kW to accelerate the same vehicle from 0 to 60 mph in 9.5s. In order to satisfy both requirements, the wheel power demand needs to be designed higher than 130 kW, while the majority of the time during the drive cycles, the vehicle will only require 20 kW or below. This discrepancy between the small average power for the driving cycle and the large power for drivability requirements is one of the main causes for the relatively low fuel economy of the

conventional non-hybrid propulsion systems, since the efficiency of ICE strongly decreases when these engines are operated at low torque.

Moreover, according to the sensitivity analysis in reference [47], the most promising and feasible approach to reduce the mechanical energy required for a cycle is to reduce the vehicle's mass. As can be seen from Table 19 and Table 20, increasing the vehicle mass will significantly impact the energy demand at the wheels, which is related to the fuel economy and the electric energy consumption. A weight analysis of various architectures was conducted and is discussed below.

Appendix.C PHEV Architecture and Component Selection

The process of architecture selection and component selection was iterative. Designs were conceived and evaluated with different components, and modified based on those evaluations. While a vast number of hybrid electric architectures have been researched and developed through the years, only a handful of them have been successfully mass produced. The UVic EcoCAR team analyzed these architectures and considered those which could be implemented within the size constraints of the 2013 Malibu. Initially, a power-split option was considered as it would allow both mechanical and electrical energy to be used optimally for vehicle propulsion. However, this required the use of a power-split device (PSD). The team was unable to find a PSD that would come with sufficient manufacturer support. This reduced the architecture options to series, parallel, or mild hybrid. The mild hybrid option was ruled out, since the donated vehicle was already configured as a mild hybrid, and the team felt that it would be difficult to implement a mild hybrid with better performance than the well-designed GM eAssist system. However, an opportunity was identified to improve on the BAS mild hybrid design by adding a large ESS and rear electric motor, making it a full hybrid. The team determined that implementing a PHEV design would be advantageous in that the utility factor would be greatly increased, improving UF-weighted fuel economy and decreasing emissions. It was decided that the three proposed architectures would therefore consist of a Series EREV, BAS+ PHEV, and Parallel PHEV.

C1. Architecture Design Process

The basic Series EREV design consists of a rear traction motor (RTM) driving the rear wheels, with a generator coupled to the ICE in the front of the vehicle. The team decided to take this design a step further by adding a front electric drive system, making it an AWD series. The availability of power to all four wheels would provide a

significant advantage in both marketing the vehicle and in meeting the power requirements identified in the previous section. Instead of one large (and expensive) motor providing all the propulsive power, two smaller motors would be selected, coupled through fixed gears to drive the front and rear wheels respectively. The ratios of the fixed gears would be selected such that one motor would operate most efficiently at city speeds, and the other more efficiently at highway speeds. A control strategy could be adopted to shift the bulk of the power demand to the most efficient source, based on vehicle speed. However, further analysis revealed that the energy conversion losses associated with two separate electric drives nullified the efficiency gains from the two-ratio concept. Also, the space constraints in the engine bay of the Malibu meant that there was no way to fit both a generator and front drive motor of sufficient size. Therefore, the design was scaled back to that of a RWD EREV. A block diagram of the series EREV architecture is shown in Fig 74.

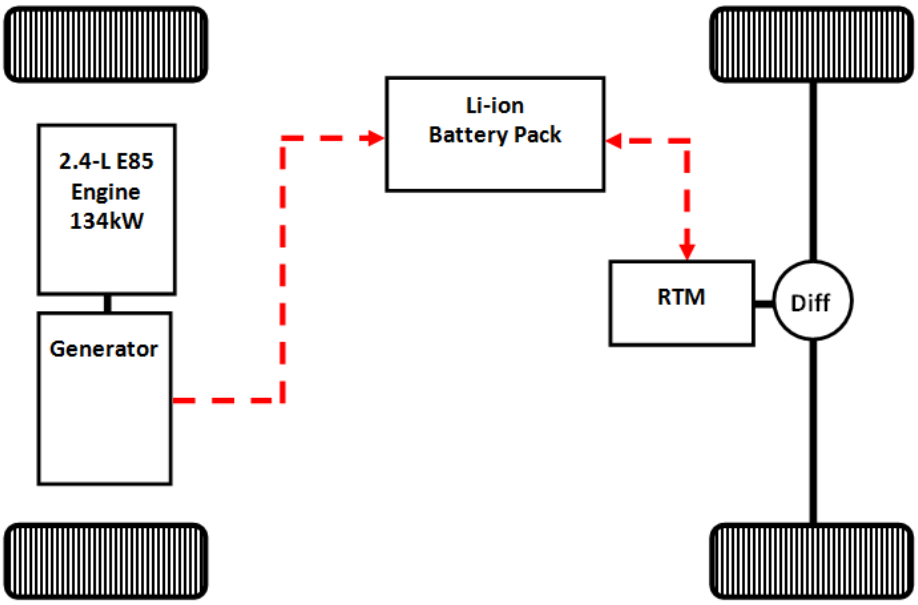

Fig 74. Layout of the proposed series EREV architecture

The second architecture considered was an upgraded BAS+ architecture referred to by the team as the ‘SuperBAS’: a BAS+ with a more powerful BAS motor, as well

as a rear traction motor and large battery. The battery and RTM make this architecture a full hybrid, giving it a significant electric-only range. The stock Malibu eAssist system would be removed and replaced with a system of the team's own design, using a significantly more powerful electric motor. This configuration was identified as having several advantageous operating modes. With the transmission set in neutral, the vehicle could essentially function as a series E-REV, with the ICE charging the batteries through the BAS system. When additional power is required, or when it is more efficient to do so, the ICE and transmission could be used to propel the vehicle. For high-performance driving situations, the BAS could provide a power-assist function to smooth out the torque curve of the ICE, and the RTM could add its power such that all available power sources propel the vehicle. A block diagram of the 'SuperBAS' architecture is shown in Fig 75.

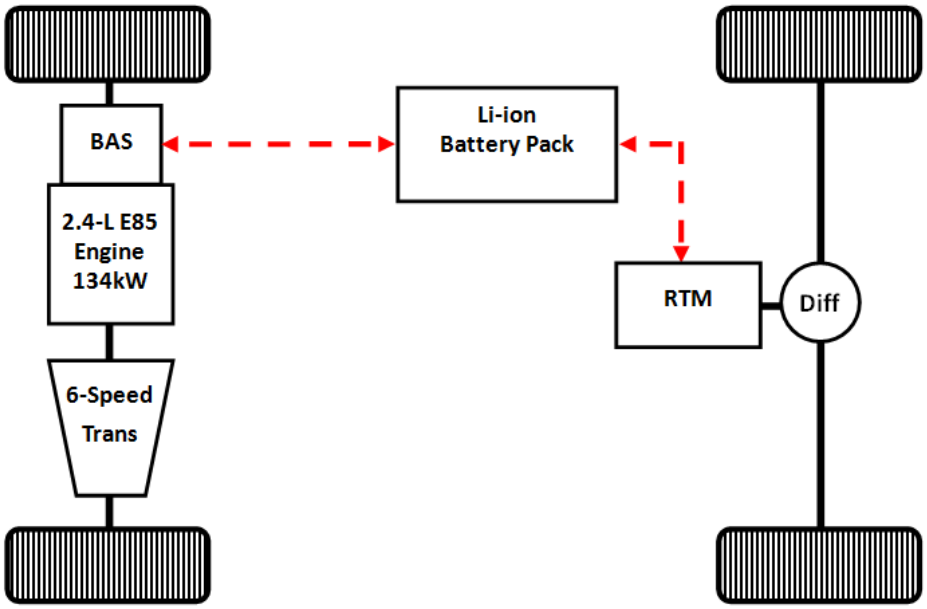

Fig 75. Layout of the proposed SuperBAS architecture

The third architecture considered was a parallel design, analyzed in both pre- and post-transmission parallel. The post-transmission parallel design was discarded once it was discovered that the differential and the transmission were a single entity within the transmission housing, making it impossible to couple an electric motor. Initially, the

parallel design called for the integration of a clutch between the engine and transmission, with an electric motor coupled into the drive system through a belt connecting it and the transmission input shaft. The clutch would replace the torque converter, allowing the engine to be decoupled from the powertrain on command, without the power losses associated with the fluid coupling. This design would offer maximum flexibility of operation; many operating modes are available including electric RWD and AWD and blended operation.

This design, while offering many performance advantages, also presented several major challenges. An electromagnetic clutch was considered as the preferred option over conventional friction and dog clutches. A powerful linear actuator would be required to open and close the dog and friction clutches, but fast-moving actuators generally operate with a reduced torque capability, making them unsuitable for this application. The electric clutch would need to fit into the transmission housing and replace the torque converter. In order to prevent engine torsional vibrations from causing damage to the system, a flexible coupling would also be required. Several solutions were explored for this, including a LUK or Sachs dual-mass flywheel to replace the stock Malibu flywheel, or a shaft coupler. Despite a lengthy search, only one manufacturer was found able to produce an electric clutch to the team's requirements. As this design grew in complexity, the team judged it to be too risky an option; its successful implementation depended largely on external factors outside the team's control such as the cooperation and engineering support of several third-party companies. Consequently, the design evolved to utilize the stock torque converter, rather than an electric clutch, to decouple the ICE. A block diagram of this design is shown in Fig 76.

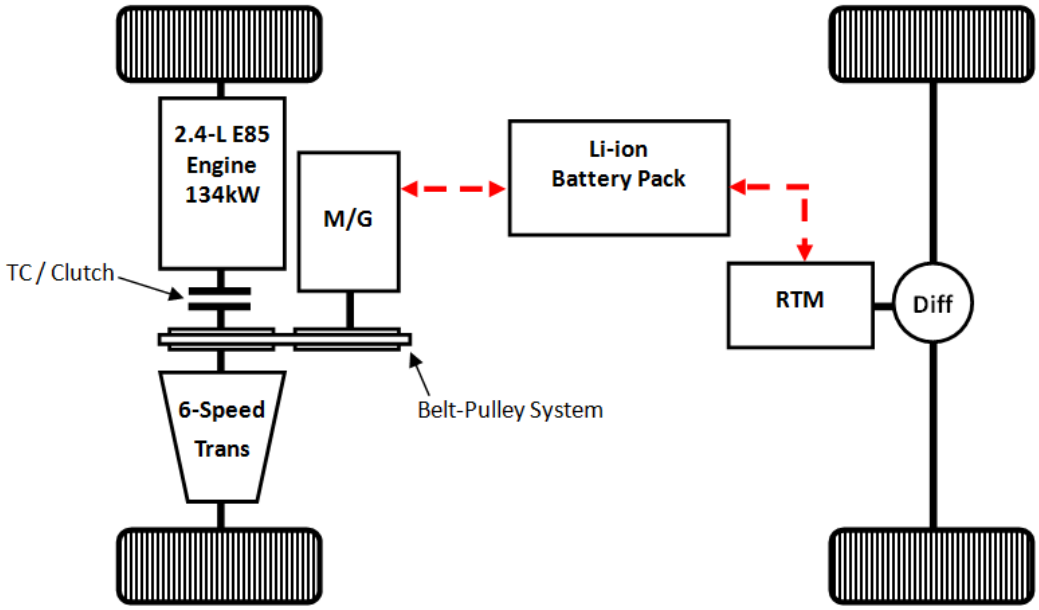

Fig 76. Layout of the proposed pre-transmission parallel architecture

C2. Initial Component Selection Process

The calculations of power and energy requirements from Section 0 were used to determine the component specifications for each configuration.

In order to minimize costs and ensure technical support, sponsor-donated components (from GM or other competition sponsors) would be preferentially used rather than independently selected, purchased components. The three unique engines donated by GM in EcoCAR 2 are the 2.4L E85 Ecotec LE9; the 1.4L gasoline turbocharged LUJ, and the 1.4L diesel LUD. The results of the WTW analysis showed E85 as the optimal fuel. Therefore, the LE9 was designated the primary engine option.

Another engine option was evaluated as a potential alternative: the use of a 1.4L LUJ recalibrated to run on E85. Information from GM indicated that the LUJ being offered in EcoCAR 2 was E85-compatible, but lacked the E85 engine control software. The LUJ is physically smaller than the LE9, and its use would make front-end mechanical packaging less difficult. However, gasoline was identified as the least-

desirable fuel in the WTW analysis, and any benefits gained from the packaging would be more than offset by the poorer performance in E&EC events. Therefore, this engine option would only be viable if the LUJ was successfully recalibrated to run E85 efficiently. Although UVic now possesses the equipment required to recalibrate an engine, the team lacked the experience required for the task. After consulting competition organizers and other teams with engine calibration experience, it was concluded that this option would be too risky for the team to undertake. In contrast, the E85 LE9 was used successfully by the team in EcoCAR1 with the equipment available at the time. Therefore, the LE9 was identified as the preferred engine for the team. To minimize integration difficulty and make the best use of the support from GM, the 6T40 6-speed automatic transmission was selected for the parallel and BAS+ designs.

The PHEV design, along with the power requirements identified in the previous section, dictate that high-power electric machines are required for a successful design. However, the space available for adding electric machines to the Malibu was limited. The size of the chosen engine and transmission drastically limited the space available for any electric motors and inverters in the engine bay, while in the rear of the vehicle, the low ground clearance and competing space requirements for fuel tank, ESS, and other components imposed a similar restriction.

Three traction motors were identified for potential use. First, the Magna E-Drive motor / differential unit was examined. This donated component offered significant advantages. The excellent integration of inverter, motor, and differential in the E-Drive would simplify mechanical and electrical integration in the team's vehicle. Also it would greatly reduce the cost of the vehicle, and enable access to Magna engineers for support. The second machine identified was in the Powerphase family of motors, from UQM. These motors offer very high power density, and the team has previous experience with a Powerphase 145 system from EcoCAR 1. However, the UQM systems are very expensive, and would require significant work to find a rear

differential compatible with them. The third electric machine identified was the Motive 80kW electric drive system, from TM4. TM4 was contacted early in the design process, and indicated its interest in working with the team. Since TM4 works with several large OEM`s that manufacture differentials, use of the TM4 motor would ease the difficult (based on EcoCAR 1 experience) task of integrating a motor and differential into the rear of the vehicle. However, this system would still require significant rear-end space for packaging. Also, the TM4 system is significantly cheaper than the UQM system.

C3. Simulation Comparison

The three architectures outlined above were modeled using Autonomie, which provides a high-level look at the performance of the architecture. The objective was to ensure that each design satisfied the EcoCAR 2 energy use, performance, and driveability targets.

Based on the estimated mass increase from the addition of the hybrid powertrain components, the vehicle mass used in the team's modeling was set at 2100kg. In order to determine overall energy consumption, charge sustaining (CS) and charge depleting (CD) modes are simulated separately. During electric-only CD mode, the engine remains inactive and the rear-traction motor (and front electric drive, for the parallel architecture) drives the vehicle. Battery parameters such as current and voltage are observed over the standard drive cycles in order to determine the electrical energy consumed, with upper and lower state-of-charge (SOC) limits set to 90% and 30% respectively. For the parallel and SuperBAS designs, a blended CD mode was also simulated, to account for their ability to use both electric and engine power to directly propel the vehicle. The CD range over these drive cycles is also determined, by extrapolating the SOC decrease and energy consumed over one cycle to determine the distance over which the SOC drops from upper to lower limits. During CS mode, the engine supplies enough power to maintain the SOC at the constant lower limit of 30%.

Fuel energy use is determined by integrating the fuel rate of the engine over each of the drive cycles. The EcoCAR 2 UF calculation methods presented in section G-2 of the non-year-specific rules were used to determine the weighted fuel economy of each architecture. The modeling results are described and tabulated below.

Series EREV

The series EREV design was first modeled using Autonomie. A standard 2WD series template was used, with the initialization files changed to suit the team's selected components. Results for fuel efficiency, emissions, and driveability of the series EREV are presented in Table 25. It was noted that although the team's design is RWD, the basic Autonomie series model is FWD, creating a possible source of error in the results.

Table 25. Autonomie Modeling Results - Series EREV Fuel Economy and Dynamic Performance

Drive Cycle	505	HWFET	US06 City	US06 Highway	EcoCAR 2 Combined 4 Cycle
CD Electrical Consumption (Wh/km)	160.42	168.07	323.32	241.269	220.53
CS Fuel Consumpiton (Wh/km)	660.57	711.32	1724.43	968.603	954.21
CD Range (km)					47.34
UF Weighted Fuel Energy Consumption (Wh/km)					954.22
UF Weighted Electric Energy Consumption (Wh/km)					220.53
UF Weighted Total Energy Consumption (Lge/100km)					6.41
Total GHG (g/km)					193.07
Total PEU (kWh/km)					0.150
Total upstream THC emissions (g/km)					0.022
Total upstream CO emissions (g/km)					0.006
Total upstream NOX emissions (g/km)					0.018
Dynamic Performance					
0-60mph Time (s)					12.8
50-70mph Time (s)					7.2
Top Speed (km/h)					130.51
Gradeability: 20min @ 100km/h					1.5%

In summary, the Pre-Transmission Parallel+RTM PHEV followed a very similar control strategy as the SuperBAS Parallel+RTM PHEV. Limitations to the design in Autonomie included the common battery problem, as well as an incapability to use the front motor for propulsive power while the engine was inactive. This constraint was improved by modeling the architecture using the ASM. A simple logic was used to maximize efficiency between the rear and front motors that was not available in Autonomie. This logic is not made complex, as the ASM control design was again

difficult to create for the system as a whole. This architecture proves great results for economy and performance, and can be improved using further optimization and component mode blending. Since only the rear traction motor can propel the vehicle in the series design, the dynamic performance is poor compared to the other two designs.

SuperBAS PHEV

Fig 77 shows the SuperBAS model built in Autonomie. Since most Autonomie templates are 2WD by default, a heavily customized model was created to define the front and rear wheel connections of the ICE/transmission and RTM respectively. A list of model components is given in Table 26.

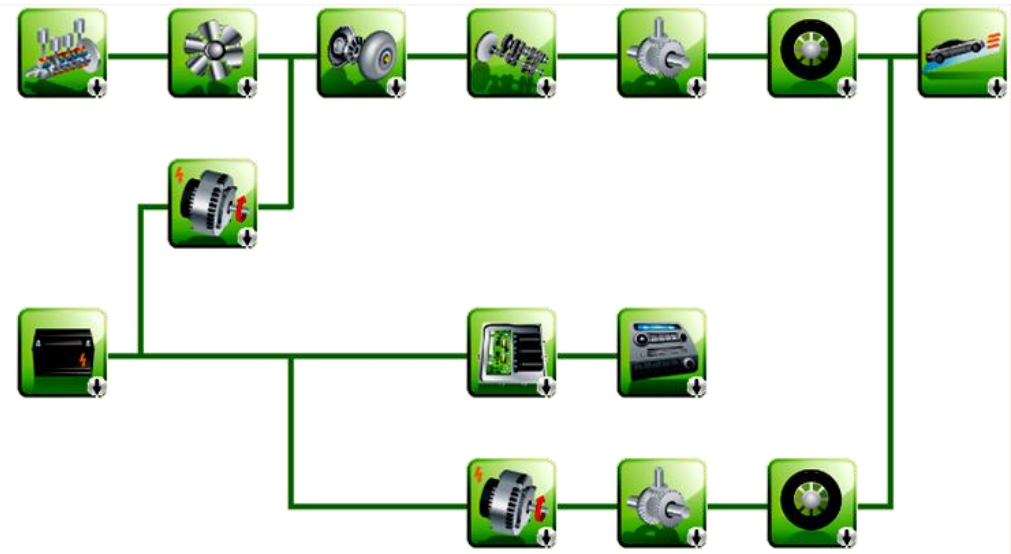

Fig 77. SuperBAS PHEV Model in Autonomie

Table 26. Components of the SuperBAS PHEV Model in Autonomie

Component	Selection and Description
Engine	The updated 2.4 L SIDI Ecotec engine model with full power capabilities is used, where the fuel consumption data for engine speeds above 4000 RPM is extrapolated.
Mechanical Accessories	Constant mechanical power loss representing components such as A/C, water pump, power steering, etc. Set to 0.
Motor 1	To represent the additional motor/generator (TM4) added to the stock BAS system, the PM motor (mot_plant_pm_35_70_escape_MG1) is

	selected and scaled to 80kW, as it has the closest operating curve to the TM4.
Clutch/Torque Converter	Default component in Autonomie: torque converter for over 150Nm: cpl_plant_clutch_1
Gearbox	6-speed 6T40 automatic transaxle with gear ratios 4.58, 2.96, 1.91, 1.45, 1.00, 0.75 and corresponding up/down shift and torque loss tables
Final Drive1(FWD)	2.89 ratio with torque loss table
Wheel Axle1(FWD)	17 inch wheel plant with rolling resistance based on coefficients supplied in the model
Chassis	Custom component by ANL representing the chassis of the 2013 Malibu and corresponding curve fit coefficients and data for aerodynamics and mass
Batteries	The VL41M Saft Li-ion battery with corresponding voltage and power curves compared to state of charge and energy/power densities is scaled at a pack capacity of 58.8Ah(16.2kWh) to represent the A123 6x15s3p battery.
Motor2(RTM)	Magna E-Drive with peak power at 90kW and continuous power at 45kW.
Final Drive2(RWD)	Ratio set at 7.82 with torque loss table
Wheel Axle2(RWD)	17 inch wheel plant with rolling resistance based on coefficients supplied in the model
Power Converter	Generic 12V power converter
Electrical Accessories	Constant electrical power loss representing components such as fans. Set to 200 W.
Driver	Normal driver with integral gain of 1000, proportional gain of 0.5

The SuperBAS was first simulated in Autonomie, using an electric-only CD mode. The UF-weighted energy consumption, emissions, and performance measurements are displayed in the following table:

Table 27. Autonomie Modeling Results - SuperBAS Fuel Economy and Dynamic Performance (electric-only CD mode)

Drive Cycle	**505**	**HWFET**	**US06 City**	**US06 Highway**	**EcoCAR 2 Combined 4 Cycle**

Electrical Consumption (Wh/km)	197.7	189.6	314.2	257.2	239.81
Fuel Consumption (Wh/km)	731.8	685.5	1170.7	882.2	885.37
CD Range (km) — EV-Only					42.14
UF Weighted Total Energy Consumption (Lge/100km)					6.25
UF Weighted Fuel Energy Consumption (Wh/km)					855.39
UF Weighted Electric Energy Consumption (Wh/km)					239.81
Total GHG (g/km)					189.89
Total PEU (kWh/km)					0.145
Total upstream THC emissions (g/km)					0.021
Total upstream CO emissions (g/km)					0.006
Total upstream NOX emissions (g/km)					0.018
Dynamic Performance					
0-60mph Time(s)					9.26
50-70mph Time(s)					5.27
Top Speed (km/h) (limited by RTM gearing)					140.02
Gradeability: 20min @ 100km/h					9.5%

A comparison between Table 28 and Table 27 shows that using the blended mode, the CD range is significantly increased. According to ANL's research in reference [34], when the trip distance is greater than the All Electric Range, using the engine throughout the trip (blended control) is preferable to depleting the battery as fast as possible. Further control strategy research in this area will be performed by the team.

Moreover, the simulation result of the CD range by using EV-only mode is much smaller than the expectation from the battery power and energy demand analysis (which can be found later in Table 29). This is because Autonomie does not have a model of the donated high power A123 Li-ion battery pack. For this analysis, the Saft Li-ion battery was scaled to approximate the capacity (58.8Ah) of the A123 Li-ion battery.

However, the difference of the discharge power between the scaled model and actual component limits the electrical capability of the vehicle model.

The Autonomie control strategy (both propulsion and braking) for the Parallel 2by2WD PHEV with two motors was used for this architecture. The engine ON threshold value was set at 55kW, which means the engine was turned on when the wheel power demand was higher than 55kW. Fig 78 shows the simulation result of the SOC over the EcoCAR 1 combined 4-cycle. The new EcoCAR 2 combined 4-cycle weights more demanding portions greater than others. Therefore, Fig 78 demonstrates the trend that the battery should deplete, but it is important to note that this trend will be more extreme for EcoCAR 2.

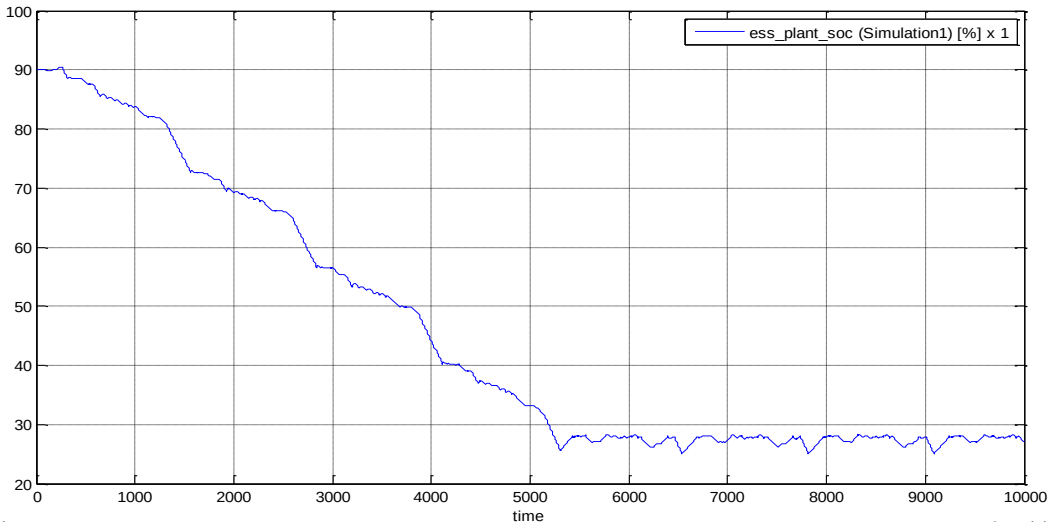

Fig 78. SOC of SuperBAS PHEV under EcoCAR 2 Combined 4-Cycle

The fuel economy, emission and range performance under the standard drive cycles are summarized in Table 28, using a blended mode in CD range. This requires ICE assistance for acceleration, during passing episodes, and at moderate-to-high speeds. It is important to note that the values presented in this table are not weighted, so more aggressive demands are not balanced appropriately with the rest of the drive cycles.

Table 28. Fuel Economy and Emissions of the SuperBAS PHEV Model

Drive Cycle	505	HWFET	US06	US06	EcoCAR 1

	(UDDS)		City	Highway	Combined 4 Cycle
Fuel Consumption (L/100km)	7.39	7.65	8.13	6.79	6.04
Electrical Consumption (Wh)	384.95	7.77	1215.18	914.43	10189.17
Electrical Consumption (Wh/mile)	107.25	0.27	151.81	147.55	98.80
CO_2 Emission (g/mile)	379.31	392.79	417.11	348.52	310.1
Load Specific CO_2 Emission (g/km/ton)	196.41	203.39	215.98	180.47	160.58
CD Range (km)					68
Fuel Consumption in CD Mode(L/100km)					2.83
Fuel Consumption in CS Mode(L/100km)					7.68
UF Weighted Energy Consumption (Lge/100km)					6.58

To size the battery, the same procedure used for energy demand analysis in the previous section is carried out here again for the EcoCAR 1 combined 4-cycle, assuming a vehicle weight at 2000kg and the efficiency from the battery to the wheel is 85%. The battery is then oversized to take into account battery aging. The battery power is oversized by 30% and its energy by 20%. Table 29 shows the requirement for the battery size. The results indicate that in order to satisfy both the discharge power requirement for the most aggressive US06 cycle and the energy requirement for about 40 mile AER, the suitable choice among the 4 provided A123 Li-ion battery are the 6x15s3p (energy= 16.2kWh, cont./peak discharge power=51/152kW) and the 7x15s3p battery pack (energy= 18.9kWh, cont./peak discharge power=60/177kW).

Table 29. Requirement for Battery Size (Vehicle Weight=2100kg)

Battery Ave/Peak Discharge Power Requirements for Drive Cycles	505 (UDDS)	13.5 / 70.60 kW
	HWFET	18.00 / 57.35 kW
	US06 City	38.54 / 168.90 kW

	US06 Hwy	34.73 / 165.27 kW
Energy to follow the EcoCAR 1 Combined 4-Cycle	175.50 Wh/km	
Battery Energy Requirements for AER(All Electric Range) on EcoCAR 1 Combined 4-Cycle	10 miles	3.53 kWh
	20 miles	7.06 kWh
	30 miles	10.59 kWh
	40 miles	14.12 kWh
	50 miles	17.65 kWh

In summary, the SuperBAS PHEV was initially modeled in Autonomie in order to quickly evaluate the design over various drive cycles. In the frequent case, UVic discovered new information that would limit the use of components and the feasibility of present designs. Therefore, Autonomie acted as a base for verifying all requirements were met in a quick and simple manner. However, there were limits in component selection and drivetrain imitation. The most accurate model of the A123 battery modeled by UVic needed to be scaled larger, as it did not provide sufficient voltage to the electric machines in order to meet the aggressive portions of drivecycles (note that the actual velocity was still extremely close to the drivecycle reference, so it was assumed reasonable). The SuperBAS model was relatively simple to model, as required components were readily available for use in the software. This was good, as the same architecture was quite difficult to replicate using the ASM approach. The ASM provided a much more accurate model in the end, although assumptions for optimization were used to simplify the design. This optimization would allow for a superior blend of optimal component use, and is currently being investigated by UVic controls strategists. This architecture proves exceptional results for economy and performance, and can be improved using further optimization and component mode blending.

Pre-Transmission Parallel PHEV

The proposed pre-transmission Parallel PHEV architecture is modeled in Autonomie to examine the fuel economy and dynamic performance. Since the proposed architecture doesn't exist in Autonomie, an effort is made through XML to integrate the clutch and the RTM into the existing template of Autonomie. The built model is shown in Fig 79.

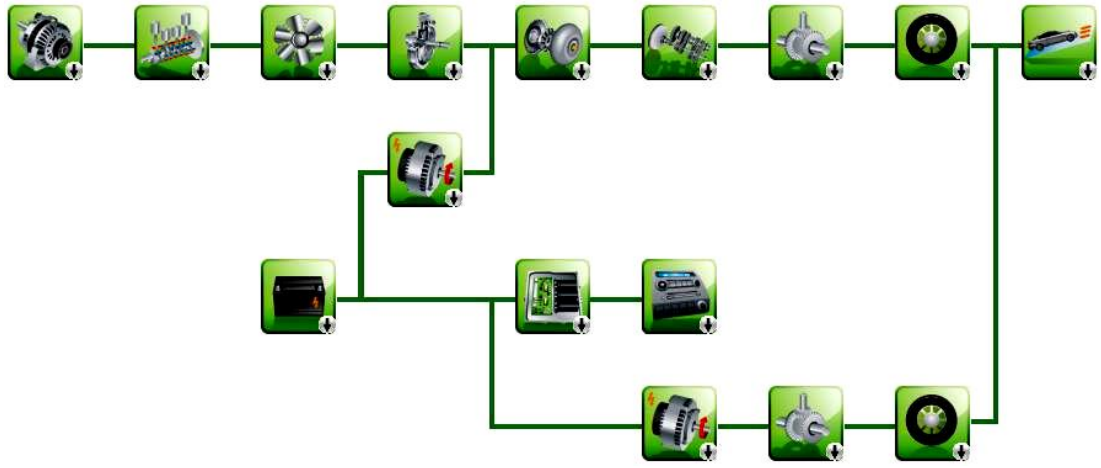

Fig 79. Pre-Transmission Parallel PHEV Model in Autonomie

The simulation results using blended mode in CD range are summarized in Table 30. Again the control strategy for the parallel 2by2WD PHEV with two motors was used for the architecture. The simulation was carried out outside GUI interface of Autonomie.

Table 30. Fuel Economy and Dynamic Performance of the Pre-Transmission Parallel PHEV Model using Autonomie

Drive Cycle	UDDS /505	HWFET	US06 City	US06 Highway	EcoCAR Combined 4 Cycle
Fuel Economy (mpg)	41.38	31.94	34.43	42.44	**45.4**
Fuel Consumption (L/100km)	5.68	7.36	6.83	5.54	**5.18**
Electrical Consumption (Wh/mile)	126.40	-0.93	166.80	168.55	**97.90**
CO2 Emission(g/mile)	291.71	377.91	350.51	284.39	**265.83**

Load Specific CO2 Emission (g/km/ton)	177.41	229.82	213.17	172.94	**161.67**
CD Range(mile)					**49.39**
Fuel Consumption in CD Mode(L/100km)					**2.1**
Fuel Consumption in CS Mode(L/100km)					**7.65**

Dynamic Performance	
0-60mph Time(s)	**9.25**
50-70mph Time(s)	**5.26**

The simulation results using EV-only mode in CD range are summarized in the following Table 31. Again, the CD range is significantly longer if using blended mode. However, under the current control strategy in Autonomie, the front motor doesn't provide power to the wheel under EV-only mode. So the results are quite close to that in SuperBAS design.

Table 31. Fuel Economy and Dynamic Performance of the Pre-Transmission Parallel PHEV Model (Vehicle Mass=2100 kg)

Drive Cycle	**505**	**HWFET**	**US06 City**	**US06 Highway**	**EcoCAR 2 Combined 4 Cycle**
CD Electrical Consumption (Wh/km)	189.01	177.42	312.14	237.78	/
CS Fuel Consumpiton (Wh/km)	716.66	686.39	1132.41	867.11	/
CD Range(mile) – EV-Only Mode					**27.76**
UF Weighted Total Energy Consumption(Lge/100km)					**5.96**
UF Weighted Fuel Energy Consumption(Wh/km)					**838.94**
UF Weighted Electric Energy Consumption(Wh/km)					**226.80**
Total GHG(g/km)					**182.25**
Total PEU (kWh/km)					**0.137**

Total upstream THC emissions (g/km)	**0.020**
Total upstream CO emissions (g/km)	**0.005**
Total upstream NOX emissions (g/km)	**0.017**
Dynamic Performance	
0-60mph Time(s)	**9.25**
50-70mph Time(s)	**5.26**
Top Speed (mph)	**138.69**
Towing Gradeability@60mph @20min	**9.45%**

The Pre-Transmission Parallel PHEV design was modeled using the ASM in a very similar fashion as the SuperBAS. The drivetrain was cut in order to separate torque requests between the front and rear differential. The real-time optimization tool is used to distribute torques optimally. However, the BAS model in the previous design is replaced with a motor that is coupled to the crank shaft on the opposite side of the engine. This motor is modeled with the same TM4-80kW specifications as the BAS. The design of this architecture uses a device that allows the motor to run while the engine is off. This device is represented by a torque converter in the stock ASM transmission, and allows the front motor to assist in driving the vehicle in all-electric mode in order to assist with power requirements and increased regenerative braking.

The control strategy is nearly identical to that of the SuperBAS PHEV design. Differences include an extra optimization technique that governs the maximum combined efficiency between the front TM4 motor and the rear traction Magna e-Drive motor. To simplify this step, the efficiency at an instantaneous front- and rear-traction motor torque and speed were observed. Whichever of either motors possessed the largest efficiency point gained priority. This change from the SuperBAS design affected the emissions data presented below.

Summary

In this section, the three hybrid powertrain architectures were simulated. Drive cycle based simulations using Autonomie and the dSPACE ASM were performed and the results of all vehicles can be found in Table 25, Table 27, Table 28, Table 30 and Table 31.

The AWD SuperBAS PHEV design allows for efficient engine operation and good EV capability. This design also reduces the power flow from the mechanical to electrical power conversion path which creates considerable losses in the series hybrid design. The BAS motor is increased in size compared to the stock Malibu BAS system to aid in vehicle propulsion. This system also largely increases the efficiency of the engine by optimizing the amount of torque and speed the engine may run at. The rear traction motor was analyzed in great detail to determine that the Magna E-Drive would provide the required performance. The performance and economy results were excellent, although it should be taken in consideration that the modeling of the system's optimization using the ASM may not be well calibrated and slightly over-optimistic due to time and information availability constraints.

The Pre-Transmission Parallel PHEV design performs similarly to the SuperBAS PHEV, with an improved electric-drive capability. The BAS is replaced with a belt-driven motor, placed in between the engine and stock transmission. A torque converter allows the engine to disengage at any time. This torque converter may be replaced by a clutch if availability permits latter in the EcoCAR2 competition. This design is much more complex than the SuperBAS system, so a trade-off for simplicity vs. performance was made using a defined feasibility study and an architecture design matrix. The performance and economy results remained exceptional; however, data proved to be slightly less economic than the SuperBAS design. This could be due to the loss from the control logic that attempts to optimize the combined front and rear motor efficiencies. Results may be improved with a more developed control strategy and further optimization.

The RWD Series PHEV was the third architecture investigated. The absence of a FWD capability results in satisfactory performance. As this architecture has only one power flow path for driving capability, it's optimization is relatively simple with the expense of efficiency due to the mechanical-electrical-mechanical power conversions. Due to the lack of power from multiple components, the vehicle performance was satisfactory.